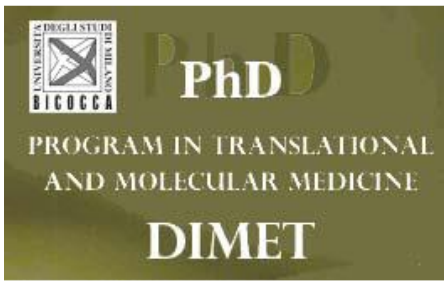

PAOLA VENCO

Matr. N°. 056703

Characterization of disease genes in neurodegeneration with brain iron accumulation through the development of cellular models

Coordinator: Prof. Andrea Biondi

Tutor: Dr. Valeria Tiranti

Co-tutor: Dr. Vania Broccoli

XXVIII CYCLE

ACADEMIC YEAR

2014-2015

CHAPTER 1

General introduction:

Neurodegeneration with brain iron accumulation (NBIA), neurodegenerative diseases and modeling approaches.

NEURODEGENERATIVE DISEASES

Neurodegeneration is a common term which identifies any pathological condition primarily affecting neurons and leading to distinct loss of nervous system structure and function (Deuschlc G. 2009) (Przedborski S. 2003).

Age is the most risk factor for neurodegenerative diseases (NDDs) that represent a major cause of disability and premature death among older people worldwide. For instance, the number of cases of Alzheimer's disease (AD) and other dementias, including Lewy body disease and frontotemporal dementia, was estimated by the World Health Organization in 2005 at almost 25 million individuals worldwide, with 5 million new cases annually (Shon and Przedborski 2011). It is currently estimated that the number of neurodegenerative diseases is approximately a few hundred, and they show a great phenotypic and clinical diversity. There are classifications based on clinical symptoms or the topography of the principal lesion, but sometimes the pathological characteristics of these diseases overlap, suggesting the necessity of a new classification that points its attention on the pathogenesis of these diseases (Kovacs G. 2016). The hypothesis that have come to prominence are: accumulation of misfolded proteins, proteasomal and autophagy dysfunction, oxidative stress, impaired calcium homeostasis, axonal transport deficits, mitochondrial dysfunction, inflammation, and white matter alterations. Many of these mechanisms are likely to be connected, so that a defect in one cellular pathway will have a "domino effect" leading to multiple stresses for the cell (Thompson LM. 2008).

Despite numerous progresses in understanding the aetiopathogenesis of neurodegenerative diseases have been done, the precise pathway that firstly leads to neuronal dysfunction and then to death isn't yet known and there are currently no therapies available. Furthermore, the overwhelming majority of neurological disease is of a sporadic nature, renders the discussion about eatiology more difficult.

However, the purpose of the experimental work I carried out during my DIMET course has been focused on a neurodegenerative syndrome identified with the acronym NBIA, which means Neurodegeneration with Brain Iron Accumulation. NBIA identifies a group of clinically and genetically heterogeneous rare pathological conditions (1 every 1 000 000 citizens), characterized by progressive extra-pyramidal disorders and by evidence of focal iron accumulation in the brain, especially in basal ganglia (Gregory and Hayflick 2013). In the following paragraphs I have reported the clinical and pathological findings for each NBIA-related genes and then, the main pathogenic themes related to neurodegenerative disorders because the major overlap seen between NBIA and more common neurodegenerative diseases may highlight conserved disease processes. So, although relatively rare as individual genetic diseases, mechanisms that lead to NBIA, share similar aspect with other diseases such as frontotemporal dementia (FTD), Parkinson's disease (PD), Alzheimer's disease (AD), Friedreich's ataxia and amyotrophic lateral sclerosis (ALS). Thus studying monogenetic orphan diseases such as NBIA, is very useful to define the processes involved in

common and genetically undefined diseases like the ones mentioned above. (Arber C. 2015).

NEURODEGENERATION WITH BRAIN IRON ACCUMULATION (NBIA)

NBIA identifies a group of clinically and genetically heterogeneous rare pathological conditions, characterized by progressive extra-pyramidal disorders and by iron accumulation in the brain, especially in basal ganglia, observed initially in autopsy studies and more recently in MRI studies (Gregory A. 2005). In NBIA, specifically, iron accumulates in the globus pallidus and in the substantia nigra. These basal ganglia, due to the fact that contain high iron levels and have a high metabolic requirement, are more susceptible to iron-related demage (Hill J. 1984). During normal aging, brain iron accumulation is evident even in neurologically healthy people (Hallgreen B. 1958). But in NBIA it occurs even in childhood or adolescence and it can extends to other site, such as cerebellum, depending on the disease. Iron deposition has been at the same time associated with various disorders, such as Parkinson's disease, Alzheimer's disease and multiple sclerosis and it has been evidenced as a potential damaging element for tissues either directly or because it changes the cellular environment, making it more prone to toxins. On the other hand, iron deposition may be just a consequence of axonal disruption (Sian-Hulsmann J. 2011) (Weinreb O. 2010).

To date, it isn't known if iron accumulation may be just an epiphenomenon, and not a primary cause of NBIA diseases, the things

that we certainly know is that iron is indispensable in mammalian metabolism because of its role in formation of haem, iron-clusters and as cofactor in numerous metabolic reactions (Rouault T.A. 2013) .

The clinical spectrum of this devastating disorder includes dystonia, parkinsonism and spasticity. Pyramidal involvement or ataxia are frequent and also retinopathy or optic atrophy may be diagnostic. Furthermore, pathological studies have identified protein aggregates and axonal swellings that are reminiscent of other common neurodegenerative disorders. As previously stated, the term "NBIA" encompasses a wide group of similar diseases, which are nevertheless distinguishable; it is thus necessary to provide the researchers with a classification, that can help avoid confusion and eventual misunderstandings. Previously NBIA, known as Hallervorden-Spatz disease, was classified in two categories based on the onset and the progression of the disease. Up to now 10 genes have been associated with specific forms of NBIA and the actual classification is based on these genetic findings, however the clinical and molecular heterogeneity of NBIA disorders causes a large fraction (around 20%) of affected patients to be without a molecular genetics diagnosis (Arber C. 2015). The table below summarizes the known genes involved in NBIA and the main molecular, clinical and neurophatological features of NBIA subtypes. Only two proteins are specifically related to iron metabolism: neuroferritonopathy and aceruloplasminemia. While the others, apparently unrelated to each, can be clustered together: some of them are related to fatty acid metabolism (PANK2 and COASY,C19orf12, PLA2G6, FA2H), DNA damage response (DCAF17), autophagy (WDR45), lysosomal activity

(ATP13A2). In 2015 another two genes has been associated with NBIA, the first, SCP2 (Horvarth R. 2015) that is related to fatty acid, and the second, GTPBP2, (Elham J. 2015) that is involved in cell proliferation and differantiotion, intracellular transport, regulation of cytoskeleton and protein synthesis (Bourne H.R. 1990).

NBIA DISORDERS AND ASSOCIATED GENES			
DISEASE	DISEASE GENE	INHERITANCE	SYMPTOMS
Neuroferritinopathy	FTL (19q13.3)	Autosomal Dominant	Extrapyramidal signs, dystonia, orofacial dystonia, cognitive decline.
Aceruloplasminemia	CP (3q23.25)	Autosomal Recessive	Iron not only in the basal ganglia but also in liver, pancreas and myocardium, cognitive impairment, diabetes mellitus, retinal degeneration, blepharospasm, facial and neck

			dystonia, chorea, dysarthria, ataxia.
Pantothenate Kinase-Associated Neurodegeneration (PKAN)	*PANK2* (20p12.3)	Autosomal Recessive	Dystonia, spasticity, cognitive decline, pigmentary retinopathy.
PLA2G6-Associated Neurodegeneration (PLAN)	*PLA2G6* (22q12.13)	Autosomal Recessive	Infantile neuroaxonal dystrophy, progressive motor and mental retardation, cerebellar ataxia, pyramidal signs.
Mitochondrial Membrane Protein Associated Neurodegeneration (MPAN)	C19orf12 (19q12)	Autosomal Recessive	Iron-containing deposits, dystonia, parkinsonism, psychiatric symptoms, spastic paraparesis.
FA2H-Associated Neurodegeneration (FAHN)	FA2H (16q23)	Autosomal Recessive	Spastic quadriparesis, severe ataxia, dystonia.

Kufor-Rakeb disease	ATP13A2 (1p36)	Autosomal Recessive	Early onset levodopa-responsive parkinsonism with pyramidal tract involvement, dementia.
Woodhouse-Sakati Syndrome	*DCAF17* (2q31.1)	Autosomal Recessive	Hypogonadism, alopecia, diabetes mellitus, mental retardation, deafness, electrocardiographic abnormalities.
β-propeller Protein-Associated Neurodegeneration (BPAN)	*WDR45* (Xp11.23)	X-Linked	Cognitive impairment, progressive dystonia-parkinsonism, corticospinal signs.
COASY protein-associated neurodegeneration (CoPAN)	COASY (17q12.21)	Autosomal Recessive	Oro-mandibular dystonia, dysarthria, spastic dystonic paraparesis, obsessive-

			compulsive behaviour
?	SCP2 (1p.32)	Autosomal recessive	Gait disturbance and deafness
?	GTPBP2 (6p.21)	Autosomal recessive	Mental retardation, ataxia, dystonia features

Table 1. **Overview of NBIA conditions and genes**. The table summarizes the currently known genes involved in NBIA. *FTL*: ferritin light polypeptide, *CP*: ceruloplasmin, *PANK2*: pantothenate kinase 2, *PLA2G6*: phospholipase A2, *C19orf12*: chromosome 19 open reading frame 12, *FA2H*: fatty acid 2 hydroxylase, *ATP13A2*: ATPase type 13A2, *DCAF17*: DDB1 and CUL4 associated factor 17, *WDR45*: WD repeat domain 45, *COASY*: CoA synthase, *SCP2*: sterol carrier protein 2, *GTPBP2:* GTP binding protein 2.

Here I propose a summary of the diseases present in the table.

1. NBIA disorders directly involving iron metabolism

1.1.Neuroferritinopathy

Neuroferritinopathy (MIM#606159) is an adult-onset autosomal dominant progressive movement disorder, due to mutations in Ferritin Light Chain gene (*FTL)*.

The first medical recognition of neuroferritinopathy relates to an English family (Curtis A.R. 2011). The proband was a woman who developed a movement disorder in middle age, but who retained all her cognitive functions; subsequent DNA analysis revealed an autosomal dominant genetic condition with symptom onset between the fourth and the sixth decade. Genetic analysis identified the cause of the syndrome in a 2 Mb region located at position 19q13.3, and

specifically in a sequence variant of Ferritin Light Chain gene (*FTL*), exon 4, constituted by an adenine insertion in position 460-461 near the 3' end of the coding region (Curtis A.R. 2011). Research conducted after the discovery of new cases in the UK revealed that a common haplotype had been inherited by all patients and consequently that all their families derived from a common ancestor. To date, seven distinct disease-causing mutations have been reported in this disease, all of them localized in exon 4 of the *FTL* gene. The most common mutation is the insertion of an extra nucleotide in the fourth exon, which causes a frame-shift and synthesis of an abnormal C-terminus (McNeill A. 2011). Ferritin(Ft) is the main protein iron storage from prokaryotes to mammals and is characterized by a highly conserved structure that consists of a virtually spherical shell with an internal cavity that can accommodate up to 4500 iron atoms.

Ferritin is a heteropolymer of 24 subunits, which can be either heavy or light in different proportions and form a proteinaceous shell that can store 4500 iron atoms (Arosio and Levi 2010).

The heavy chain has a ferroxidase activity and the light chain aids mineralisation within the ferritin structure. The C-terminus is involved in the formation of the hydrophobic channel of the ferrin shell. So, when is mutated, it is incorporated into the ferrin heteropolymer, but leads to a poisoning of the holo-ferritin structure, potentially at the iron entry pore (Burn and Chinnery 2006) leading to an iron-porous ferritin structure (Friedman A. 2011). The mutated peptide assembles with the H- and L- subunits to form ferritin shell, which is unable to incorporate iron properly. This leads to iron excess in the cytosol (cytLIP), which induces iron-dependent ferritin translation, generating

a self-maintained vicious cycle, and at the same time stimulating ROS production and oxidative damage. In long period this causes impairment of the proteasome, ferritin aggregation, and cell death. The result is that iron leaks out of ferrin (Friedman A. 2011) . This cause iron-dependent oxidation, particularly in cells that normally express high amounts of FTL. Recently, it has also been reported a greater propensity to oxidation of the mutated chains, both *in vitro* and *in vivo*, stressing that oxidative stress is a key component of the pathogenesis (Baraibar M. A. 2010) .

Clinically, the major extrapyrimidal symptoms, which manifest between the third and the sixth decades of life are chorea, dystonia, bradykinesia or a mixture of the three, with choreiform movements, tipically asymmetrical and more evident in the face, orolingual musculature and upper limbs. Dystonia affects face, tongue, arms and legs and is usually asymmetrical as well. A number of patients experience reduced facial expression and gait instability. Dysarthria is common and dysphagia can also be a late feature, while eye movements are usually well preserved. The diagnosis of neuroferritinopathy is still quite difficult, as its symptoms can easily be confused with those deriving from Huntington's disease, Parkinson's disease and idiopathic torsion dystonia, and it can also be confused with an unclassified movement disorder syndrome.[14] In patients, serum ferritin level tends to be reduced (Crompton E. 2002).

An abnormal deposition of iron and ferritin is found in the brain of neuroferritinopathy patients. At MRI their locations are usually in the basal ganglia, in the cerebellum and motor cortex; histologically, in

glia and neurons. Importantly, evidence of iron deposition has been seen in presymptomatic familial carriers of the disease, leading to the hypothesis that iron accumulation begins in childhood and worsens until symptoms begin, in the fourth decade of life. (Keogh M. J. 2012).

Mitochondrial abnormalities have been highlighted and an increased oxidative stress of the cells, possibly due to iron, was shown via peroxidation and nitrosylation (Mancuso M.M. 2005). Indeed, several animal and cell systems have confirmed an increase in oxidative stress in *FTL* mutant models: through mitochondrial and nuclear DNA damage, proteasomal insufficiencies and damage to proteins and lipid via reactive species. Iron chelators were able to reverse cell sensitivity, promoting iron as the main cause of disease (Cozzi A. 2010).

In conclusion, analysis of protein suggest that the pathogenesis could be caused by a reduction in ferritin iron storage capacity and by enhanced toxicity associated with iron-induced ferritin aggregates, where as data on cellular models, confirmed by the study on transgenic mouse model, imply that the pathogenesis could be mostly related to iron- dependent oxidative damage. Thus, time should be invested now in the development of therapeutic agents aimed at blocking the detrimental cascade of oxidative events. Some promising results have been recently obtained in more common diseases, such as Parkinson's disease and might be extended to these cases (Devos D. 2014).

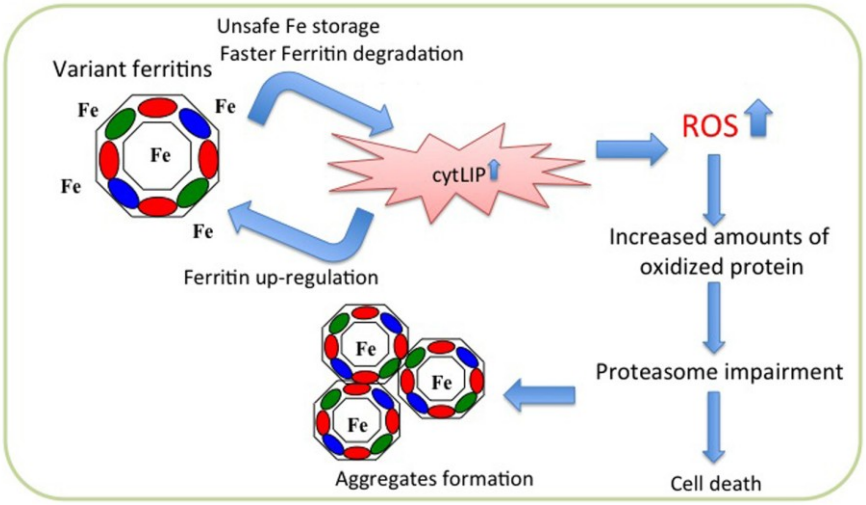

Figure 1. **Scheme of pathogenetic molecular mechanism of neuroferritinopathy**. The mutated peptide (greenellipse) assembles with the H- (redellipse) and L (blueellipse) subunits to form ferritin shell, which is unable to incorporate iron properly. This leads to iron excess in the cytosol (cytLIP), which induces iron-dependent ferritin translation, generating a self maintained vicious cycle, and at the same time stimulating ROS production and oxidative damage. In long period this causes impairment of the proteasome, ferritin aggregation, and cell death. (Levi and Finazzi 2014)

1.2.Aceruloplasminemia

Aceruloplasminemia is a disease originating from loss-of-function mutations in the ceruloplasmin (*CP*) gene, first discovered in 1987.

The gene is located on chromosome 3, at position 3q23.25 and its product is a protein expressed by astrocytic foot processes.

Ceruloplasmin is a glycoprotein containing many copper atoms that acts as a ferroxidase. It helps the iron export activity of ferroportin and leads to its binding to glycosyl phosphatidylinositol (GPI); in astrocytes it is necessary for iron export.

Aceruloplasminemic patients cannot oxidize ferrous ions (Fe^{2+}) delivered into their CNS, to ferric ions(Fe^{3+}) so that the reduced atoms are free to lead to un-regulation in a different pathway concerning non transferrin-bound iron uptake. This mechanism, coupled with the inability of astrocytes to export iron, is thought as responsible for the astrocytic iron overload observed in patients (Brissot P. 2012).

Eventually, iron will not reach neurons, that will consequently die because of iron deficiency and exposure to toxins released by the surrounding dying astrocytes.

Furthermore, mutant forms of ceruloplasmin could possibly promote cell death on the basis of a non-iron related mechanism (Kono S. 2006).

The most affected brain area is that of the basal ganglia (Jeong and David 2003), where loss of neurons and accumulation of globular structures which have been interpreted as astrocytic remnants are evident (Schneider and Bhatia 2013). Particularly affected seem to be the dentate nuclei, the globus pallidus, the putamen, the caudate, thalamus and the red nuclei. Iron accumulation is also evident in liver, pancreas and myocardium (Gregory A. 2005).

From the clinical point of view, patients present with adult-onset neurological disease, diabetes mellitus and retinal degeneration.

With the pathological proceeding, there is the comparison of cognitive impairment, cerebellar ataxia and craniofacial dyskinesia (Schneider S.A. 2012). Diagnostically serum cepuplasmin is undetectable, copper and iron serum levels are low, while ferritin is elevated (Schneider S.A. 2012).

2. NBIA disorders caused by defects in autophagy

β-propeller-protein-associated neurodegeneration (BPAN)

WDR45 (WD Repeat domain 45), a gene located at position Xp11.23, is responsible for a form of NBIA, called β-propeller-protein associated neurodegeneration (BPAN), first described by Haack in 2012. Even thought the gene is on chromosome X, males and females present the same clinical phenotype, and the disease is always sporadic, due to *"the novo"* mutations in the WDR45 gene. (Haack T.B. 2012). It codes for a protein (WIP14) with a seven-blated beta-propeller structure and a phosphoinositide-binding motif for membrane interaction. It is a member of the WD repeats protein family and one of the four mammalian homologous of yeast Atg18, and important regulator of autophagy, specially in autophogosome formation (Lu Q. 2011) (Dall'Armi C. 2013). In lymphoblast cells from BPAN patients, the protein amount is clearly reduced and there is a block in the autophagic flux (Saitsu H. 2013).

The patients affected show a definite phenotype, named SENDA, characterized by childhood onset cognitive impairment without progression which proceeds in adult age and became a progressive dystonia-parkinsonism and dementia with corticospinal signs.The MRI shows clear sign of iron accumulation in the SN in the early disease stage, while in GP is a later event (Haack T.B. 2012).

There are many pathologies in which autophagy is involved: Pakinson's disease, Crohn's disease, cancer and spastic paraperesis, but this disorder represent the first direct link between the autophagy

machinery and neurodegeneration. So it will be of great interest to analyze the correlation with iron homeostasis.

3. NBIA disorders caused by defects in lysosomal metabolism

Kufor-Rakeb disease

This recently-discovered NBIA pathology comes from patients mutated in a gene called *ATP13A2*, also known as *PARK9*; this gene is located on chromosome 1, at position 1p36. It is a rare autosomal disorder characterized by juvenile onset parkinsonism and dementia, neuronal ceroid-lipofuscinosis and NBIA (Di Fonzo A. 2007) (Bras J. 2012) (Schneider S.A 2010).

The protein encoded by *ATP13A2* is a lysosomal 5 P-type ATPase that functions as a divalent cation transporter. The analysis of the fibroblasts from patients with *ATP13A2* mutations have showed severe perturbation of lysosomal function, with impaired degradation of substrate, reduced processing of lysosomal enzyme and decreased autophagosome clearance. This leads to cytotoxic effects together with α-synuclein and zinc accumulation. Moreover fibroblasts (and olfactory neurons) have evidenced impaired maintenance of mitochondria, with network fragmentation (Grünewald A. 2012), mitochondrial DNA alterations, reduced membrane potential and ATP production (Nunnari and Suomalainen 2012). Maybe these dysfunction are linked to the increased cytosolic heavy metal status of the cell.

Post-mortem studies have not been described yet, but, with brain imaging technique it is possible to observe generalized atrophy, with

putaminal and caudate nuclei iron deposition (Schneider and Bhatia 2013) .

4. NBIA disorders caused by defects in DNA damage response

Woodhouse-Sakati Syndrome

The Woodhouse-Sakati syndrome, first described in 1983, is a recessive disease which does not necessary involve iron accumulation in the brain but that has nevertheless been welcomed in the NBIA group. This is because it involves lipid metabolism, another main pathway whose dysfunctions have been recognized shared by most NBIA pathologies (Alazami A.M. 2008).

Patients suffering from this condition present mutations in *DCAF17* (DDB1 and CUL4 Associated Factor 17). *DCAF17* encodes a nucleolus transmembrane protein of unknown function, which actively associates with CUL4 and DDB1 (Cullin 4 ubiquitin ligase complex/damaged DNA binding protein 1) (Jin J. 2006). This association links DCAF17 to DNA damage and cell cycle control.

Patients affected by the Woodhouse-Sakati syndrome suffer from a multisystemic disorder characterized by hypogonadism, alopecia, diabetes mellitus, mental retardation, deafness and electrocardiographic abnormalities (Alazami A.M. 2008).

5. NBIA disorders caused by defective lipid metabolism

The remaining five disease genes have a direct or an indirect role in fatty acid metabolism, and the reason for iron accumulation is less clear. Here I will summarize each of these five different diseases and the potential implication of lipid metabolism in NBIA, pointing the attention on Coenzyme A, that play an important role in two NBIA syndromes.

5.1.1 **NBIA caused by defective coenzyme A biosynthesis**

Coenzyme A

Coenzyme A (CoA) is an essential cofactor of enzymatic reactions. CoA is utilized in about 100 biosynthetic and degrading reactions, where it acts as a high-energy carrier of acetyl and acyl groups, including tricarboxylic acid cycle and fatty acid metabolism.

The CoA biosynthetic pathway is higly conserveted and it involves five universal enzymatic steps, which use pantothenate (vitamin B5), ATP, and cysteine. [Figure 2].It is initiated by pantothenate kinase (PANK), which converts pantothenic acid into 4'-phosphopantothenic acid. The 4'-phosphopantothenoylcysteine synthase (PPCS) and phosphopantothenoylcysteine decarboxylase catalyze the formation of 4-phosphopantothenoylcysteine and 4'-phosphopantetheine (4'PP), respectively. The last two steps of CoA biosynthesis are mediated by CoA synthase (COASY), which possesses 4'PP adenylyltransferase (PPAT) and dephospho-CoA kinase (DPCK) activities to couple

phosphopantetheine with ATP and subsequently phosphorylate the 3'-hydroxyl group to generate CoA. (Aghajanian and Worral 2002).

In mammals, the first step, catalysed by PANK, is the rate limiting one, whereas the last two steps are catalysed by COASY, a mitochondrial bifunctional enzyme having a PPAT (4-phosphopantetheine-adenylyl transferase) and a DPCK (dephospho-CoA kinase) activities. In other organisms, such as bacteria and yeast, PPAT and DPCK activities reside in two different enzymes: Cab4 and Cab5 in yeast, CoAD and CoAE in bacteria.

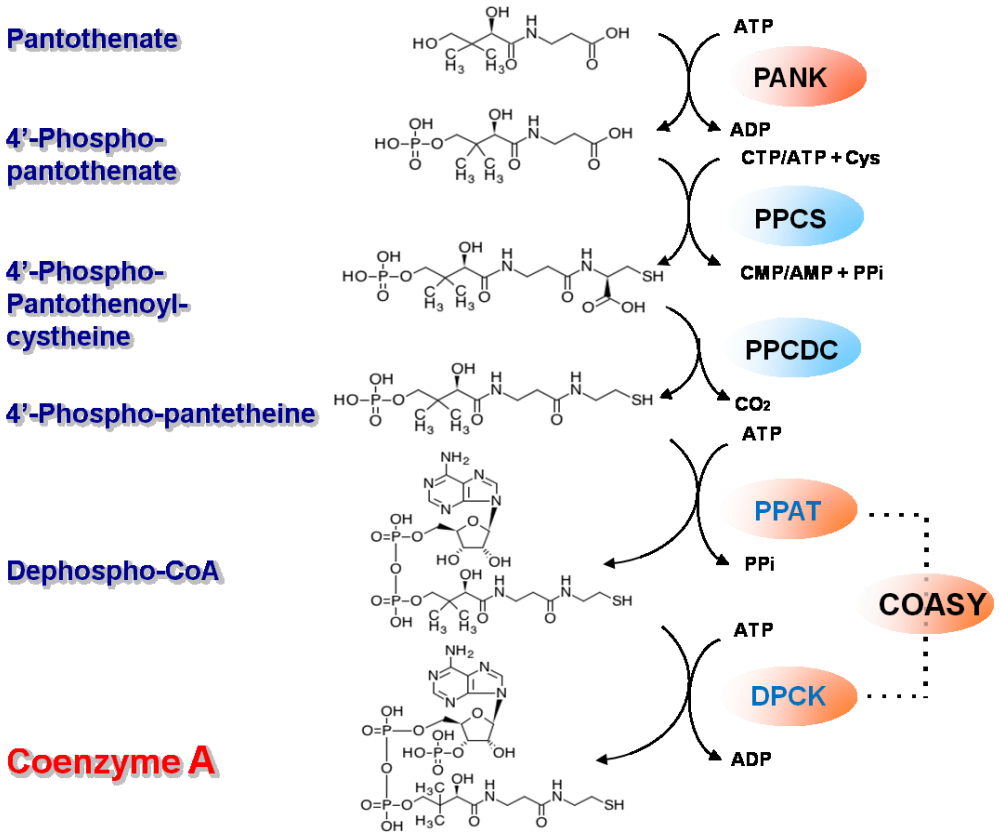

Figure 2. **Coenzyme A biosynthetic pathway in human**

CoA consists of 3'-phosphoadenosine linked through the 5' position of the ribose, to pantothenic acid via pyrophosphate linkage. The carboxyl end of pantothenic acid is then attached to β-mercaptoethylamine with an amide linkage. The active form of CoA, acetyl-CoA, derives from a thioester composed of the –SH group of the mercaptoethylamine moiety and acetate. The thiol group at the end is essential to the chemical reactions where CoA is involved in, for this reason the enzymes involved in CoA biosynthesis are highly specific in incorporating cysteine, but not other amino acids (Strauss and Begley 2005).

Tissue levels can vary widely depending on the organ in question, diet and fed/fasting state. The ratio of free CoA to acyl-CoA is important for regulating many key metabolic enzymes, such as acyl-CoA synthetase, PDH (pyruvate dehydrogenase) and 2-OG (2-oxoglutarate) dehydrogenase. The level of CoA is regulated by numerous extracellular stimuli, including hormones, glucocorticoids, nutrients and cellular metabolites (Tahiliani and Beinlich 1991) and a link between the complex signaling mTOR pathway, which is implicated in numerous metabolic and signaling processes, and CoA biosynthesis has been proposed (Nemazanyy I. 2014).

CoA is primaly required in mitochondria for the citric acid cycle, in chloroplasts for fatty acid synthesis, and in peroxisomes for *β*-oxidation (Agrimi G. 2012). The compartmentalization of CoA in all eukaryotes appears to be highly regulated: cytosol and organelles maintaining separate CoA pools whose levels can modulate fluxes through CoA-dependent reactions. Mammalian cytosolic concentrations are estimated to be in the range 0.02–0.14 mM in

animal tissues, whereas mitochondrial concentrations are much higher: from 2 to over 5 mM (Leonardi R. 2005). Most studies on the regulation of CoA metabolism in mammalian cells and tissues were carried out several years ago by Fritz A. Lipmann, who received the Nobel prize in 1953 for the discovery and characterization of CoA. The research on CoA biosynthesis/regulation has recently received novel interest thanks to the identification of mutations in genes encoding CoA biosynthetic enzymes in mammals and to the discovery of a link to neurodegeneration.

This strongly reinforces the essential role of CoA biosynthetic pathway in the development and functioning of the nervous system.

5.1.2 **Pantothenate Kinase Associated Neurodegeneration (PKAN)**

The history of Pantothenate Kinase Associated Neurodegeneration (PKAN) is strictly linked to the discovery of NBIA pathologies. It dates back to 1922, when Julius Hallervorden and Hugo Spatz described what has since then been known as the Hallervorden-Spatz syndrome, which shares similarities with the group of NBIA disorders, to which it has consequently been assigned (Hallervorden and Spatz 1922). In 2001 the gene causing Hallervorden-Spatz syndrome was finally identified by linkage analysis; it turned out to be *PANK2* gene, located on chromosome 20, at position 20p12.3 and responsible of the expression of Pantothenate Kinase type 2 responsible for the first out of five steps in Coenzyme A biosynthesis (Zhou B. 2001).

After the rising of concerns regarding unethical activities of both Hallervorden and Spatz during the Second World War, a new disease nomenclature was proposed in 2002. According to this more recent NBIA designation, based on the name of the genes implied in the aetiology of the respective pathologies, Hallervorden-Spatz syndrome is better known as Pantothenate Kinase Associated Neurodegeneration (PKAN) and accounts for about 50-70% of NBIA cases. The majority of PKAN patients present combinations of dystonia, parkinsonism, dysarthria, spasticity, mental retardation and pigmentory retinopathy (Hayflick S.J. 2003). There are two distinct manifestations of this disease: classical and atypical. The first one PKAN has early onset, usually before six years of age, with a mean age of onset ranging between three and four years and a following rapid step-wise progression. Affected children show gait abnormalities, dystonia, dysarthria, rigidity with corticospinal tract involvement that ultimately leads to spasticity, hyper-reflexia and extensor-toe sign; some of them are given a diagnosis of Attention Deficit Hyperactivity Disorder (ADHD) before understanding that they are actually suffering from a PKAN syndrome. Losing of the ability to ambulate happens between 10 and 15 years after disease onset, and some of the children show developmental delay. Classic PKAN progresses at a non-uniform rate, even though the actual reasons for this characteristic are still unclear (Gregory A. 2005)

PKAN also presents an atypical form, characterized by a later onset and a slower progression if compared to classic PKAN; the average age of onset is 13-14 years of age.

Speech difficulty is often the first recognized feature in this case, frequently accompanied by psychiatric symptoms, including depression, emotional lability, impulsivity and violent outbursts.

Motor involvement is less severe than in classic PKAN patients and it progresses more slowly, with the loss of independent ambulation arising between 15 to 40 years after disease onset.

Peculiarities of the atypical disease are repetitive actions, freezing and palilalia, a speech disorder in which a word or a phrase is rapidly repeated. Freezing during ambulation is similar to the one observed in Parkinson's disease, and is often present when turning corners or when the subject experiences surface variations (Dusek and Schneider 2012). Several studies have underlined the extreme variability in PKAN patients both genotipically and phenotypically, so as to bring a wider vision of the aetiopathology of this syndrome (Gregory A 2009).

Clinically, there is a strong correlation between loss of enzymatic activity and disease onset. PKAN patients with null mutations usually present with an early-onset and rapidly progressive form of the disease.

At MRI, patients show a typical sign known as "eye of the tiger": a region of hyperintensity possibly due to tissue necrosis and oedema, surrounded by an area of hypointensity possibly originating from iron deposition, in the medial globus pallidus (McNeill A. 2011).

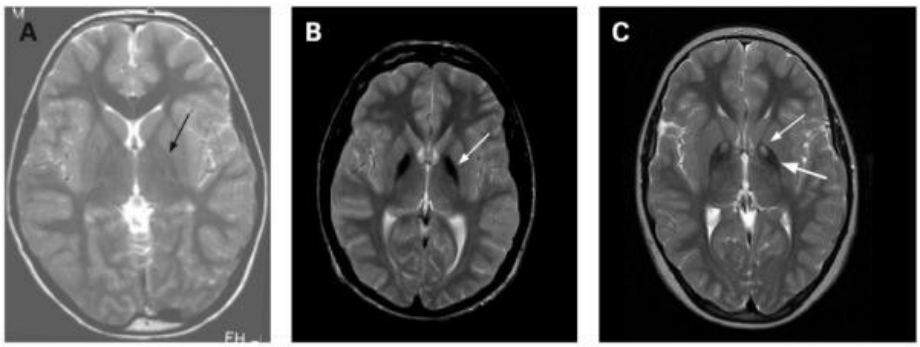

Figure 3. **T2-weighted MRI profiles.** It is shown a control (A), a NBIA patient (B) and a PKAN patient (C) with che classical 'eye of the tiger' sign. Hyperintense (white) signals indicative of tissue rarefaction are seen surrounded by areas of hypointensity (black areas) attribute to iron accumulation and visible also in B**.** (Gregory A 2009)

According to nine post-mortem cases (Kruer MC. 2011), the pathology of the disease was almost located in the CNS and particularly in the GP, where was evident a strong reduction of neurons and synapsis. In particular in the GP area, iron was increased in the cytoplasm of degenerating neurons, implying that neurons manifest iron overload before their death. Astrocytes showed marked iron overload in the GP of patients, but there was no iron accumulation in microglia and oligodendrocytes. Optic nerves and cerebellum were not affected.

As was described above, PKAN is a pathology arising from mutations in PANK2 gene, which is a seve exon gene, alternatively spliced to form two transcript variants. It codes for Pantothenate Kinase, a 48 kDa protein (Zhang Y-M. 2006), that catalyze the phosphorylation of vitamin B5 (pantothenate) in 4'-phosphopantothenate, the first committed step in CoA biosynthesis.

Mammals have four catalytically active PANK isoforms, all sharing a catalytic core identical for more than 80%. PANK4 is proposed to be non-fuctional while PANK1 and PANK3 are active in the cytosol.

PANK2 contains a residue that direct the protein to the mitochondria, where it can exert its activity (Hörtnagel K. 2003).

PANK2 tissue distribution has also been proved to be variable, with murine PANK2 reaching its highest concentration level in the testes, whereas the human isoform has primarily been found in liver and brain (Leonardi R 2007) .

Redundancy of PANK enzymes may explain why PKAN patients can survive to the first or second decade of life. Probably, the different isoforms can compensate each other to maintain adequate CoA levels.

A full comprehension of the PANK2 mechanisms and their correlation with neurodegeneration process and iron accumulation is not clear yet, even thought there are many data obtained by different approach (*in vivo* and *in vitro* studies).

Different animal models have been proposed using *Mus musculus* and *Drosophila melanogaster*.

Homozygous mice do not develop brain iron accumulation or neurological traits, but develop retinal problems and azoospermia, a condition which has also been associated to human patients (Gregory A. 2005), that could depend on the different PANK2 patterns of expression in the organism.

Moreover the difference between mice and human expression, explains why knock-out mice do not, in fact, show most PKAN neurologic features, even though homozygous mice do manifest retinal degeneration (Kuo Y.M. 2005). A subsequent study showed

that neurological symptoms occurred only when *Pank 2-/-* mice were deprived of pantothenic acid. Neurons from *Pank 2-/-* mice have an altered mitochondrial membrane potential, a defective respiration and a neurological phenotype that can be elicited in ketogenic diet (Brunetti D 2014) (Brunetti D. 2012) .

Drosophila have one PANK2 homologue, *fumbl*. The animals without this gene manifested locomotor defects, neurodegeneration and interestingly, for the mechanism of the disease, lipid dyshomeostatis and low CoA levels. Of extreme relevance, panthetine addiction to the diet of the mutant flies determined the correction of the effects described. (Bosveld F. 2008) (Wu Z. 2009) .

As concern biochemical in vitro studies, PKAN patients have increased serum levels of lactic acid and pantothenate, and defects in lipid metabolism, mainly reduced lipid and cholesterol biosynthesis (Leoni V. 2012). Altogether these results are not able to indicate the exact pathophysiology of PKAN, and the reason why iron accumulated in the brain, but some hypothesis can be done. According to the Johnson and colleagues (Johnson M. 2004), in healthy brains phosphopantothenate condenses with cysteine, while in PKAN patients phosphopantothenate is deficient, because of loss of phosphorylation activity by PANK2, and mitochondrial cysteine is thus accumulated. Cysteine successfully binds iron and subsequently undergoes auto-oxidation, resulting in free radical production. But after the discovery of forms of NBIA with iron deposits but without increased cysteine levels, other theories based on the association between iron and lipid were proposed. Alterations in phospholipids metabolism due to CoA-deficiency may injure the membranes, with

consequent oxidative stress that leads to iron accumulation (Leonardi R. 2005). The importance of CoA biosynthesis is confirmed also by the recent identification of mutations in COASY in other NBIA patients. CoA is central to metabolism, and is also required for synthesis of fatty acids and amino acids. It is interesting to notice that PANK2 and COASY share not only the same pathway but also the same localization, the mitochondria. Mitochondria are the main sites of iron utilisation in the cell. (Levi and Rovida 2009). This organelle employs iron for the biosynthesis of the iron sulphur cluster and heme cofactors, which are prostetic groups of many proteins involved in key biological processes (Stehling O. 2014).

In view of these reported results, PKAN could ultimately be explained with a not sufficient Pantothenate Kinase activity in the brain, particularly involving PANK2 isoform, the most present in human brain; these defects could also lead to increased oxidative stress. This last hypothesis is supported by the observation that PKAN primarily involves the globus pallidus and the retina, which have both high metabolic demands and cellular environments susceptible to oxidative stress. In summary there is an interaction between lipid metabolism, iron metabolism and mitochondrial functions in cellular and animal models of PKAN patient, but more studies are required to understand the reasons for specific cell death.

5.1.3 **Coenzyme A Synthase Protein Associated Neurodegeneration (COPAN)**

Recently, a novel subtype of NBIA, denominated CoPAN (CoA Synthase Protein Associated Neurodegeneration) (MIM #609855), has been associated with mutations in Coenzyme A synthase (*COASY)* gene (Dusi S. 2014). *COASY* gene codes for a bi-functional mitochondrial enzyme converting 4-phosphopantetheine into dephospho-CoA and then to coenzyme A. COASY is composed by two domains: the first one has a phosphoadenyl transferase (PPAT) activity, while the second one has a dephospho-CoA kinase (DPCK) activity (Aghajanian and Worral 2002). There are two COASY isoforms, α and β produced from alternate splicing. The longer β isoform is brain specific and has an additional prolice-rich protein interaction domain but has identical enzymatic activity, to the ubiquitous α isofomorm (Nemazanyy I 2006). Reported clinical signs were: gait abnormalities, dystonia, dysarthria, spastic paraparesis, cognitive impairment, behavioural disturbances and motor axonal neuropathy. Iron accumulation was evident at MRI. The two mutation identified in NBIA patients, affects a highly conserved aminoacid residue in the catalytic site of the DPCK domain, a region extremely conserved from yeast to human. Fibroblast from the patients showed decreased levels of the mutant protein and reduced amount of acetyl-CoA. Mutant dephospho-CoA kinase domain do not have his enzymatic activity *in vitro*, whereas CoA levels in patients and controls appear normal. This finding suggests that CoA biosynthesis might be abolished in the presence of mutation, but that there is an alternative pathway for CoA synthesis that has to be found.

The recent role of COASY in NBIA, strongly reinforces the essential role of CoA in the development and functioning of the nervous system (Dusi S. 2014) . This has been previously suggested by other studies showing a reduction of CoA levels in dPank-deficient Drosophila fumble mutants (Rana A. 2010) and in mice lacking both *PANK1* and *PANK2* genes (Garcia M. 2012). Moreover, the demonstration of COASY interaction with components of the PI3K/mTOR/S6K signaling cascade poses an interesting link between CoA biosynthesis and the regulation of cellular metabolism (Breus O. 2004) (Nemazanyy I. 2014)

5.2 NBIA caused by defective fatty acid metabolism

5.2.1 Phospholipase A2, group VI-associated neurodegeneration (PLAN)

The first disease to be recognized as a distinctive non-PKAN type of NBIA disease was PLAN, a heterogeneous group of neurodegenerative conditions caused by mutation in PLA2G6.

Mutations involving PLA2G6 gene (also known as iPLA2β) encoding phospholipase A2 group VI calcium-indipendent have been found as having a primary role in two different pathologies: infantile neuroaxonal dystrophy (NAD), and atypical neuroaxonal dystrophy.

In infantile neuroaxonal dystrophy (NAD), a pediatric form of NBIA, symptoms occurs before 2 years of age and the most frequent feature is psychomotor regression, accompanied by hypotonia and tetraparesis. Often ataxia or gait instability also occur, together with optic atrophy, nystagmus and strabismus (Morgan N.V. 2006).Other clinical signs include decrease in nerve conduction velocity,

denervation evidence on EMG and fast rhythms on EEG. As seen with PKAN classification, INAD has an atypical form as well. This has different and heterogeneous characteristics, with patients experiencing later onset disease and a slower progression, variable ataxia, spasticity and neurobehavioral abnormalities. (Schneider and Bhatia 2013). Contrary to PKAN, iron accumulation is not a universal feature of PLAN. Half of INAD patients show abnormally high iron levels especially in the globus pallidus, without the "eye of the tiger" sign (Kurian and Hayflick 2013).

Neuropathologically, these patients have been reported presenting axonal spheroids throughout the nervous system, with predominant accumulation at axonal endings (Kimura K. 1991). Other observed features include neurofibrillary tangles, historically related to Alzheimer's disease, α-synuclein-positive Lewy bodies and dystrophic neuritis, characteristics that may suggest a possible common pathogenic pathway shared by NBIA and other neurodegenerative disorders, such as Parkinson's disease or Alzheimer's disease. (Morgan N.V. 2006).

PLA2G6, locus 22q13.1, encodes for a mitochondrial Calcium independent group VI phospsholipase A_2 , which is responsible for 70% of total PLA2 activity in the brain. (Liou J.Y., 2005). It is obiquitously expressed (Song H. 2010),with at least five splice variant. The mature protein catalyzes the hydrolysis of glycerophospholipids at the *sn*-2 position, giving rise to lysophospholipids and free fatty acid, which on its side promotes phospholipid remodelling, arachidonic acid release, leukotriene and prostaglandin synthesis and apoptosis (Morgan N.V. 2006). PLA2G6

role in neurodegeneration may occur via the inability to remodel oxidized and damage phospholipids in neuronal cells and subcellular membranes. As concern membranes, polyunsatured inner-membrane mitochondrial components, such as cardiolipin, are extremely sensitive to ROS, suggesting the potential involvement of mitochondria in the pathogenesis of this disease. This hypothesis is also proved by two other evidences. First, the protective role of PLA2G6 against staurosporine-induced apoptosis (Seleznev K. 2006). Second mice lacking *Pla2g6* exhibit degenerating mitochondria throughout the nervous system (Beck G. 2011). Protein dysfunction may altered lipid composition of plasma membrane, vesicles, and endosomes, subsequently resulting in abnormal regulation of membrane trafficking.

Finally, there is evidence for a non-cell autonomous effect of PLA2G6 disruption. Docosahexaenoic acid (DHA) is an essential fatty acid that cannot be synthesised in neurons. Astrocytes produce and release it thank to PLA2G6 action (Green J.T. 2008). Knockdown of the enzyme in astrocytes leads to a reduction of arachidonic acid and DHA in neurons and increased prostaglandin production, which could lead to increased apoptosis.

In conclusion mitochondrial involvement, lipid turnover and Tau pathology are implicated in this NBIA subtype, and, in contrast to PKAN, it may be that metal has not a relevant role in PLAN pathogenesis.

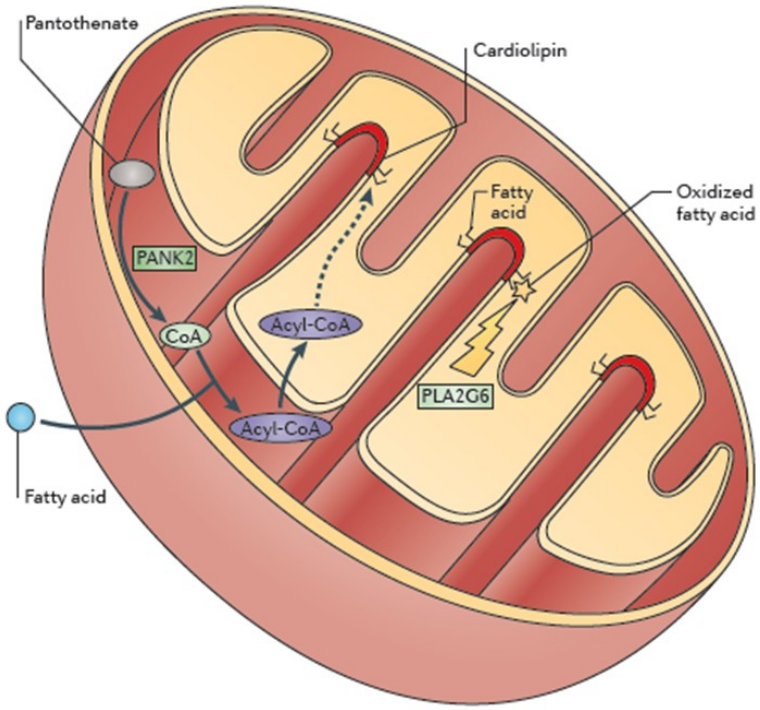

Figure 4. **PANK2 and PLA2G6 in mitochondria.** Mutations in *PANK2* and in *PLA2G6* may interfere with synthesis and remodelling of cardiolipin. PANK2 is needed for the formation of CoA from pantothenate. CoA condenses with fatty acids to form acyl-CoA, which crosses into the mitochondrial matrix using the carnitine carrier system. Acyl-CoA in the mitochondrial matrix either delivers fatty acids for incorporation into complex intra-mitochondrial lipids, such as cardiolipin, or may alternatively undergo oxidation by the mitochondrial respiratory chain to generate ATP. The matrix membrane contains cardiolipin that enables the inner membrane to bend and turn. PLA2G6 may remove damaged fatty acids to allow incorporation of flexible unsaturated fatty acids, such as linoleic acid, from the acyl-CoA pool in the matrix. (Rouault T.A. 2013).

5.2.2 **Mitochondrial Membrane Protein-Associated Neurodegeneration (MPAN)**

Mitochondrial Membrane Protein Associated Neurodegeneration, a recessive NBIA disorder, takes its name from the localization of the protein encoded by the orphan gene C19orf12.

In 2011 mutations in chromosome 19 open reading frame 12 were found in approximately 80% of Polish NBIA patients without any *PANK2* mutation by Hartig and colleagues (Hartig M.B. 2011); other mutations were recognized and later analyzed in 2012 by Schulte and colleagues. And now is estimated that MPAN accounts for around 30% of NBIA cases (Hogarth P. 2013). C19orf12 is higly conserved in evolution. In humans, chimps and chickens it encodes for two protein isoforms originating from two alternative first exons, each with two predicted transmembrane domains. The wild-type gene product localizes to mitochondria, but also in the endoplasmic reticulum (ER) and MAM (Mitochondria Associated Membrane) (Venco P. 2015).

Despite its mitochondrial localization, MPAN-associated mutations do not affect the mitochondrial bioenergetics in fibroblasts under basal conditions (Hartig M.B. 2011).

Although the function of the protein is still unknown, the peptide is known as ubiquitously present, with high expression levels in brain, blood cells, adipose tissue where it is upregulated during adipocyte differentiation. The average age of onset is 9 years and the rate of progression is relatively slow (Dezfouli M. 2013). Clinical symptoms are dysarthria, gait difficulties, dystonia, parkinsonism, psychiatric symptoms and spastic paraparesis, and in this sense the pathology is

similar to PKAN. Neuropathologically, the patients show iron-containing deposits in the globus pallidus and substantia nigra, with the hippocampus presenting a small number of α-synuclein-containing spots and numerous tau-positive pyramidal cells.

Loss of myelin in the pyramidal tracts of the spinal cord and optic nerve is also present, especially in the optic tract, as observed by Hartig and colleagues (Hartig M.B. 2011).

MPAN has been successfully modelled in *Drosophila*, that exhibit neurological defects despite absence of iron accumulation (Iuso A. 2014).

5.2.3 **Fatty Acid Hydroxylase-associated Neurodegeneration (FAHN)**

Mutations in FA2H (Fatty Acid 2-Hydroxylase) gene, located on chromosome 16 at position 16q23, is responsible of Fatty Acid Hydroxylase-associated Neurodegeneration (FAHN) (Kruer M.C. 2010).

FA2H codes for a 43kDa-NADPH-dependent mono-oxygenase residing in ER membranes. The protein has a C-terminal sterol desaturase domain, which contains an iron binding histidine motif and is responsible for catalytic activity, and an N-terminal cytochrome b5 haem-binding domain, involved in redox activity and electron donation (Alderson N.L. 2004) (Hama H. 2010). FA2H produces the 2-hydroxylated fatty acids that are incorporated into sphingolipids (Dan P. 2011). 2-hydroxylated fatty acids are precursors for the synthesis of ceramide, a critical component of myelin sheaths (Eckhardt M. 2005) .

FAHN is clinically characterized by spasticity, movement disorder, ataxia, dystonia, optic atrophy and oculomotor abnormalities, which later progress to intellectual impairments and seizures (Rouault T.A. 2013).

Brain MRI highlights profound white-matter changes, cerebellar atrophy and thin corpus callosum (Kruer M.C. 2010) ; iron accumulation is mainly detected in the globus pallidus, substantia nigra and subcortical and periventricular regions.

Three main pathogenetic mechanism can be hypothesized: first FA2H has a critical role in the maintenance of myelin, and its dysfunction can lead to myelin instability; second 2-hydroxylation could also have an effect to the size and number of membrane domains, which in turn can influence signalling between myelinating cells and neurons; third sphingolips may function ad signalling molecules that regulate neuronal and glia cells. Mice models confirmed the first hypothesis, because demyelination and profound axonal loss in diverse brain areas where found. (Hama H. 2010). But the second and the third pathogenic hypothesis are now gaining strength. (Potter K.A. 2011). Finally, as concern the link between iron accumulation and sphingolipid metabolism, further studies are need to understand their relationship.

NEURODEGENERATIVE DISEASES AND NBIA

After having presented the molecular and clinical complexity of NBIA, here I try to highlight emerging themes that have in common not only different NBIA syndromes, but also neurogenerative diseases. This overlap between NBIA and neurodegenerative diseases is demonstrated by neuropathological evidence, clinical manifestation and molecular dysfunctions and it maybe will bring to new discovery about mechanism causing neuronal health.

1. Iron

Iron is one of the most important elements for our body, because it is indispensable for the formation of haem and iron-sulphur clusters and it acts as a cofactor in numerous metabolic reactions.

Assumed by alimentation by duodenal enterocytes, iron travels through plasma bound to the glycoprotein transferrin, which has two high-affinity binding sites for Fe (III) and maintains iron in a soluble form and limits toxic radicals.

In humans, plasma transferrin is usually 30% saturated with iron; if this level diminishes to less than 16%, there is iron deficiency, whilst if it increases to levels higher than 45%, we talk of iron overload. Iron is primarily used by erythroid precursors in the synthesis of heme. Reticuloendothelial macrophages clear senescent erythrocytes and release the iron from heme to export it to the circulation or store it in the hepatocytes (Fleming and Ponka 2012). These cells have an important role in the production of hepcidn, an ormone that regulates the release of iron from enterocytes and macrophages by degrading

the iron exporter ferroportin. Iron uptake in cells is performed via a clathrin-dependent endocytotic process. Once in the cell, iron is ferroxidased by ferritin heteropolymers, composed of 24 subunits, which can be either light (FtL) or heavy (FtH1). Both types of chain are ubiquitously expressed, and it is only their ratio that varies according to the kind of cell considered and to the presence of stimuli like inflammation or infection.

FtH1 brings on a ferroxidase activity, which is necessary for the internal deposition of iron, while FtL makes iron nucleation easier and increases the turnover of the protein's catalytic site. Ferritin's action gives the cells a chance to lock up the excess of iron in a redox-inactive form, so as to prevent iron-mediated cell and tissue damage. (Harrison and Arosio 1996)

Iron homeostasis inside the cell is furthermore regulated at the post-transcriptional level by Iron Regulatory Protein 1(IRP1) and Iron Regulatory Protein 2 (IRP2); both these proteins can inhibit translation initiation if bound to the respective hairpin structures on ferritin H(Heavy)- or L(Light)- chain, ferroportin, ALAS2 (AminoLevulinic Acid Synthase), mitochondrial aconitase (ACO2) or hypoxia-inducible factor 2α mRNAs. (Gali B. 2008)

Genetic ablation experiments have shown that the expression of both IRPs is essential, even though their activities are seemingly redundant. Phosphorilation of these proteins could also regulate their function, even though the exact mechanisms by which this regulation can possibly affect first iron metabolism and ultimately cell metabolism is still under study. (Hentze M.W. 2010)

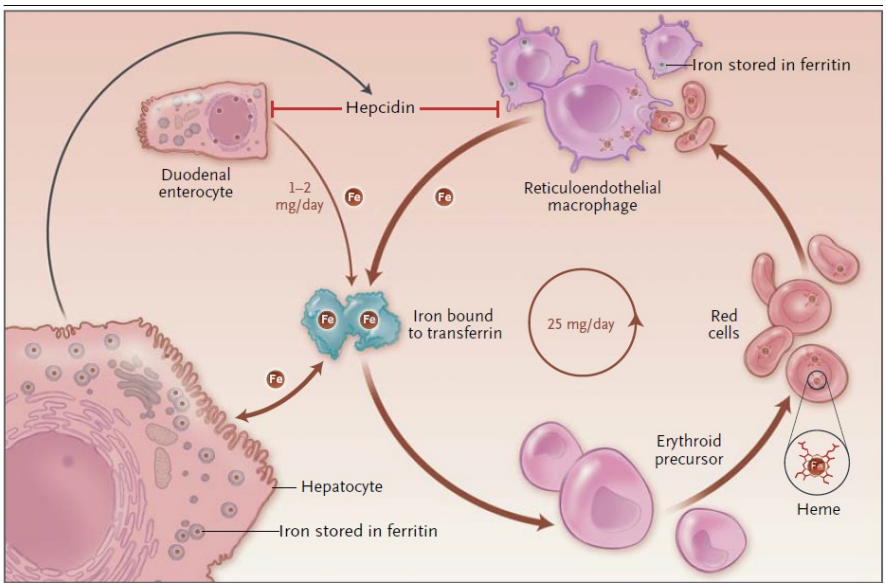

Figure 5. **Iron cycle** (Fleming and Ponka 2012) .

Iron-overload disorders are a spectrum of different progressive and sometimes irreversible diseases caused by defects in hepcidin-ferroportin axis, erythroid maturation, iron transport and less common disorder like NBIA, where iron is a specific hallmark of the pathology, but also present in the plethora of symptoms od Alzheimer, Parkinson's and Huntington disease. (Fleming and Ponka 2012). Interestingly, iron accumulation is not always correlated to a disease, in fact it's a phenomenon, which happens in the brain during ageing in neurologically healthy people, in areas primarily associated with motor activity that are already iron-rich. (Hallgreen B. 1958). In NBIA disease iron accumulates in defined areas of the brain, basal ganglia, but sometimes also in cerebellum. Iron has been evidenced as a potential damaging element for tissues either directly or because it changes the cellular environment, making it more prone to toxins, by catalyzing the production of reactive oxygen species. In absence of a

model (in vivo or in vitro) that clearly recapitulate the iron accumulation, some researchers have proposed the idea that it may be just an epiphenomenon, and not a primary cause of NBIA diseases. This hypothesis is confirmed by the fact that iron chelation therapy was able to reduce iron in the brain, but not all the symptoms (Cossu G. 2014) (Zorzi G. 2012); moreover defects in one single gene, like PLA2G6 lead to variable iron accumulation. So iron deposition may be just a consequence of axonal disruption. In that case, iron dyshomeostatis could be explained by mitochondria and by their role as iron sink or by their importance in mitophagy. Altered mitochondria could alter iron. Questa frase non è tanto Chiara, cosa volevi dire?

2. Fatty acid and phospholipid metabolism

Metabolic dysfunction, specifically lipid dysfunctions, are often associated with neurological diseases (Esposito G. 2008) (Evans SJ 2012) (Jadoon A. 2012) also due to the peculiar lipid composition of neurons, that guarantees the correct functioning of the nervous system. Moreover, in the last few years, the identification of NBIA disease genes, implicated in lipid metabolism, pointed out on a possible link between phospholipids and neurodegeneration. Lipid impairment could bring neurological dysfunction by determining anomalies in cellular membranes, modification in cellular signalling involved in inflammation, neuronal excitability and myelin maintenance. (Brunetti D. 2012). Second, the fact that the majority of NBIA-related genes implicate mitochondria, or ER entails a fundamental role of these organelles for the correct functioning of neuronal cells. Mitochondrial

membrane abnormalities, for example involving cardiolipin, an important component of the mitochondrial inner membrane, could cause the respiratory deficiency and ROS production seen in many NBIA subtypes. (Beck G. 2011).

3. Mitochondrial dysfunction

Mitochondria have been widely recognized as the election site for cell's energetic. (Benard G. 2007). But their role is not confined only to bioenergetics: in fact, they play a fundamental action in other processes, such as intracellular Ca^{2+} homeostasis, ROS formation, apoptosis and iron cellular handling. (Detmer and Chan 2007) Mitochondria produce more than 90% of our cellular energy (ATP) by oxidative phosphorilation (OXPHOS), which occurs at the level of mitochondrial respiratory chain (MRC). So their main function is clearly energy production, which plays a decisive role in life/death of the cells. In particular, neuronal function and survival depend on a continuous supply of glucose and oxygen, used to generate ATP through glycolysis and mitochondria respiration. A perturbation in energy metabolism, can lead to irreversible neuronal injury.

Faulty mitochondria have been thought to contribute to several ageing-related neurodegenerative diseases, such as PD, AD and ALS.

The exact role of mitochondria in the pathogenesis of NBIA is not clearly understood, but there are several observations that support this link. Many disease-genes code for mitochondrial protein and in different NBIA subtypes it is reported mitochondrial dysfunction, which occurs as respiratory deficiency, oxidative damage, and morphological defects.

4. Misfolded proteins

Many neurodegenerative diseases are caused by accumulation of specific protein aggregates in the brain with a regional pattern specific to each disease. AD is characterized by extracellular deposition of amyloid-β (Aβ) protein in the form of senile plaques and by intraneuronal accumulation of hyperphosphorylated tau as neurofibrillary tangles (Hardy J. 2006) (Selkoe DJ. 2004). In PD, the synaptic protein α-synuclein accumulates in neuronal cell bodies and axons; these aggregates are referred to as Lewy bodies and Lewy neuritis, respectively (Goedert M. 2001). In Huntington's disease (HD) and other diseases with the expansion of triplet repeats, proteins with expanded polyglutamine (polyQ) accumulate in the nucleus and cytoplasm (Ross and Poirier 2004). Accumulation of misfolded prion proteins also occurs in Creutzfeldt–Jakob disease (CJD) (Prusiner SB. 2001). The proteins that accumulate in neurodegenerative diseases are typically misfolded and yield a β-sheet structure that promotes aggregation and fibril formation (Soto C. 2003). In the paragraphs above we make a list of the unfolded proteins present in NBIA, like Tau pathology, Lewy bodies and Lewy neuritis, which can be responsible of cell death in NBIA.

Genetic factors but also environmental factors, such as oxidative or metabolic stress, can increase the production of misfolded proteins.

In eukaryotic cells there are two main pathways responsible for protein and organelle clearance: the ubiquitin-proteasome system (UPS) and the autophagy-lysosome system.

Proteasome are barrel-shaped multiprotein complexes that predominantly degrade short-lived nuclear and cytosolic proteins after their C-terminal ubiquitination.

Autophagy, literally “self-eating”, describes a catabolic process in which cell constituents such as organelles and proteins are delivered to the lysosomal compartment for degradation.

Increasing evidences suggest that impairment in UPS and autophagy is a common feature in several brain diseases (McNaught and Jenner 2001). These dysfunctions may be caused directly by mutations in genes that encode proteins involved these pathways; or by the abnormal protein accumulation may further overwhelm degradative systems and, as a result, even more proteins start accumulating within the cells (Bence NF 2001) .

If unfolded proteins cannot be refolded and targeted for degradation, they may be sequestered into a specific cellular site to generate an intracellular inclusion body, as an aggresome (Johnston J.A. 1998). Axonal swellings, that are the pathological hallmark of PLAN, contain mitochondrial components, ubiquitinated proteins and cytoskeletal alterations that finally could lead to axonal transport defects.

According to current knowledge, the formation of this aggresome would have a protective function, reducing the random accumulation of potential toxic protein oligomers and aggregates and preventing abnormal interactions of these aberrant species with other proteins or cell organelles (Chen B. 2011)

5. Calcium homeostasis

Calcium, as Ca^{2+} cation, is an essential intracellular signal, important in many cellular functions and processes, including muscle contraction, neuronal transmission as in an excitatory synapse, cellular motility, fertilisation, cell growth or proliferation, learning, memory (as with synaptic plasticity). For neuronal transmission, neurons use Ca^{2+} as intracellular messenger that mediates the physiological response of neurons to chemical and electrical stimulation. In all eukaryotic cells, the cytosolic concentration of Ca2+ ([Ca2+]c) is tightly controlled by complex interactions among pumps, channels, exchangers and binding proteins, and relatively small and/or local changes in its concentration modulate a wide range of intracellular actions. Under resting conditions, free cytosolic Ca^{2+} levels in neurons are maintained around 200 nM, but their concentration can rise to low micromolar values upon electrical or receptor–mediated stimulation. Ca^{2+} in resting condition is maintained around the value of 100nM, significantly lower than extracellular (1mM). This condition is guaranteed by the low permeability of the plasma membrane to ions and by by powerful calcium-binding and calcium-buffering proteins (e.g. calbindin or parvalbumin) and partly by an active uptake into internal stores by the Sarco/ER calcium-ATPase (SERCA) at the ER membrane or by the mitochondrial uniporter (Berridge MJ. 2003). This fine regulation of Ca^{2+} allows this ion to act as one of the most important second messenger in signal transduction pathways. The increase of intracellular Ca^{2+} can be elicited through two fundamental mechanisms: 1) the Ca^{2+} mobilization from intracellular stores, mainly the endoplasmic reticulum (ER) and Golgi apparatus, or 2) the entry

from the extracellular space, where the concentrations are several magnitudes higher compared to cytosolic calcium levels (Berridge MJ. 2003). Calcium can be released into the cytosol from ER via activation of inositol 1,4,5-triphosphate receptors (InsP3Rs) or ryanodine receptors (RyRs). The main route inducing Ca^{2+} release from intracellular stores involves the IP3 Receptor (IP3R), a transmembrane protein located on the ER and Golgi membrane, which exposes on the cytosolic face the IP3 binding site, while it forms a Ca^{2+} channel in the transmembrane domain. Usually, this finely tuned control of Ca^{2+} fluxes and Ca^{2+} load is compromised in normal aging and even more in pathological states. The major factor responsible for impairment of neuronal Ca^{2+} homeostasis is oxidative stress. This situation makes neurons vulnerable to a form of Ca^{2+}-mediated death, called excitotoxicity, in which glutamate receptors are over activated leading to rise of intracellular Ca^{2+} concentrations beyond tolerable levels (Arundine and Tymianski 2003). Mitochondria play an important role in the regulation of Ca^{2+} levels. It has been demonstrated that both genetic manipulations and pharmacological treatments, enhancing mitochondrial Ca^{2+} sequestration, can protect neurons against excitotoxicity (Duchen MR. 2000).

Alterations of Ca^{2+} homeostasis are observed in several neurodegenerative diseases including PD, AD, ALS and HD. Rare examples support a direct role of Ca^{2+} homeostasis deregulation as the first hit towards neurodegeneration, however there are evidences that highlights the presence and the importance of calcium deregulation in progression of several neurodegenerative process (Wojda U. 2008). As concern NBIA, calcium signaling was shown to be defective in

astrocytes from PLA2G6 mutant mice (Strokin M. 2007) and in MPAN patients (Venco P. 2015).

6. Autophagy

The term autophagy literally means “self-eating’’ and it is used to describe lysosomal-mediated degradation of intracellular contents, which can be divided into three basic mechanisms: 1) chaperone-mediated autophagy, 2) microautophagy, and 3) macroautophagy. Macroautophagy, hereafter referred to as autophagy, is a major pathway for bulk degradation of cytoplasmic constituents and organelles. In this process, parts of the cytoplasm and intracellular organelles are sequestered within characteristic double- or multi-membrane autophagic vacuoles (named autophagosomes) and are finally delivered to lysosomes for bulk degradation and recycling. (Lamb CA. 2013)It is a highly regulated process that can either be involved in the turnover of long-lived proteins or can specifically target distinct organelles (for example, mitochondria in mitophagy and the endoplasmic reticulum (ER) in reticulophagy), thereby eliminating supernumerary or damaged organelles. (Hamasaki M. 2013) .Thus autophagy is a constitutive cellular event, through which superfluous, damaged or aged cells or organelles are eliminated. Beyond this homeostatic function, autophagy is also a process by which cells adapt their metabolism to starvation, hormonal stimulation and drug treatments. It plays an important role in cellular quality control in neurons because the denatured or aggregated proteins and the dysfunctional organelles are not reduced by dilution during cell division in neurons. So, impaired autophagic processes in neurons

lead to improper homeostasis and neurodegeneration. Specifically the impairment is due to an unbalance between autophagosome formation and autophagic degradation. The accumulation of autophagosomes in neurons is associated with neurodegenerative diseases, such as Alzheimer's disease, Parkinson's disease, and Huntington's disease. (Jiang and Mizushima 2014)

Excessive autophagy can lead to excessive degradation of cytosolic components and neuronal cell death.

As concerning NBIA, autophagy has a clear role in Kufor-Rakeb Syndrome and in SENDA caused by mutations in WDR45, but autophagic defects have been reported also in MPAN. (Venco P. 2015).

The supposed link between autophagy and NBIA (in genes that are not strictly correlated with this process), is lipid metabolism for the autophagolysosome formation and mitochondria for the involvement in the bulking of autophagic vesicles.

7. Oxidative stress

Oxidative stress results from exposure to high levels of reactive oxygen species (ROS), which are not detoxified by cellular antioxidizing agents (Fleury C. 2002). ROS are generally small, short-lived and highly reactive molecules, formed by incomplete one-electron reduction of oxygen. ROS include both free radicals, such as superoxide ($O_2^{\cdot -}$), nitric oxide ($NO^{\cdot}$) and hydroxyl ($OH^{\cdot}$) radicals and other molecular species, such as hydrogen peroxide (H_2O_2) and peroxynitrite ($ONOO^-$). These species are produced by ionizing radiation of biological molecules, as a byproduct of respiration in

mitochondria or are synthesized by specific enzymes of the NADPH oxidase (NOX) and dual oxidase (DUOX) family. NOX and DUOX oxidize NADPH and reduce oxygen across the plasma membrane to generate superoxide, which can then form (H_2O_2), which crosses the membrane and enters the cell (Suh YA. 1999).

ROS can interact with different substrates in the cell, such as proteins, lipids and DNA. Oxidation of proteins may involve structural alterations or destroy the active sites of enzymes. Other examples of protein modifications caused by ROS are nitration, carbonylation, and protein-protein cross linking, generally leading to protein loss of function and accumulation into cytoplasmic inclusions with alterations of degradation systems (Dalle-Donne I. 2005).

Oxidative modification of unsaturated fatty acids can result in lipid peroxides, which in some cases disrupt both the plasma membrane and membranes of subcellular organelles, such as mitochondria.

Oxidation of DNA may lead to mutations. In fact, it is known that the frequency of mtDNA mutations is higher that nDNA, because it is exposed to the action of ROS produced by oxidative phosphorylation (OXPHOS), the metabolic pathway in which the mitochondria produce energy in the form of ATP. Various defense mechanisms have been developed to protect cells against oxidative stress, such as up-regulation of antioxidants, removal of specific proteins by the ubiquitin–proteasome system (Grune T. 2003) and removal of damaged proteins and organelles by autophagy. Antioxidant enzymes include superoxide dismutase (SOD), glutathione peroxidase, and catalase. In addition there are non enzymatic antioxidant compounds, such as glutathione (GSH) and vitamin E. GSH is the most abundant

small non protein molecule in cells and it is the main antioxidant in CNS. Reduced GSH can interact directly with free radicals for their removal. Vitamin E appears to neutralize the effect of peroxide and to prevent lipid peroxidation in membranes. I will talk about autophagy in next paragraph, but now it is important to mark its role in response to ROS. This is highlighted by the accumulation of oxidized proteins in aged cells under normal growth conditions (Donati A. 2001), where autophagic pathways are compromised with age (Kiffin R. 2006) and in age-related disorders, such as Alzheimer's disease (Cataldo AM. 1996) and diabetes mellitus (Sooparb S. 2004), where there is also a decrease in autophagy. The brain is considered to be particularly susceptible to ROS damaging. In fact, even if it represents only ~2% of the total body weight, the brain accounts over than 20% of the total consumption of oxygen (Halliwell B. 2006). Therefore, oxidative stress can be important in aetiology of various neurodegenerative diseases. In fact postmortem brain tissues from patients with different neurodegenerative diseases demonstrated increased ROS in affected brain regions. A clear example from genetics is the presence of *SOD1* mutations in 20% of familial cases of ALS. Looking at NBIA, the overall data indicate oxidative stress, driven by heavy metal accumulation, as the primary pathogenesis for aceruloplasminemia and neuroferritinopaty (Kono e Miyajima 2006). The PKAN patients' fibroblasts showed altered oxidative status, reduced antioxidant defense, and impaired cytosolic and mitochondrial aconitase activities compared to control cells. (Campanella A. 2012). Thus, studies should be invested now in development of drugs that block the cascade of

oxidative events, following the results carried on Parkinson's disease (Devos D. 2014).

8. Axonal transport

Axonal transport is a cellular process essential in neurons because of their size and their role in the reception and transmission of nerve impulses to and from the CNS. Impairment of axonal transport has recently emerged as a common factor in several neurodegenerative disorders even thought the causal relationship between axonal transport defects and degeneration remains unclear. (Hirokawa N. 2010)

Typically, neurons are composted of a cell body, multiple dendrites and a single axon. Dendrites and cell bodies play a role in collection and processing of information, and the axon is responsible for the transmission of information to other neurons via synapses. Axonal transport is responsible for movement of proteins, lipids, mitochondria and for the clearance of misfolded proteins and it occurs along the cellular cytoskeleton. There are three major components of the neuronal cytoskeleton: microtubules, actin and intermediate filaments. Microtubules are formed from the dynamic polymerization of αβ-tubulin dimers. Microtubules polymerize outward from the centrosome, then undergo a stochastic transition, resulting in a very rapid depolymerization. This dynamic behavior is required for the normal outgrowth of axons and growth cones, specialized ends of growing axons (or dendrites) that generate the motive force for elongation.

Also the cytoskeletal actin provides both dynamics and stability to this structure. Actin monomers assemble into a flexible helical polymer with two distinct ends: one fast growing extremity and one with a slower growth.

The third major component of the cellular cytoskeleton includes intermediate filaments, the most common of which are neurofilaments in mature motor neurons. Once assembled, these filaments lack overall polarity, and do not undergo the dramatic remodeling characteristic of actin and microtubules. Neurofilaments primarily provide structural stabilization to the cell, and regulate the radial growth of axons. (Millecamps and Julien 2013)

It is interesting to note that aggregation of neurofilaments is a common marker of neurodegenerative disease (Liu Q. 2004).

Molecular motors, specialized enzymes that use ATP hydrolysis energy to move along the cellular cytoskeleton, are responsible for active transport in neurons. Long-distance travelling within the motor neuron is driven primarily by microtubule-based motor proteins, while actin filament-based motors drive shorter distances, or dispersive movements. Microtubules motors include members of the kinesin superfamily and cytoplasmic dynein; myosin drive transport of vesicles and organelles along actin filaments. Conventional kinesins are the major species of plus-end directed molecular motors in the brain (Wagner et al., 1989), being involved in anterograde transport (from cell body to synapses) of various membrane-bounded organelles, including mitochondria, synaptic vesicles and axolemmal precursors, among others (Leopold PL. 1992) (Elluru RG. 1995). Conventional kinesin is a heterotetramer composed of two heavy

chains (kinesin-1s, KHCs) and two light chains (KLCs) (DeBoer SR. 2008). Retrograde transport (from axonal end to cell body) is carried out by the multisubunit motor protein complex cytoplasmic dynein (CDyn) (Susalka e Pfister KK. 2000).This transport consists mainly of endosomal/lysosomal organelles that carry corrupted proteins back to the cell bodies for degradation but also neurotrophic factors required for neuronal survival.

A lot of evidence suggests that neurodegenerative diseases may be a direct consequence of axonal transport alterations. Mutations have been found in various subunits of conventional kinesin (Reid E. 2002)and CDyn (Hafezparast M. 2003) resulting in selective degeneration of specific neuronal subtypes. Moreover other mechanisms, such as abnormal activation of protein kinases and aberrant patterns of protein phosphorylation, that are not associated with mutations in molecular motors, represent major hallmarks in neurodegenerative diseases (Wagey and Krieger 1998). As concerning NBIA, PLAN and BPAN, there has been found neurofibrillary tangles that maybe have a connection with impairment in axonal transport. (Arber C. 2015)

MODELLING APPROACHES

As its said in the title, my PhD program is about the characterization of disease genes through the development of cellular models. So, it is important to dedicate some paragraphs to the novel modelling approaches used during my work, to the current state of the field and the future challenges about reprogramming.

1. Induced Pluripotent Stem Cells (iPSCs)

Ever since the first isolation of Embryonic Stem Cells (ESCs) in 1981 from mouse by two independent groups, leaded by Evans and Kaufman and by Martin, (Evans and Kaufman 1981) (Martin GR. 1981) then in 1998 from human by Thomson's group, has research tried to find a way to make a ethically acceptable use of stem cells. (Thomson JA. 1998)
ESCs (Embryonic Stem Cells), in fact, though theoretically capable of renewing into every kind of cell, arise ethical issues that cannot be avoided, as these cells derive from the inner cell mass of blastocysts.

Trying to reprogram already differentiated cells, reverting their fate, has for long been a chimera, but at the same time one of the major aims of science. In this way new cells would be at disposal for treatment of degenerative disease as, for example, juvenile diabetes, Parkinson's disease, heart failure, cord injury and burns. In 1952, Briggs and King demonstrated that nuclear transfer from a blastula stage embryo to enucleated *Rana pipiens* eggs was actually possible and brought to the development of normal tadpoles (Briggs and King

1952); in the 1960s, Gurdon and his colleagues managed to produce adult frogs via nuclear transfer of tadpole intestine cell nuclei into enucleated *Xenopus laevis* eggs. (Gurdon 1962)

It was thus understood that developmental genes could be activated also in differentiate cells.

As early as in 1976, Miller and Ruddle demonstrated that after fusion with Embryonal Carcinoma Cells (ECCs), thymocytes actually acquire pluripotency; later, two independent experiments both made by Tada and colleagues, obtained pluripotent cells via electrofusion with Embryonic Germ Cells (EGCs) in 1997 and via electrofusion with mouse ESCs in 2001.

In 1996 a ultimate result was obtained with the birth of Dolly, the first cloned sheep; from then on, other animals have successfully been cloned, including cows and dogs.

The final goal was re-programming by fusion with human ESCs, a result reached for the first time in 2005 by Cowan's group and later in 2006 by Yu and colleagues. (Cowan CA. 2005)

All the above-mentioned studies have resulted in the comprehension that both egg cytoplasm and ES Cells have factors which can actively reprogram somatic cell nuclei and render them back to a pluripotent state.

This technology has nevertheless different problems, not least the creation of tetraploid cells and the subsequent teratoma formation that, even if it is a clue peculiar to pluripotent potential, also impedes the therapeutic use of these cells.

Furthermore, these fused cells could possibly give rise to immune rejection after transplantation.

The innovative result of the possibility of inducing stemness in already-differentiated, adult, somatic cells was obtained by Takahashi and Yamanaka in 2006, using a group of pluripotency-inducing factors. In their seminal work, Takahashi and Yamanaka tested different groups of factors and in the end they identified four factors necessary in the reprogramming process: Oct-3/4, Sox2, c-Myc and Klf4 (Takahashi and Yamanaka 2006). First in 2007, scientists were able to generate iPSCs from human fibroblast, using the same four factors that were applied to reprogram mouse fibroblasts and a retroviral approach. (Takahashi K. 2007) Further analysis confirmed not only that cells obtained in this way expressed markers typical of human Embryonic Stem Cells, but also that ES cell-specific genes were active in these hiPS Cells. Different methods were used to test the pluripotency and the self-renewal of these cells: Embryoid Body and teratoma formation, marker genes expression, alkaline phosphatise analysis, gobal gene expression. The question is if iPSCs are similar or identical to ESC. Still much debate is going on about this issue and more work has to be done in order to appreciate and highlight the true reason of similarity and difference between ESCs and iPSCs. (Yamanaka 2008)

A recent review written by Yamanaka points out that the high similarity observed between ESCs and iPSCs could be due to the fact that ESCs do not exist under physiological conditions, but are selected in culture with the cultivation of cells from the embryo's Inner Cell Mass (ICM); they should thus be considered artificial, hand-made. (Yamanaka S. 2012)

Contrasting results come from the comparison of hiPSCs and hESCs, regarding DNA methylation, gene expression, teratoma-forming propensity.

Many of these cells have subtle or severe chromosomal abnormalities: large sample sizes are needed to further strengthen the possible difference between iPSCs and ESCs, even if the relatively low efficiency of reprogramming makes it difficult to obtain the necessary amount of pluripotent cells. (Pera 2011) It has been widely accepted that ESCs and iPSCs are not epigenetically, transcriptionally, genetically or functionally identical, though it is still to be demonstrated whether these differences are due only to normal biological variations or if they are a consequence of the reprogramming event. (Wernig 2008)

Ever since the first discovery of iPSCs, one of the major hurdles to be overcome was the relatively low efficiency of the reprogramming process. Therefore, there has always been a search for new methodological advances that could help to ameliorate iPSCs' production. First of all the delivering methods that are currently being used in research: integrating vectors and non-integrating vectors.

In the first category, we may find retroviral vectors and lentiviral vectors; in the second one there are plasmid vectors, episomal plasmids, adenoviruses, synthesized RNAs and proteins, and Sendai viruses, which was the method that we choose in our lab.

iPSCs' potential applications

Accepting the idea that iPSCs are artificial cells type and that much work remains to be done to improve and refine them, undoubtedly reprogramming technologies have an important potential use for modelling and treating diseases. Regarding the use of iPSCs as research tool, they have the advantage of providing the scientific world with a chance to study the developmental process for multiple times with the same pool of cells. Another important application of iPSCs is the production of cell lines from patients suffering from different diseases, thus providing researchers with a tool of immense importance. Although production of disease phenotype from differentiated iPSCs *in vitro* is the necessary first step towards disease modelling, the identification of novel pathways or drugs that could affect the disease process is the ultimate goal of this approach.

Induced Pluripotent Stem Cells could also be useful in recording pre-symptomatic abnormalities: actual hurdles to this further application are the necessity of ameliorating the efficiency of differentiation in order to decrease the risk of teratoma and the development of new delivery methods to target the organs of interest. Another major issue is the possibility that *in vitro* modelling does not reproduce the actual *in-vivo* pathological evolution in age of onset, nature of disorder and in the complexity of the causative genetic defects. (Wu and Hocheddlinger 2011)

Another important research field is cancer research; nowadays it has been recognized that cancer cells inhibit induction of iPSCs, but in the future, as iPSCs' technology and production improve, it will hopefully be possible to reprogram defined cancer cells, erasing their epigenetic

alterations that gave rise to the oncogenic profile and making them physiologically normal again. (Kim 2013)

In order to promote research in all these application fields, immunodeficient mice are continuously used and humanized animals are going to be a fundamental tool for the expanding potential of this brand new technology.

Some researchers have also proposed that Induced Pluripotent Stem Cells could be a useful tool for the conservation of endangered species, via the reprogramming of cryopreserved fibroblasts. (Selvaraj V. 2011)

But one of the most exciting aspects of iPSC technology is the possibility of generating autologous cells for cell-replacement therapy. A major breakthrough regarding the use of iPSCs for research has been the obtainment of sickle cell-anemia iPS Cells murine model. (Hanna 2007). In this pioneering study, iPS Cells obtained from patients suffering from sickle cell anemia were corrected for the mutation via homologous recombination and were transplanted into humanized mice anemia model, recovering the normal phenotype.

The risk of teratoma formation is a huge challenge for iPSCs-based therapy. Most of the experiments are in fact conducted on immune-deficient animals and it is not clear if the risk would be similar or greater in patients with a functional immune system.

This issue has been partly overcome by the direct reprogramming approach, which skips the pluripotent stage.

Direct reprogramming produces somatic cells with a limited lifespan, while both ESCs and iPSs have limitless growth and could be thus

more useful for scientific research, providing the laboratories with a potentially infinite cell culture.

Another challenge for therapy lies in the fact that ES/iPSCs-derived cell lines are for the most part immature, as they resemble the embryonic status of differentiation.

An important issue that it is still under debate is whether the engrafted cells derived from iPSCs can function together with the existing cells.

Some studies have highlighted the possibility that reprogrammed fibroblasts could successfully integrate into mouse fetal brain and improve the symptoms of Parkinson's disease (Vierbuchen and Wernig 2011). It is not known, however, if the factors causing the disease can also lead to the degeneration of the reprogrammed and transplanted cells: this does not anyway preclude the possible future use of iPSCs for clinical and therapeutic transplant applications.

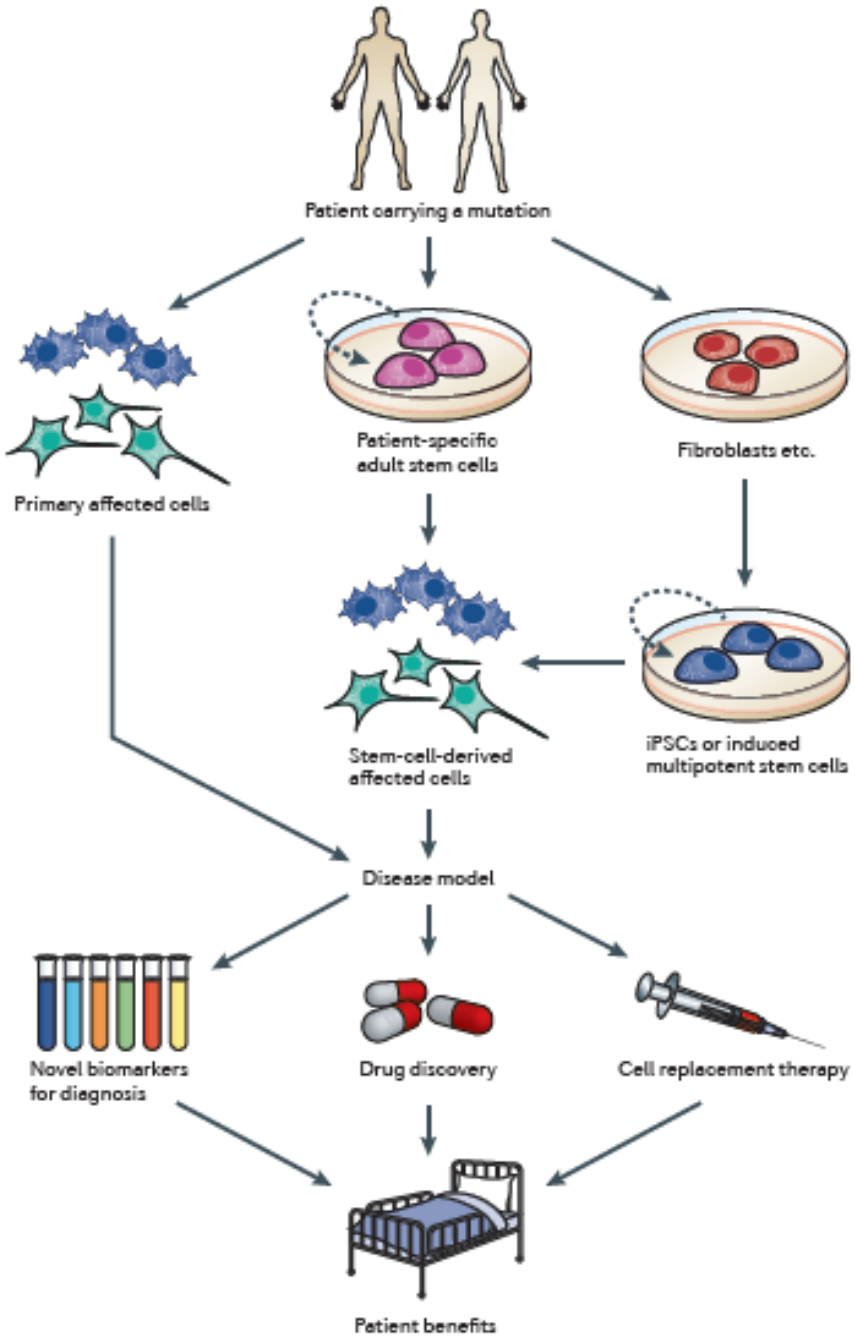

Figure 6. **Generation and application of patient-specific disease models**. (Sterneckert JL. 2014)

2. Direct reprogramming

A very short paragraph must be dedicated to the direct reprogramming, an alternative method to override the different ethical concerns involving iPSCs' generation.

In this case, somatic cell types are directly converted into one another without first reverting to a pluripotent state. There have been numerous successful results using this approach, and it has been possible to differentiate exocrine pancreatic cells to β-cells, and fibroblasts to myocytes, neurons or hepatocytes. By means of direct reprogramming, the up-regulation of target gene expression is rapid, and cell identity is stable after the removal of all exogenous factors.

Reprogramming efficiency varies widely depending on the type of cells that are being used; it is thought that closely related cell types, which are epigenetically speaking, more similar, are also more prone to an efficient conversion.

In their review, Vierbuchen and Wernig revisit all the different methods and explain some of the possible mechanisms lying under the mechanism of direct reprogramming. (Vierbuchen and Werning 2010)

Possible applications of direct reprogramming

Possible applications of direct reprogramming technology include the chance of using these cells for transplants, pharmaceutical research and disease modelling.

Compared to iPSCs, directly reprogrammed cells do not form teratoma and do not recapitulate embryonic tissue generation; they are thus more viable for modelling of those diseases generated at terminal stages in adult age (Vierbuchen T. 2011).

Despite this important practical drawbacks, it has already been tried to transplant direct reprogrammed fibroblasts into mouse models, as was the case with iPSCs technology: a group guided by Kim, in fact, observed the functional integration of neurons obtained from mouse fibroblasts via direct reprogramming in a mouse model of Parkinson's disease (Kim J. 2011).

Further research is needed to enlighten and increase our knowledge of possible main therapeutic applications of direct reprogramming technique.

THERAPEUTIC APPROACHES TO NBIA

The reason why there is no currently cure for NBIA is that is still not clear its pathogenesis. In fact to date, the approach is primarily symptomatic, which a particularly attention to reducing abnormal movements and spasticity. Dopaminergic drugs, anticholinergics, tetrabenazine may be efficacious. For psychiatric symptoms and behaviour disturbances, deep brain stimulation can produce some benefit. (Zorzi G., 2012)

However, these approaches are rarely fully satisfactory and do not slow disease progression. As concern PKAN, the potential utility of pantethine has generated much interest within NBIA community (Rana A., 2010).

Even if it is still not know if the iron play a significant role in this disease, or if it is just an epiphenomenon, it is still remaining the hallmark of this syndrome and an effectively target for therapy. So in a recent study presented by Cossu in 2014, the oral iron-chelator deferiprone produced significant (median 30%) reduction in globus pallidus iron content, ranging from 15 to 61% in adult patients with a late onset (Cossu G., 2014). The clinical assessment of NBIA patients is very complex and variable, so many studies have to be done in order to propose a therapeutic common option.

SCOPE OF THE THESIS

The purpose of the experimental work I carried out during my DIMET course has been focused on using novel tools to both discover new disease genes and develop new *in vitro* and *in vivo* models for NBIA disorders in order to understand their pathogenetic mechanisms.

My work contributed to the publications of three papers, one under submission, and one review.

In the second chapter of this thesis, there is the article concerning the characterization of C19orf12 gene, coding for a mitochondrial membrane protein, which mutations are responsible for a subtype of NBIA called MPAN (Mitochondrial membrane Protein Associated Neurodegeneration). We showed that wild-type C19orf12 protein is localized not only in the mitochondria but also in the Endoplasmic Reticulum (ER), and MAM (Mitochondria Associated Membrane). Using a GFP-tagged protein, we demonstrated that mutations of C19orf12, cause mis-localization of the protein. Moreover high mitochondrial calcium concentration and inability to respond to oxidative stress were found in MPAN fibroblasts

The clinical and molecular heterogeneity of NBIA disorders causes a large fraction (around 20%) of affected patients to be without a molecular genetics diagnosis. So I worked on a project based on identification of new disease genes by exome sequencing on selected patients, and we found that mutations in CoA Synthase (COASY) were responsibible for a form of NBIA, named CoPAN (COASY protein-associated neurodegeneration). Chapter three contains the paper reporting the first mutations in COASY.

Due to the fact that existing cellular models and PKAN mice don't recapitulate the neuropathological signs typical of the human disorder, we tried to obtain new cellular models. We generated human induced pluripotent stem cells (hiPSC) reprogramming PKAN fibroblasts. Their derived neurons exhibited functional impairments, such as, premature death, increased ROS production, aberrant mitochondria, reduction of respiratory capacity and major membrane excitability defects. Chapter four reported these findings.

Chapter five reviews currently alteration of coenzyme A biosynthetic pathway in neurodegeneration with brain iron accumulation syndromes.

REFERENCES

Aghajanian, S., and D. Worral. "Identification and characterization of the gene encoding the human phosphopantetheine adenylyltransferase and dephospho-CoA kinase bifunctional enzyme (CoA synthase)." *Biochem 356*, 2002: 13-18.

Agrimi G., Russo A, Scarcia P, Palmieri F. «The human geneSLC25A17 encodes a peroxisomal transporter of coenzyme A, FAD andNAD+ .» *Biochem. J. 443*, 2012: 241-247.

Alazami A.M., Al-Saif A., Al-Semari A., Bohlega, S., Zlitni, S., Alzahrani, F., Bavi, P., Kaya, N., Colak, D., Khalak, H., Baltus, A., Peterlin, B., Danda, S., Bhatia, K.P., Schneider, S.A., Sakati, N., Walsh, C.A, Al-Mohanna, F., Meyer, B., Alkuraya,. «Mutations in C2orf37, encoding a nucleolar protein, cause hypogonadism, alopecia, diabetes mellitus, mental retardation, and extrapyramidal syndrome.» *Am. J. Hum: Gen. 83*, 2008: 684-91.

Alderson N.L., Rembiesa B.M., Walla, M.D., Bielawska, A., Bielawski, J., Hama, H. «The human FA2H gene encodes a fatty acid 2-hydroxylase.» *Biol. Chem. 279*, 2004: 48562-8.

Arber C., LI A., Houlden H.,Wray S. «Insights into molecular mechanisms of disease in neurodegeneration with brain iron accumulation: unifying theories.» *Neurophatol. App. Neurobio.*, 2015.

Arosio, P, and S. Levi. "Cytosolic and mitochondrial ferritins in the regulation of cellular iron homeostasis and oxidative damage." *Biochim Biophys Acta*, 2010.

Arundine, M., and M., Tymianski. " Molecular mechanisms of calcium dependent neurodegeneration in excitotoxicity." *Cell Calcium* , 2003: 34, 325–337.

Baraibar M. A., Muhoberac B. B., Garringer H. J., Hurley T. D., Vidal R. «Unraveling of the E helices and disruption of 4 fold pores are associated with iron mishandling in a mutant ferritin causing neurodegeneration.» *J.Biol. Chem. 285*, 2010: 1950-1956.

Beck G., Sugiura, Y., Shinzawa, K., Kato, S., Setou, M., Tsujimoto, Y., Sakoda, S., Sumi-Akamaru, H. «Neuroaxonal dystrophy in calcium-independent phospholipase A2βdeficiency results from insufficient remodeling and degeneration of mitochondrial and presynaptic membranes.» *J. Neurosci. 31*, 2011: 11411-20.

Benard G. «Mitochondrial bioenergetics and structural network organization.» *Journal of Cell Science*, 2007: 120: 838-848.

Bence NF, Sampat RM, Kopito RR. « Impairment of the ubiquitin-proteasome system by protein aggregation.» *Science*, 2001: 292: 1552-1555.

Berridge MJ., Bootman MD, Roderick HL. « Calcium signalling: dynamics, homeostasis and remodelling.» *Nat Rev Mol Cell Biol* , 2003: 4:517-529.

Bosveld F., Rana A., Van der Wouden P.E., Lemstra W., Ritsema, M., Kampinga, H.H., Sibon, O.C. «De novo CoA biosynthesis is required to maintain DNA integrity during development of the Drosophila nervous system.» *Mol. Gen 17*, 2008: 2058-69.

Bourne H.R., Sanders D.A., McCormick F. « The GTPase superfamily: a conserved switch to diverse cell functions.» *Nature*, 1990: 248:125-132.

Bras J., Verloes A., Schneider S.A., Mole S.E., Guerreiro R.J. «Mutation of the parkinsonism gene ATP13A2 causes neuronal ceroid-lipofuscinosis.» *Hum. Mol. Genet. 21*, 2012: 2646-50.

Breus O., Panasyuk G., Zhyvoloup A., Panayotou G., Gout I.T., Filonenko V. «Specific interaction between S6K1 and CoA synthase: a potential link betwen the mTor/S6K pathway, CoA biosynthesis and energy metabolism.» *Febs*, 2004: 578: 357-62.

Briggs, R., and T., King. "Transplantation of living nuclei from blastula cells into enucleated frogs' eggs." *Proc. Natl. Acad. Sci*, 1952: 38: 455-463.

Brissot P., Ropert, M., Le Lan, C., Loréal, O. «Non-transferrin bound iron: a key role in iron overload and iron toxicity.» *Biochim. Biophys. Acta 1820*, 2012: 403-410.

Brunetti D, Dusi S, Giordano C., Lamperti C., Morbin M., Fugnanesi V., Marchet S., Fagiolari G., Sibon O., Moggio M., d'Amati G., Tiranti V.,. «Panthetine treatment is effective in recovering the disease phenotype induced by ketogenic diet in a pantothenate kinase-associated neurodegeneration mouse mode.» *Brain*, 2014: 137: 57-68.

Brunetti D., Dusi S., Morbin M., Uggetti A., Moda F., D'Amato I., Giordano C., d'Amati G., Cozzi A., Levi S., Hayflick S., Tiranti V. «Pantothenate kinase-associated neurodegeneration: altered mitochondria membrane potential and defective respiration in Pank2 knock-out mouse model.» *Hum Mol Genet 21*, 2012: 5294-305.

Burn, J., and P.F, Chinnery. "Neuroferritinopathy." *Semin. Pediatr. Neurol. 13*, 2006: 176-181.

Campanella A., Privitera, D., Guaraldo, M., Rovelli, E., Barzaghi, C., Garavaglia, B., Santambrogio, P., Cozzi, A., Levi, S. «Skin fibroblasts from pantothenate kinase-associated neurodegeneration patients show altered cellular oxidative status and have defective iron-handling properties.» *Hum. Mol. Genet. 21*, 2012: 4049-59.

Cataldo AM. « Properties of the endosomal–lysosomal system in the human central nervous system: disturbances mark most neurons in

populations at risk to degenerate in Alzheimer's .» *J. Neurosci.* , 1996: 16, 186–199.

Chen B., Retzlaff M, Roos T, Frydman J. «Cellular strategies of protein quality control. .» *Cold Spring Harb Perspect Biol*, 2011: 3: a004374.

Cossu G., Abbruzzese, G., Matta, G., Murgia, D., Melis, M., Ricchi, V., Galanello, R., Barella, S., Origa, R., Balocco, M., Pelosin, E., Marchese, R., Ruffinengo, U., Forni, G.L. «Efficacy and safety of deferiprone for the treatment of pantothenate kinase-associated neurodegeneration (PKAN) and neurodegeneration with brain iron accumulation (NBIA): results from a four years follow-up.» *Parkinsonism. Relat. Disord. 20*, 2014: 651-4.

Cowan CA., Atienza, J., Melton, D.A., and Eggan, K. «Nuclear reprogramming of somatic cells after fusion with human embryonic stem cells.» *Science* , 2005: stem cells. Science 309, 1369–1373.

Cozzi A., Rovelli E., Frizzale G., Campanella A., Amendola M., Arosio P., Levi S. «Oxidative stress and cell death in cells expressing L-ferritin variants causing neuroferritinopathy.» *Neurobiol Dis*, 2010: 37(1): 77-85.

Crompton E. «Neuroferritinopathy: A Window on the Role of Iron in Neurodegeneration.» *Blood Cells, Molecules, and Diseases*, 2002: 29(3): 522-531.

Curtis A.R., Fey C., Morris C.M., Bindoff L.A., Ince P.G., Chinnery P.F., Coulthard A., Jackson M.J., Jackson A.P., McHale D.P., Hay D., Barker W.A., Markham A.F., Bates D., Curtis A., Burn J. «Mutation in the gene encoding ferritin light polypeptide causes dominant adult-onset basal ganglia disease.» *Nat. Genet. 28*, 2011: 350-5.

Dall'Armi C., Devereaux K.A., Di Paolo G. «The role of lipids in the control of autophagy.» *Curr. Biol. 23*, 2013: R33-45.

Dalle-Donne I., Scaloni A, Giustarini D, Cavarra E, Tell G, Lungarella G, Colombo R, Rossi R, Milzani A. . « Proteins as biomarkers of oxidative/nitrosative stress in diseases: the contribution of redox proteomics. .» *Mass Spectrom. Rev*, 2005: 24, 55–99.

Dan P., Edvardson, S., Bielawski, J., Hama, H., Saada, A. «2 Hydroxylated sphingomyelin profiles in cells from patients with mutated fatty acid 2 hydroxylase.» *Lipid Health Dis 10*, 2011: 84.

DeBoer SR., You Y, Szodorai A, Kaminska A, Pigino G, Nwabuisi E, Wang B, Estrada-Hernandez T, Kins S, Brady ST, Morfini G. . « Conventional kinesin holoenzymes are composed of heavy and light chain homodimers.» *Biochemistry* , 2008: 47:4535– 4543.

Detmer, S., and D., Chan. "Functions and dysfunctions of mitochondrial dynamics." *Nature*, 2007: 8: 870-879.

Deuschlc G. «Essential tremor—neurodegenerative or nondegenerative disease towards a working definition of ET.» *Mov Disord R*, 2009: 24: 2033–2041.

Devos D., Moreau C, Devedjian JC, Kluza J, Petrault M, Laloux C, Jonneaux A, Ryckewaert G, Garçon G, Rouaix N, Duhamel A, Jissendi P, Dujardin K, Auger F, Ravasi L, Hopes L, Grolez G, Firdaus W, Sablonnière B, Strubi-Vuillaume I, Zahr N, Destée A, C. «Targeting chelatable iron as a therapeutic modality in Parkinson's disease.» *Antioxi Redox Signal*, 2014: 21(2): 195-205.

Dezfouli M. «PANK2 and C19orf12 Mutations Are Common Causes of Neurodegeneration With Brain Iron Accumulation.» *Movement Disorders*, 2013: 28(2): 228-232.

Di Fonzo A., Chien H.F., Socal M., Giraudo S., Tassorelli C., Iliceto, G., Fabbrini, G., Marconi, R., Fincati, E., Abbruzzese, G., Marini, P., Squitieri, F., Horstink, M.W., Montagna, P., Libera, A.D., Stocchi, F., Goldwurm, S., Ferreira, J.J., Meco,. «ATP13A2 missense mutations in

juvenile parkinsonism and young onset Parkinson disease.» *Neurology 68*, 2007: 1557-62.

Donati A. « Age-related changes in the autophagic proteolysis of rat isolated liver cells: effects of antiaging dietary restrictions. .» *A Biol. Sci. Med. Sci. 56, B375–B383*, 2001: 56, B375–B383.

Duchen MR. «. Mitochondria and calcium: from cell signalling to cell death.» *J. Physiol.* , 2000: 529, 57–68.

Dusek, P., and S.A., Schneider. "Neurodegeneration with brain iron accumulation." *Co-neurology*, 2012: 25(4): 499-506.

Dusi S., Valletta L., Haack T.B., Tsuchiya Y., Venco P., Pasqualato S., Goffrini P., Tigano M., Demchenko N., Wieland T., Schwarzmayr T., Strom T.M., Invernizzi F., Garavaglia B., Gregory, A., Sanford, L., Hamada, J., Bettencourt, C., Houlden,Tiranti, V. «Exome sequence reveals mutations in CoA synthase as a cause of neurodegeneration with brain iron accumulation.» *Am. J. Hum. Genet. 94*, 2014: 11-22.

Eckhardt M., Yaghootfam, A., Fewou, S.N., Zöller, I., Gieselmann, V. «A mammalian fatty acid hydroxylase responsible for the formation of alpha-hydroxylated galactosylceramide in myelin.» *Biochem. J. 388*, 2005: 245-54.

Elham J., Mohammad R., Gholam A., Shahriar N.,. «Identification of mutation in GTPBP2 in patients of a family with.» *Neurobiology of Aging*, 2015.

Elluru RG., Bloom GS, Brady ST. « Fast axonal transport of kinesin in the rat visual system: functionality of the kinesin heavy chain isoforms. .» *Mol Biol Cell* , 1995: 6:21– 40.

Esposito G., Giovacchini G, Liow JS. «Imaging neuroinflammation in Alzheimer's disease with radiolabe arachidonic acid and PET.» *J Nucl Med*, 2008: 49(9): 1414-21.

Evans SJ, Prossim AR, Harrington GL,. «Fats and Factors: lipid profiles associate with personality factors and suicidal history in bipolar subjects.» *Plos One*, 2012: 7(1):e29297.

Evans, MJ., and MH., Kaufman. "Establishment in culture of pluripotential cells from mouse embryos." *Nature*, 1981: 292, 154–156.

Fleming, R., and P., Ponka. "Iron Overloa in Human Disease." *N Eng J Med*, 2012: 366: 348-358.

Fleury C. «Mitochondrial reactive oxygen species in cell death signaling.» *Biochimie*, 2002: 84: 131-141.

Friedman A., Arosio P., Finazzi D., Koziorowski D., Galazka-Friedman J. «Ferritin as an important player in neurodegeneration.» *Parkinsonism Rela. Disord. 17*, 2011: 423-430.

Gali B., Ferring-Appel D., Kaden S.,. «Iron regulatory proteins are essential for intestinal function and control key iron absorption molecules in the duodenum.» *Cell Met*, 2008: 7:79-85.

Garcia M., Leonardi R., Zhang YM., Rehg JE, Jackowski S. «Germline deletion of pantothenate kinases 1 and 2 reveals the key roles for CoA in postnatal metabolism.» *Plos One*, 2012.

Goedert M. «Alpha-synuclein and neurodegenerative diseases.» *Nat. Rev. Neurosci.* ., 2001: 2, 492–501.

Green J.T., Orr, S.K., Bazinet, R.P. «The emerging role of group VI calcium-independent phospholipase A2 in releasing docosahexaenoic acid from brain phospholipids.» *J. Lipid. Res. 49*, 2008: 939-44.

Gregory A, Polster BJ., Hayflick J,. «Clinical and genetic delineation of neurodegeneration with brain iron accumulation.» *J Med Genet.*, 2009: 46(2): 73-80.

Gregory A., Hayflick S.J.,. " Neurodegeneration with brain iron accumulation. ." *Folia Neuropathol.* , 2005: 43(4): 286-296.

Gregory, A., and SJ., Hayflick. "Pantothenate Kinase-Associated Neurodegeneration." *Gene Reviews*, 2013: 1993-2015.

Grune T. «Selective degradation of oxidatively modified protein substrates by the proteasome.» *Biochem. Biophys. Res.*, 2003: 305, 709–718.

Grünewald A., Arns B., Seibler P., Rakovic A., Münchau, A., Ramirez, A., Sue, C.M., Klein, C. «ATP13A2 mutations impair mitochondrial function in fibroblasts from patients with Kufor-Rakeb syndrome.» *Neurobiol. Agiing. 33*, 2012: 1843, e1-7.

Gurdon, JB.,. «The developmental capacity of nuclei taken from intestinal pithelium cells of feeding tadpoles.» *Embryol exp morph*, 1962.

Haack T.B., Hogarth, P., Kruer, M.C., Gregory, A., Wieland, T., Schwarzmayr, T., Graf, E., Sanford, L., Meyer, E., Kara, E., Cuno, S.M., Harik, S.I., Dandu, V.H., Nardocci, N., Zorzi, G., Dunaway, T., Tarnopolsky, M., Skinner, S., Frucht, S., Hanspal, E. «Exome sequencing reveals de novo WDR45 mutations causing a phenotypically distinct, X linked dominant form of NBIA.» *Am. J. Mum. Gen. 91*, 2012: 1144-1149.

Hafezparast M., Klocke R, Ruhrberg C, Marquardt A, Ahmad-Annuar A, Bowen S, Lalli G, Witherden AS, Hummerich H, Nicholson S, Morgan PJ, Oozageer R, Priestley JV, Averill S, King VR, Ball S, Peters J, Toda T, Yamamoto A, Hiraoka Y. «iMutations in dynein link motor neuron degeneration to defects in retrograde transport.» *Science* , 2003: 300:808–812.

Hallervorden, J., and H. Spatz. "Eigenartige Erkrankung im extrapyramidalen System mit besonderer Beteilung des Globus

pallidus und der Substantia nigra." *Z Ges Neurol Psychiatr 1*, 1922: 79: 254-302.

Hallgreen B., Sourander P. «The effect of age on the non-haemin iron in the human brain.» *J Neurochem.*, 1958: 3(1):41-51.

Halliwell B. « Oxidative stress and neurodegeneration: where are we now? Journal of Neurochemistry .» *Oxidative stress and neurodegeneration: where are we now? Journal of Neurochemistry* , 2006: vol. 97, no. 6, pp.1634–1658.

Hama H. «Fatty acid 2-Hydroxylation in mammalian sphingolipid biology.» *Biochim. Biophys. Acta. 1801*, 2010: 405-14.

Hamasaki M., Furuta N, Matsuda A, Akiko Nezu, Akitsugu Yamamoto, Naonobu Fujita. «Autophagosomes form at ER–mitochondria contact site.» *Nature*, 2013: 495:389-349.

Hanna, H. «Treatment of Sickle Cell Anemia Mouse Model with IPS Cells Generated from Autologous Skin.» *Science*, 2007: 318: 1920-1923.

Hardy J. «A hundred years of Alzheimer's disease research.» *Neuron*, 2006: 52, 3–13.

Harrison, PM., and P., Arosio. "The ferritins: molecular properties, iron storage, function and cellular regulation." *Biochim Biophys Acta*, 1996: 1275:161-203.

Hartig M.B., Iuso., A., Haack, T., Kmiec, T., Jurkiewicz, E., Heim, K., Roeber, S., Tarabin, V., Dusi, S., Krajewska-Walasek, M., Jozwiak, S., Hempel, M., Winkelmann, J., Elstner, M., Oexle, K., Klopstock, T., Mueller-Felber, W., Gasser, T., Trenkwalder,. «Absence of an orphan mitochondrial protein, c19orf12, causes a distinct clinical subtype of neurodegeneration with brain iron accumulation.» *Am. J. Hum. Genet. 89*, 2011: 543-50.

Hayflick S.J., Westaway S.K., Levinson, B., Zhou, B., Johnson, M.A., Ching, K.H., Gitschier, J. «Genetic, clinical, and radiographic delineation of Hallervorden-Spatz syndrome.» *N. Eng. J. Med. 348*, 2003: 33-40.

Hentze M.W., Muckenthaler M.U., Galy B., Camaschella C.,. «Two to Tango: Regulation of Mammalian Iron Metabolism. .» *Cell*, 2010: 142: 24-38.

Hill J., Switzer R.,. «The regional distribution and cellular localization od iron in the rat brain.» *Neuroscience*, 1984: 11(3): 595-603.

Hirokawa N. «Molecular motors in neurons: transport mechanisms and roles in brain function, development, and disease.» *Neuron*, 2010: 68: 610-638.

Hogarth P., Gregory, A., Kruer, M.C., Sanford, L., Wagoner, W., Natowicz, M.R., Egel, R.T., Subramony, S.H., Goldman. J.G., Berry-Kravis, E., Foulds, N.C., Hammans, S.R., Desguerre, I., Rodriguez, D., Wilson, C., Diedrich, A., Green, S., Tran, H., Reese,. «New NBIA subtype: genetic, clinical, pathologic, and radiographic features of MPAN.» *Neurology 80*, 2013: 268-75.

Hörtnagel K., Prokisch H., Meitinger T.,. « An isoform of hPANK2, deficient in pantothenate kinase-associated neurodegeneration, localizes to mitochondria.» *Hum. Mol. Genet* , 2003: 12: 321-327.

Horvarth R. «SCP2 mutations and neurodegeneration with brain iron accumulation.» *Neurology*, 2015.

Iuso A., Sibon, O.C.M., Gorza, M., Heim, K., Organisti, C., Meitinger, T., Prokisch, H. «Impairment of Drosophila orthologs of the human orphan protein C19orf12 induces bang sensitivity and neurodegeneration.» *Plos One 9*, 2014: e89439.

Jadoon A., Chiu CC, McDermott L.,. «Associations of polyunsaturated fatty acids with residual depression or anxiety in older people with major depression.» *J Affected Disorder*, 2012: 1363:918-25.

Jeong, S.Y, and S. David. "Age-related changes in iron homeostasis and cell death in the cerebellum of ceruloplasmindeficient mice." *J. Neurosci. 26*, 2006: 9810.19.

Jeong, S.Y., and S., David. "Glycosylphosphatidylinositol-anchored ceruloplasmin is required for iron efflux from cells in the central nervous system." *J. Biol. Chem. 278*, 2003: 27144-27148.

Jiang, P., and Mizushima. "Autophagy and human diseases." *Cell Research*, 2014: 24:69-79.

Jin J., Arias E.E, Chen J., Harper J.W., Walter J.C. «A family of diverse Cul4-Ddb1-interacting proteins includes Cdt2, which is required for S phase destruction of the replication factor Cdt1.» *Mol. Cell 23*, 2006: 709-21.

Johnson M. «Mitochondrial localization of Human PANK2 and Hypotheses of Secondary Iron Accumulation in Pantothenate Kinase-Associated Neurodegeneration.» *Ann. N. Y. Acad. Sci.*, 2004: 1012: 282-298.

Johnston J.A., Ward CL, Kopito RR. « Aggresomes: a cellular response to misfolded proteins.» *J Cell Biol*, 1998: 143: 1883-1898.

Keogh M. J., Jonas P., Coulthard A., Chinnery P.F., Burn J. «Neuroferritinopathy: a new inborn error of iron metabolism.» *Neurogenetics*, 2012: 13(1):93-6.

Kiffin R. «Oxidative stress and autophagy.» *Antioxid. Redox Signal*, 2006: 8, 152–162.

Kim J. «Functional Integration of Dopaminergic Neurons Directly Converted from Mouse Fibroblasts.» *Cell Stem Cell*, 2011: 9: 413.419.

Kim, J. « An iPSC line from human pancreatic ductal adenocarcinoma undergoes early to invasive stages of pancreatic cancer progression. .» *Cell Rep.* , 2013: 3: 2088–2099 .

Kimura K. «Terminal axon pathology in infantile neuroaxonal dystrophy.» *Pediatr. Neurol*, 1991: 7: 116-120.

Kono S., Suzuki H., Oda T., Miyajima, H., Takahashi, Y., Shirakawa, K., Ishikawa, K., Kitagawa, M. «Biochemical features of ceruloplasmin gene mutations linked to aceruloplasminemia.» *Neuromolecular Med. 8*, 2006: 361-74.

Kono, S., e Miyajima. «Molecular and pathological basis of aceruloplasminemia.» *Biol. Res. 39*, 2006: 15-23.

Kovacs G. «Molecular Pathological Classification of Neurodegenerative Diseases: turning towards precision medicine.» *Int J Mol Sci*, 2016.

Kruer M.C., Boddaert, N., Yoon, M.Y., Hama, H., Gregory, A., Malandrini, A., Woltjer, R.L., Munnich, A., Gobin, S., Polster, B.J., Palmeri, S., Edvardson, S., Hardy, J., Houlden, H., Hayflick, S.J.,. «Defective FA2H leads to a novel form of neurodegeneration with brain iron accumulation (NBIA).» *Ann. Neurol. 68*, 2010: 611-18.

Kruer MC., Hiken, M., Gregory, A., Malandrini, A., Clark, D., Hogarth, P., Grafe, M., Hayflick, S.J., Woltjer, R.L. «Novel histopathologic findings in molecularly-confirmed pantothenate kinase-associated neurodegeneration.» *Brain 134*, 2011: 947-58.

Kuo Y.M., Duncan J.L., Westaway S.K., Yang, H., Nune, G., Xu, E.Y., Hayflick, S.J., Gitschier, J. «) Deficiency of pantothenate kinase

2 (Pank2) in mice leads to retinal degeneration and azoospermia.» *Hum. Mol. Genet. 14*, 2005: 49-57.

Kurian, M., and S., Hayflick. "Pantothenate kinase-associated neurodegeneration and PLA2G6-associated neurodegeneration: review of two major neurodegeneration with brain iron accumulation phenotypes." *Int. Rev. Neurobiol*, 2013.

Lamb CA., Yoshimori T., Tooze SA.,. «The autophagosome: origin unknown, biogenesis complex .» *Nature Reviews*, 2013: 14:759-769.

Leonardi R, Rock , Jackowski, S., Zhang,. «Activation of human mitochondrial pantothenate kinase 2 by palmitoylcarnitine.» *Proc Natl Acad Sci. 104*, 2007: 1494-9.

Leonardi R., Zhang YM, Rock CO, Jackoski S. «Coenzyme A: Back in action.» *Prog Lipid Res*, 2005: 44:125-153.

Leoni V., Strittmatter L., Zorzi, G., Zibordi, F., Dusi, S., Garavaglia, B., Venco, P., Caccia, C., Souza, A.L., Deik, A., Clish, C.B., Rimoldi, M., Ciusani, E., Bertini, E., Nardocci, N., Mootha, V.K., Tiranti, V. «Metabolic consequences of mitochondrial coenzyme A deficiency in patients with PANK2 mutations.» *Mol Genet Metab. 105*, 2012: 463-71.

Leopold PL., McDowall AW, Pfister KK, Bloom GS, Brady ST .. « Association of kinesin with characterized membrane-bounded organelles.» *Cell Motil Cytoskeleton* , 1992: 23:19 –33.

Levi, and Rovida. "The role of iron in mitochondrial function." *Biochim Biophys Acta. 1790*, 2009: 629-636.

Levi, S., and D., Finazzi. "Neurodegeneration with brain iron accumulation: update on pathogenic mechanism." *frontiers in pharmacology*, 2014.

Liu Q., Xie F, Siedlak SL, Nunomura A, Honda K, Moreira PI, Zhua X, Smith MA, Perry M. « Neurofilament proteins in neurodegenerative diseases.» *Cell. Mol. Life Sci. (2004);61 3057–3075*, 2004: 61 3057–3075.

Lu Q., Yang P., Huang X., Hu, W., Guo, B., Wu, F., Lin, L., Kovács, A.L., Yu, L., Zhang, H. «The WD40 repeat PtdIns(3)P-binding protein EPG-6 regulates progression of omegasomes to autophagosomes.» *Dev. Cell. 21*, 2011: 343-57.

Mancuso M.M., Davidzon G.M., Kurlan R.M.M., Tawil R.M., Bonilla E.M., Di Mauro S.M., Powers J.M.M. «Hereditary ferritinopathy: a novel mutation, its cellular pathology, and pathogenetic insights.» *J. Neuropathol. Exp. Neurol. 64*, 2005: 280-94.

Martin GR. « Isolation of a pluripotent cell line from early mouse embryos cultured in medium conditioned by teratocarcinoma stem.» *Proc. Natl. Acad.* , 1981: 78, 7634–7638.

McNaught, KS., and P., Jenner. "Proteasomal function is impaired in substantia nigra in Parkinson's disease." *Neurosci Lett*, 2001: 297: 191-194.

McNeill A., Chinnery P.F. "Neurodegeneration with brain iron accumulation." *Hand. Clin. Neurol. 100*, 2011: 161-172.

Millecamps, S., and SP., Julien. "Axonal transport deficits and neurodegenerative diseases." *Nature Review*, 2013: 14: 161-180.

Morgan N.V., Westaway, S.K., Morton, J.E.V., Gregory, A., Gissen, P., Sonek, S., Cangul, H., Coryell, J., Canham, N., Nardocci, N., Zorzi, G., Pasha, S., Rodriguez, D., Desguerre, I., Mubaidin, A., Bertini, E., Trembath, R.C., Simonati, A., Schanen, C.,. «PLA2G6, encoding a phospholipase A2, is mutated in neurodegenerative disorders with high brain iron.» *Nat. Gen. 38*, 2006: 752-4.

Nemazanyy I, Panasyuk G, Breus O., Zhyvoloup A., Filonenko V., Gout I.T.,. «). Identification of a novel CoA synthase isoform, which is primarily expressed in the brain.» *Biochem. Biophys. Res. Commun. 341*, 2006: 995-1000.

Nemazanyy I., Panasyuk G., Zhyvoloup A., Panayotou G., Gout I.T., Filonenko, V. «Specific interaction between S6K1 and CoA synthase: a potential link between the mTOR/S6K pathway, CoA biosynthesis and energy metabolism.» *FEBS Lett. 578*, 2014: 357-62.

Nunnari, J., and A. Suomalainen. "Mitochondria: in sickness and in health." *Cell 148*, 2012: 1145-59.

Pera, MF.,. «Stem cell: the dark side of induced pluripotency .» *Nature*, 2011: 471: 46-47.

Potter K.A., Kern M.J., Fullbright, G., Bielawski, J., Scherer, S.S., Yum, S.W., Li, J.J., Cheng, H., Han, X., Venkata, J.K., Khan, P.A.A., Rohrer, B., Hama, H. «Central nervous system dysfunction in a mouse model of FA2H deficiency.» *Glia 59*, 2011: 1009-21.

Prusiner SB. « Shattuck lecture – neurodegenerative diseases and prions.» *N. Engl. J. Med.* , 2001: 344, 1516–1526.

Przedborski S., Vila M., Jackson-Lewis V. «Neurodegeneration: what is it and where are we?» *J Clin Invest*, 2003: 111: 3–10.

Rana A., Seinen E., Siudeja K., Muntendam R., Srinivasan, B., Van der Want, J.J., Hayflick, S., Reijngoud, D.J., Kayser, O., Sibon, O.C. «Pantethine rescues a Drosophila model for pantothenate kinase-associated neurodegeneration.» *Proc. Nat. Acad. Sci. USA. 107*, 2010: 6988-93.

Reid E., Kloos M, Ashley-Koch A, Hughes L, Bevan S, Svenson IK, Graham FL, Gaskell PC, Dearlove A, Pericak-Vance MA, Rubinsztein DC, Marchuk DA. « A kinesin heavy chain (KIF5A) mutation in

hereditary spastic paraplegia (SPG10).» *Am J Hum Genet* , 2002: 71:1189.

Ross, CA, and MA., Poirier. "Protein aggregation and neurodegenerative disease." *Nat. Med.*, 2004: S10–S17.

Rouault T.A. «Iron metabolism in the CNS: implications for neurodegenerative diseases.» *Nat. Rev. Neurosci. 14*, 2013: 551-6.

Saitsu H., Nishimura T., Muramatsu K., Kodera, H., Kumada, S., Sugai, K., Kasai-Yoshida, E., Sawaura, N., Nishida, H., Hoshino, A., Ryujin, F., Yoshioka, S., Nishiyama, K., Kondo, Y., Tsurusaki, Y., Nakashima, M., Miyake, N., Arakawa, H., Kato, M., Miz. «De novo mutations in the autophagy gene WDR45 cause static encephalopathy of childhood with neurodegeneration in adulthood.» *Nat. Genet. 45*, 2013: 445-9.

Schneider S.A, Quinn ,N.P., Lees A.J., Houlden H., Hardy J., Bhatia K.P. «ATP13A2 mutations (PARK9) cause neurodegeneration with brain iron accumulation.» *Mov. Disorder. 25*, 2010: 978-84.

Schneider S.A., Hardy J., Bathia K.P. « Syndromes of Neurodegeneration with Brain Iron Accumulation (NBIA): and Update on Clinical Presentations, Histological and Genetics Underpinnings, and Treatment Considerations. .» *57. Schneider S.A., Hardy J., Bathia K.P., Syndromes of Neurodegeneration with Brain Iron Accumulation (NBIA): and Update on Clinical Presentations, Histological and GeneMovement Disorders*, 2012: 27(1): 42.

Schneider, S.A., and K.P. Bhatia. "Excess iron harms the brain: the syndromes of neurodegeneration with brain iron accumulation (NBIA)." *J. Neural. Transm*, 2013: 120: 695-703.

Seleznev K., Zhao, C., Zhang, X.H., Song, K., Ma, Z.A. «Calcium-independent phospholipase A2 localizes in and protects mitochondria during apoptotic induction by staurosporine.» *J. Biol. Chem. 281*, 2006: 22275-88.

Selkoe DJ. «Cell biology of protein misfolding: the examples of Alzheimer's and Parkinson's diseases.» *Nat. Cell Biol*, 2004: 6, 1054–1061.

Selvaraj V., Wildt D., Pukazhendthi S,. «Induced pluripotent stem cells for conserving endangered species?» *Nature methods*, 2011: 8:810-815.

Shon, E., and S. Przedborski. "Mitochondria: the next (neuro)degeneration." *Neuron*, 2011: 70:1033-1053.

Sian-Hulsmann J., Mandel S., Youdim M. B., Riederer P. «The relevance of iron in the pathogenesis of Parkinson's disease.» *J. Neurochem.118*, 2011: 938-957.

Song H., Bao, S., Lei, X., Jin, C., Zhang, S., Turk, J., Ramanadham, S. «) Evidence for proteolytic processing and stimulated organelle redistribution of iPLA(2)beta.» *Biochim. biophys. acta. 1801*, 2010: 547-58.

Sooparb S. «Suppression of chaperone-mediated autophagy in the renal cortex during acute diabetes mellitus.» *Kidney Int*, 2004: 65, 2135–2144.

Soto C. « Unfolding the role of protein misfolding in neurodegenerative diseases.» *Nat Rev Neurosci*, 2003 : 4(1):49-60. .

Stehling O., Wilbrecht, C., Lill, R. «Mitochondrial iron–sulfur protein biogenesis and human disease.» *Biochi 100*, 2014: 61-77.

Sterneckert JL., Peter Reinhardt,Hans R. Schöler. «Investigating human disease using stem cell models.» *Nature review*, 2014: 15: 625-630.

Strauss, E., and T.P. Begley. "The selectivity for cysteine over serine in coenzyme A biosynthesis." *Chem Bio 6*, 2005: 284-286.

Strokin M., Sergeeva, M., Reiser, G. «Prostaglandin synthesis in rat brain astrocytes is under the control of the n-3 docosahexaenoic acid, released by group VIB calciumindependent phospholipase A2.» *J. Neurochem. 102*, 2007: 1771-82.

Suh YA. « Cell transformation by the superoxide superoxide-generating oxidase.» *Nature*, 1999: 401, 79–82.

Susalka, SJ., e i Pfister KK. « Cytoplasmic dynein subunit heterogeneity: implications for axonal transport. .» *J Neurocytol* , 2000: 29:819–829.

Tahiliani, A. G., and C.J. Beinlich. "Pantothenic acid in health and disease." *Vitam Horm. 46*, 1991: 165-228.

Takahashi K., Tanabe K, Ohnuki M, Narita M, Ichisaka T, Tomoda K, Yamanaka S,. «Induction of Pluripotent Stem Cells from Adult Human Fibroblasts by Defined Factors.» *Cell*, 2007: 131: 861-872.

Takahashi, K, and S., Yamanaka. "Induction of pluripotent stem cells from muose embryonic and adult fibroblast cultures by defined factors." *Cell*, 2006: 126: 663-676.

Thompson LM. «Neurodegeneration: a question of balance.» *Nature*, 2008: 452(7188):707-8.

Thomson JA., Itskovitz-Eldor, J., Shapiro, S.S., Waknitz,M.A., SwierSwiergiel,. «Embryonic stem cell lines derived from human blastocysts.» *Science 282, 1145–1147.*, 1998: 282, 1145–1147.

Venco P., Bonora, M., Giorgi, C., Papaleo, E., Iuso, A., Prokisch, H., Pinton, P., Tiranti, V. «Mutations of C19orf12, coding for a transmembrane glycine zipper containing mitochondrial protein, cause mis-localization of the protein, inability to respond to oxidative stress and increased mitochondrial Ca^{2+}.» *Front. Genet. 6*, 2015: 185.

Vierbuchen T. «Direct lineage conversions: unnatural but useful?» *Nature Biotechnology*, 2011: 29(10): 892-907.

Vierbuchen, and Werning. " Direct conversion of fibroblasts to functional neurons by defined factors." *Nature*, 2010: 463(7284): 1035-1041.

Vierbuchen, T., and M. Wernig. "Direct lineage conversions: unnatural but useful?" *Nature Biotechnology*, 2011: 29(10): 892-907.

Wagey, RT., and C. Krieger. "Abnormalities of protein kinases in neurodegenerative diseases." *Prog Drug Res*, 1998: 51:133–183.

Weinreb O., Amit T., Mandel S., Kupershmidt L., Youdim M. B. «Neuroprotective multifunctional iron chelators: from redox-sensitive process to novel therapeutic opportunities.» *Antioxid. Redox. Signal. 13*, 2010: 919-949.

Wernig. « A drug-inducible system for direct reprogramming of multiple somatic cell types. .» *Nature Biotechnology*, 2008: 26(8): 916-924.

Wojda U., Salinska E, Kuznicki J. «Calcium ions in neuronal degeneration.» *IUBMB Life*, 2008: 60:575-590.

Wu Z., Li C., Lv S., Zhou B. «Pantothenate kinase-associated neurodegeneration: insights from a Drosophila model.» *Hum. Mol. Genet. 18*, 2009: 3659-3672.

Wu, SM., and K Hocheddlinger. "Harnessing the potential of induced pluripotent stem cells for regenerative medicine." *Nature Cell Biology*, 2011: 13:5:497-482.

Yamanaka. «Induction of pluripotent stem cells from mouse fibroblasts by four transcription factors.» *Cell Prolif.*, 2008: 41(1): 51-56.

Yamanaka S. «Induced Pluripotent Stem Cells: Past, Present and Future.» *Cell Stem Cell*, 2012: 10: 678-684.

Zhang Y-M., Rock, C.O., Jackowski, S. «Biochemical properties of human pantothenate kinase 2 isoforms and mutations linked to pantothenate kinase-associated neurodegeneration.» *J. Biol. Chem 281*, 2006: 107-14.

Zhou B., Westaway S.K., Levinson B., Johnson M.A., Gitschier, J., Hayflick, S.J. «A novel pantothenate kinase gene (PANK2) is defective in Hallervorden-Spatz syndrome.» *Nat. Genet. 28*, 2001: 345-349.

Zorzi G., Ziboldi F., Chiapparini L., Nardocci N. «Therapeutic advances in neurodegeneratio with brain iron accumulation.» *Sem Pediatric Neurology*, 2012.

CHAPTER 2

Mutations of C19orf12, coding for a transmembrane glycine zipper containing mitochondrial protein, cause mis-localization of the protein, inability to respond to oxidative stress and increased mitochondrial Ca^{2+}

Paola Venco *1,* ***Massimo Bonora*** *2 ,* ***Carlotta Giorgi*** *2 ,* ***Elena Papaleo*** *3 ,* ***Arcangela Iuso*** *4, 5 ,* ***Holger Prokisch*** *4, 5 ,* ***Paolo Pinton*** *2 and* ***Valeria Tiranti*** *1*

1Unit of Molecular Neurogenetics – Pierfranco and Luisa Mariani Center for the study of Mitochondrial Disorders in Children,

IRCCS Foundation Neurological Institute "C. Besta", Milan, Italy, 2 Section of Pathology, Oncology and Experimental Biology and Laboratory for Technologies of Advanced Therapies Center, Department of Morphology, Surgery and Experimental Medicine, University of Ferrara, Ferrara, Italy, 3 Structural Biology and NMR Laboratory, Department of Biology, University of Copenhagen, Copenhagen, Denmark, 4 Institute of Human Genetics, Klinikum rechts der Isar, Technische Universität München, Munich, Germany, 5 Institute of Human Genetics, Helmholtz Zentrum München, Munich, Germany

Front. Genet. Published: 19 May 2015. 6:185. doi: 10.3389/fgene.2015.00185

Abstract

Mutations in *C19orf12* have been identified in patients affected by Neurodegeneration with Brain Iron Accumulation (NBIA), a clinical entity characterized by iron accumulation in the basal ganglia. By using western blot analysis with specific antibody and confocal studies, we showed that wild-type C19orf12 protein was not exclusively present in mitochondria, but also in the Endoplasmic Reticulum (ER) and MAM (Mitochondria Associated Membrane), while mutant C19orf12 variants presented a different localization. Moreover, after induction of oxidative stress, a GFP-tagged C19orf12 wild-type protein was able to relocate to the cytosol. On the contrary, mutant isoforms were not able to respond to oxidative stress. High mitochondrial calcium concentration and increased H_2O_2 induced apoptosis were found in fibroblasts derived from one patient as compared to controls. C19orf12 protein is a 17 kDa mitochondrial membrane-associated protein whose function is still unknown. Our *in silico* investigation suggests that, the glycine zipper motifs of C19orf12 form helical regions spanning the membrane. The N- and C-terminal regions with respect to the transmembrane portion, on the contrary, are predicted to rearrange in a structural domain, which is homologs to the N-terminal regulatory domain of the magnesium transporter MgtE, suggesting that C19orf12 may act as a regulatory protein for human MgtE transporters. The mutations here described affect respectively one glycine residue of the glycine zipper motifs, which are involved in dimerization of transmembrane helices and predicted to impair the correct localization

of the protein into the membranes, and one residue present in the regulatory domain, which is important for protein-protein interaction.

Introduction

The acronym NBIA identifies a group of clinically and genetically heterogeneous rare pathological conditions, characterized by progressive extra-pyramidal disorders and by evidence of focal iron accumulation in the brain, especially in basal ganglia, and globus pallidus, observed in MRI studies.

Recently, thanks to the identification of new disease genes in these years there has been an increasing knowledge about NBIA, but pathomechanisms underlining these disorders are still not completely clear. Up to now 10 genes have been associated with specific forms of NBIA (Kalman et al., 2012). Only two forms inherited as autosomal dominant and recessive traits respectively are caused by mutations in genes coding for proteins directly involved in iron metabolism: neuroferritinopathy due to ferritin light chain gene (*FTL)* (MIM#606159) mutation (Chinnery et al., 2007) and aceruloplasminemia linked to mutations in the ceruloplasmin gene (CP) (MIM#117700) (McNeill et al., 2008).

The other forms with autosomal recessive or X-linked transmission are due to mutations in genes (Rouault, 2013) coding for proteins with a variety of functions including: Coenzyme A biosynthesis, fatty acid metabolism, autophagy, and still unknown roles. This is the case for the *C19orf12* gene, coding for a mitochondrial membrane protein, which mutations are responsible for a form of

disease called MPAN for Mitochondrial membrane Protein Associated Neurodegeneration (Hartig et al., 2012). Mean age at onset is 9 years and the clinical phenotype is characterized by: progressive spastic para and tetraparesis, generalized dystonia, optic atrophy, motor axonal neuropathy, and psychiatric signs. T2-weighted MRI reveals hypointensities in the globus pallidus and substantia nigra. Mutations of *C19orf12* were also found in a patient with Parkinson disease (Hartig et al., 2012) and post mortem examination of the brain of one MPAN patient revealed Lewy bodies, tangles, spheroids, and tau pathology, indicating a possible overlap between NBIA and more common neurodegenerative diseases. There is no direct link between *C19orf12* mutations and the clinical phenotype of the patients, although preliminary evidence suggests for this gene a role in lipid homeostasis (Hartig et al., 2012). Recently, a Drosophila model (Iuso et al., 2014) has been generated, which shows neurological problems that can resemble the clinical features present in patients.

To gain insight into the functional properties of wild-type and mutant encoded proteins, corresponding to homozygous mutations Q96P and G58S, identified in two affected patients (Panteghini et al., 2012), we performed immunolocalization and confocal assays under normal and stress conditions. Since no structural information are available on *C19orf12,* we also exploited molecular modeling techniques and we predicted that the protein has transmembrane helices with glycine-zipper motifs and a soluble domain that is homologous to the N- regulatory domain of

bacterial MgtE transporter. The mutations identified in the patients are predicted to structurally destabilize both the glycines of the transmembrane zipper motif and the soluble domain, where the Q96P especially may impair the helical structure of the fourth α-helix of the homology model, which correspond to helix α6 of the bacterial domain.

Methods

Cloning Procedures and Plasmid Vectors Mutagenesis

Human *C19orf12* was cloned in the pCMV-AC-GFP (OriGene) vector containing a C-terminal green fluorescent protein. cDNA was amplified by PCR from pCMV-AC-GFP construct with primers carrying c-myc tag (underlined sequence) described below, and cloning in the pcDNA3.1(-), in order to obtain a recombinant protein with a smaller tag than the GFP-one. The cDNA was PCR amplified with these primers:

Fw: 5′-TCTGCCGCCGCGATCGCCATGGAGA-3′

Rv: 5′-CGGTTATCACAAGTCCTCTTCAGAAATGAGCTT TTGCTCGTCATCATACTGGATCTCGG-3′

The mutant versions corresponding to the G58S and Q96P were obtained by site directed mutagenesis (QuikChange II Site-Directed Mutagenesis Kit Stratagene). The corresponding modified primers used to generate mutated allele are as follows:

G58S Fw: 5′-GGGGGTTTGGTGGGCAGCCCACCGGGAC TCGCC-3′

G58S Rv: 5′-GGCGAGTCCCGGTGGGCTGCCCACCAA ACCCCC-3′

Q96P Fw: 5′-CCCCCTGCCGAGCCACAGAGGCTCTTTA ACGAAGCC-3′

Q96P Rv: 5′-GGCTTCGTTAAAGAGCCTCTGTGGCTCG GCAGGGGG-3′

We use also a vector containing the mkate2 red fluorescent protein (Envrogen) additionally to the GFP in order to perform live imaging experiments. Cloning Procedures and Plasmid Vectors pmKate2-N-c19orf12 was obtained as follows. The two original plasmids pCMV6-AC-GFP and pmKate2-N contained appropriate restriction sites to allow cloning in the EcoRI-XhoI for the first one and EcoRI-SalI for the second one. XhoI and SalI produce compatible cohesive ends and produce recleavable ligation products. All cloned fragments were sequenced to check the absence of mutations. Restriction-enzyme digestions, *Escherichia coli* transformation, and plasmid extractions were performed with standard methods.

Cell Culture, Transient Transfection, Stable Transduction

HeLa and HEK-293 cells were grown in Dulbecco's modified Eagle's medium (DMEM) (Euroclone), supplemented with 10% fetal bovine serum (FBS). Cells were seeded 36 h before transfection onto round glass coverslips for imaging or 13-mm diameter petri dishes for aequorin experiments, or in 10-cm petri dishes for immunoblot and fractionation experiments. Cells were allowed to grow to 50% confluence, then transfected with a

standard calcium phosphate procedure (Sambrook and Russell, 2006) and used in the experiments 36-h post-transfection.

Quantitative Colocalization Analysis

HeLa cells were co-transfected with wild-type or mutant C19orf12 fused in frame with mkate2 fluorescent marker and with the ER marker GFP-Sec61-β. Thirty six hour after transfection, cells were stained with the mitochondrial dye Mitotracker Deep Red 200 nM in PBS for 10 min at 37°. After washing cells were imaged with and LSM510 confocal microscope equipped with a Plan-Apochromat 63X/1.4 n.a. Oil objective and acquired with a pixel size of 142 nm.

Live Imaging

HeLa cells were co-transfected with GFP-tagged C19orf12 wild-type or mutant chimeras and the mitochondrial marker mtDsRed using calcium phosphate method. Thirty six hour after transfection, time-lapse recording were performed with a Nikon Swept Field Confocal equipped with CFI Plan Apo VC60XH objective (numerical aperture, 1.4) (Nikon Instruments, Melville, NY, USA) and an Andor DU885 electron multiplying charge- coupled device (EM-CCD) camera (Andor Technology Ltd, Belfast, Northern Ireland), the overall image sampling was below the resolution limit (X and Y pixel size: 133 nm). Coverslips were placed in an incubated chamber with controlled temperature, CO2 and humidity; images were then acquired with a differential frequency during the experiment: cells were placed in 1 mM Ca2+ KRB and

basal fluorescence images were acquired for 5 min; then cells were stimulated with H2O2 (500 μM final), and fluorescence images were acquired for 1 h and 30 min.

Image Analysis

Acquired images were then analyzed by using open source software Fiji. Images were corrected for spectral bleedthrough using the Spectral Unmixing plugin (available at http://rsbweb.nih.gov/ij/plugins/spectral-unmixing.html). Then, single cells were analyzed, and, for each of those, the Manders' overlap coefficient was obtained using the JACOP plugin (available at http://rsb.info.nih.gov/ij/plugins/track/jacop.html).

Mitochondria Preparation and Fractionation

Isolated mitochondria from cultured cells were obtained according to the protocol described (Fernandez-Vizarra et al., 2010).

Isolated mitochondria were resuspended in 100 ml of potassium phosphate buffer [(PP) buffer, 20 mM, pH 7.8, KCl 150 mM] and sonicated 10 s for three times at 10 Amp. The suspension was centrifuged at 164000 g for 30 min at 48C. Supernatant (mitochondrial matrix and inter-membrane space) was collected, and pellet (mitochondrial membranes) was resuspended in 100 ml of PP buffer.

MAM and ER Fraction Preparation

Hek cells (Wieckowski et al., 2009) were harvested, washed in phosphate-buffered saline medium, pelleted by centrifugation at 500 × g for 5 min, resuspended in homogenization buffer (0.25 M sucrose and 10 mM Hepes pH 7.4) and gently disrupted by dounce homogenization. The homogenate was centrifuged twice at 600 × g for 5 min to remove cellular debris and nuclei, and the supernatant was centrifuged at 10.300 × g for 10 min to pellet crude mitochondria. The resultant supernatant was centrifuged at 100.000 × g for 1 h in a Beckman 70 Ti rotor at 40C to pellet microsomes, which were resuspended in homogenization buffer. The mitochondrial pellet, resuspended in isolation medium (250 mM mannitol, 5 mM Hepes (pH7.4), and 0,5 mM EGTA) was layered on top of 8 ml of Percoll medium [225 mM mannitol, 25 mM Hepes (pH 7.4), 1 mM EGTA, and 30% Percoll (v/v)] in a 10-ml polycarbonate ultracentrifuge tube and centrifuged for 30 min at 95.000 × g. A dense band containing purified mitochondria, recovered approximately 3/4 down the tube, was removed, diluted with isolation medium, washed twice by centrifugation at 6.300 × g for 10 min to remove the Percoll, and finally resuspended in isolation medium. MAM, removed from the Percoll gradient as a diffuse white band located above the mitochondria, were diluted in isolation medium and centrifuged at 6.300 × g for 10 min. The supernatant containing MAM was centrifuged at 100.000 × g for 1 h in a Beckman 70 Ti rotor, and the resulting pellet was resuspended in the homogenization buffer. The quality of the preparation was checked by western blot analysis using different

markers for the fractions obtained: IP3R was used as marker of ER, tubulin as marker of cytoplasm and the Voltage Dependent Anion Channel (VDAC) as marker for mitochondria.

Immunoblot and Immunocytochemistry Analysis

Immunoblot and Immunocytochemistry Analysis Thirty micrograms of proteins were used for each sample in denaturing sodium dodecyl sulfate–polyacrylamide gel electrophoresis (SDS–PAGE). Western blot analysis was performed as described (Tiranti et al., 1999), using the ECL-chemiluminescence kit (Amersham) according to the manufacturer's protocol.

Antibodies

For immunodetection of the C19orf12 protein, western-blot analysis with a antisera specific for C19orf12 (1:1000) was performed, as previously described (Hartig et al., 2012). An anti-Myc monoclonal antibody (OriGene) was used at a final concentration of 1μg/ml. An anti-NADH dehydrogenase ubiquinone 1 alpha subcomplex subunit 9 (NDUFA9) antibody was used (Invitrogen) at final concentration of 0.5 μg/ml. A mouse monoclonal anti-b-TUBULIN antibody was used at a final concentration of 1 μg/ml (Sigma-Aldrich). An anti-ethylmalonic encephalopathy 1 rabbit polyclonal antibody was used at 1:2000 dilution (Tiranti et al., 2004). An anti-VDAC (1:3000) from Abcam (Cambridge, UK). An anti-IP3R3 (1:300) from BD Biosciences (San Jose, CA, USA). Secondary anti-rabbit and anti-mouse antibodies were used at 1:7000 and 1:5000 dilutions, respectively.

Automated Nuclei Count Analysis

Fibroblasts were seeded at 50,000 cells on a 25-mm coverslip, allowed to grow for 48 h and then treated with H2O2. Coverslips were stained with 10 μM Hoechst, placed in an incubation chamber with a controlled temperature and mounted on an Axiovert 200 M microscope equipped with a motorized stage. Nuclei were acquired with a 10x Fluar objective (Zeiss) and a CoolSnap HQ CCD camera. Twenty random fields were acquired with the random stage scan tools in MetaMorph and analyzed with the nuclei count application.

Autophagy Induction and Inhibition

Twenty four hours after seeding, cells were extensively washed with PBS to remove any traces of the previous medium and then exposed to EBSS (Sigma-Aldrich) or to NH4Cl 2 mM for 3 h at 37◦C and with controlled humidity and CO_2.

Autophagosomes Count

HeLa cells were seeded as previously stated then transfected with a mix of LC3-EGFP cDNA in pcDNA3 and C19orf12-mKate2 or pmKate2 using the transfection procedure previously described. Thirty six hours after transfection cells were stained with Hoechst 1 μM then imaged with an Axiovert 200 M microscope equipped with a motorized stage and a CoolSnap HQ CCD camera. Ten random fields were acquired using a Zeiss 40X water immersion lens (N.A. 1.2). Images were then processed and autophagosomes

counted using a custom made pipeline for the open source software Cell Profiler (Carpenter et al., 2006).

Aequorin Measurements

Cells grown on 13 mm round glass coverslips at 50% confluence were transfected with the mitochondria targeted aequorin. All aequorin measurements were carried out in 1 mM Ca2+ KRB buffer (NaCl 135 mM, KCl 5 mM, MgSO4 1 mM, K2HPO40.4 mM, Glucose 5.5 mM, HEPES 20mM). Agonists and other drugs were added to the same medium, as specified in the figure legends. Experiments were stopped by lysing the cells with 100 μM digitonin in hypotonic Ca2+-rich solution (10 mM CaCl2 in H2O), thus discharging the remaining aequorin pool. The light signal was collected and calibrated into [Ca2+] values, as previously described (Bonora et al., 2013).

Molecular Modeling

The prediction of the transmembrane region has been carried out by MEMSAT3 (Jones, 2007) and its secondary structure propensity by McGuffin et al. (2000). The sequence of the predicted soluble regions of *C19orf12* (*C19orf1*1−40and *C19orf12*80−151) was used as a target sequence for homology modeling. The model was obtained by Modeller version 9.11 (Eswar et al., 2006) using the structure of its closer homolog, i.e., the Mg2+ transporter belonging to the MgtE class isolated from *Thermus thermophilus* (PDB entry 2yvy, chain A, residues 31–134, resolution 2.30 Å, (Hattori et al., 2007) as a template.

C19orf12 shares 26% of sequence identity and 56% of sequence similarity with the template. The guide alignment for the prediction has been derived by HHPred (Söding et al., 2005) and then manually corrected to improve the match between the secondary structural elements of the template and the predicted secondary structural elements of the target, as well as to improve local sequence identity (Supplementary Figure 3). Model quality has been evaluated by AIDE program (Mereghetti et al., 2008).

Results

Wild-Type and Mutants C19orf12 Sub-Cellular Localization in Native Conditions

Prediction based on the amino acid sequence of human C19orf12 and fractionation experiments indicated that it was a mitochondrial membrane-bound 17-kDa protein (Hartig et al., 2012).

To demonstrate sub-cellular localization we performed Western-blot analysis on HeLa cells transfected with MYC- tagged *C19orf12* cDNA. Western-blot analysis showed that wild- type *C19orf12* gene product was present into the mitochondrial membranes but also in the lysate and cytosol (**Figure 1A**).

Because of its putative function in lipid metabolism (Hartig et al., 2012) we reasoned that the protein could have additional sub-cellular localizations. To demonstrate this we isolated different HEK293 fractions containing: crude mitochondria, pure

mitochondria, membrane associated mitochondria (MAM), and ER.

Western-blot analysis of the different sub-cellular fractions using a specific C19orf12 antibody, indicated that the wild-type protein was present in both mitochondria and ER (**Figure 1B**) under naïve condition. Moreover, a small fraction of the protein was also detected in the MAM, which represent physical association between mitochondria and endoplasmic reticulum important for the transport of phospholipids (Patergnani et al., 2011; Marchi et al., 2014).

Antibodies specific to proteins known to be located into different sub-cellular compartments were used as controls. In particular, Inositol 3 Phosphate receptor 3 (IP3R3) was used as marker of ER, tubulin as marker of cytoplasm and the VDAC as marker for mitochondria.

To understand the localization of the mutant C19orf12 proteins, we performed Western-blot analysis on HeLa cells transfected with *C19orf12* versions, carrying the point mutations G58S and Q96P. The level of overexpression of Myc-tagged versions in relation to endogenous C19orf12 was evaluated by Real-time PCR and an histogram is reported in Supplementary Figure 1.

In the presence of G58S mutation, located in the predicted transmembrane domain, the mutant protein is also found in the mitochondrial matrix (**Figure 1C**). On the contrary the Q96P mutation has no effect on the localization of the protein, which is mainly present in the mitochondrial membranes (**Figure 1D**) as observed for the wild-type protein.

Wild-Type and Mutants C19orf12 Live Imaging Analysis

To further corroborate the data obtained by Western-blot we performed experiments of live imaging in cells transfected with mkate2-tagged wild-type C19orf12, G58S, and Q96P mutant versions.

Cells transfected with the wild-type displayed a network-like intracellular staining with small tubular structures resembling the ER tubules and thicker structures similar to mitochondria (**Figure 2**). This localization was confirmed by confocal colocalization microscopy. mKate2 signal in fact display significant colocalization with the ER marker GFP–Sec61-β and also with the mitochondrial marker mitotracker Deep Red (as indicated by the high values of Pearson's and Mander's coefficients representing respectively the correlation between the two signals and the proportion of mKate2 signal overlapping with mitochondria or ER). The G58S presented with a predominant cytosolic distribution that generates asymmetric behaviors in the colocalization indexes (**Figure 2**). Differently from what observed with the wild-type chimera, the Q96P displayed a vesicles pattern with a partial co-localization vs. the mitochondrial and ER compartments (as displayed by a reduction in the Pearson's coefficients) (**Figure 2**). Overall, the colocalization experiment confirms the data obtained by western-blot analysis (**Figure 1**) on different sub-cellular fractions.

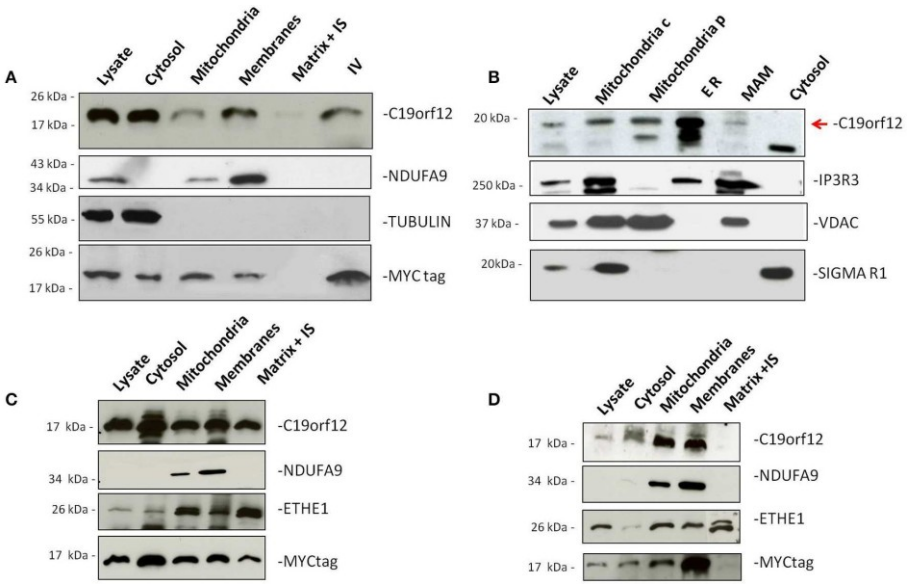

FIGURE 1 | Subcellular localization of wild-type and mutant C19orf12. HeLa cells transfected with wild-type C19orf12MYC construct and mutant versions G58S−C19orf12MYC construct (C), and Q96P−C19orf12MYC construct (D), were harvested to obtain mitochondria and other fractions. Equal amount of proteins (30 μg) from each fraction were resolved by SDS-PAGE and immunostained with antibodies against C19orf12 and MYC to specifically detect protein sub-localization. Anti-NDUFA9, TUBULIN, and ETHE1 were used as control of mitochondrial membranes, cytosol fractions and mitochondrial matrix respectively. (B) Detection of naïve C19orf12 (red arrow) by immunoblotting in HEK 293 cells fractionation. The lower band is probably an unspecific signal. Mitochondria c, crude mitochondria; Mitochondria p, pure mitochondria; ER, endoplasmic reticulum; MAM, mitochondria-associated membrane. IS, Intermembrane space. IV, *In vitro* translation product. Anti-IP3R, VDAC, and Sigma-1R were used as ER, mitochondria and MAM markers respectively

Response to Oxidative Stress

To test response to oxidative stress we treated cells transfected with wild-type and mutant C19orf12 GFP-tagged versions, with 500 μM H2O2 for 80 min and we followed the cellular localization of the protein by live imaging during time. After 30 min from H2O2 addition, we observed that the wild-type changed its

localization pattern from reticular to cytosolic and generated bright aggregates in proximity to the mitochondrial network (**Figure 3**). In addition, after persistent exposure to oxidative stress, it generates bright aggregates that partially colocalize with mitochondrial network (**Figure 3B**).

On the contrary, both mutant G58S (**Figure 4**) and Q96P (**Figure 5**) versions display minor redistribution as indicated by the variation in the Pearson's coefficient. Only the mutant Q96P displayed a significant increase in Pearson's coefficient that remains in any case lower then 0.5, usually considered as threshold for a relevant correlation (Bolte and Cordelières, 2006) suggesting that this mutant increases its cytosolic distribution without affecting dramatically its mitochondrial localization.

We also tested apoptotic cell death after H2O2 treatment and we observed that fibroblasts derived from the patient carrying the G58S change were more sensitive to treatment and showed a high percentage of cells death as compared to two control fibroblasts (**Figure 6**). We could not test the Q96P mutation since patient' fibroblast were not available.

Analysis of Mitochondrial Ca2+ Homeostasis

In order to measure mitochondrial Ca2+ handling (Marchi et al., 2014) in controls and patient-derived fibroblasts we carried out mitochondrial [Ca2+] ([Ca2+]m) measurements using the mitochondrial-targeted aequorin probe (Bonora et al., 2013). To this end we stimulated the cells with an agonist, ATP, acting on receptors coupled, through Gq proteins, to the production of

inositol 1,4,5 trisphosphate (IP3) and in turn to the opening of the IP3 receptor. Both in control and cells harboring the G58S mutation, ATP stimulation caused a rapid rise in [Ca2+]m followed by a gradually declining sustained plateau. In patient-derived fibroblasts, the [Ca2+]m increases evoked by stimulation with ATP were significantly greater than in controls (**Figure 7**

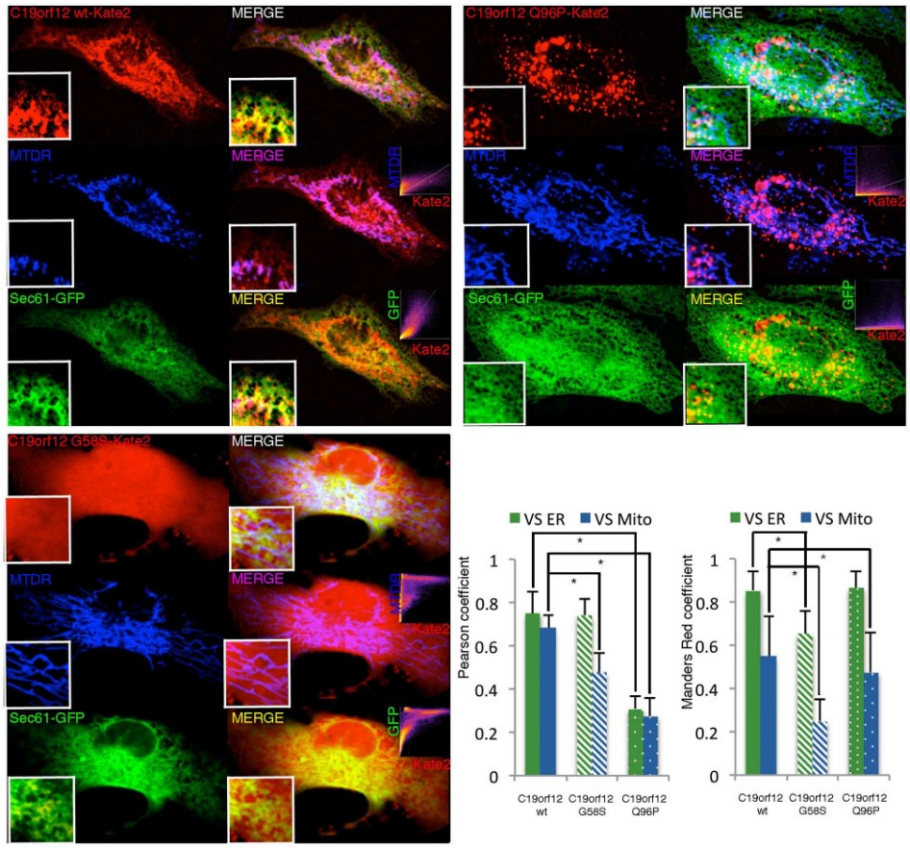

FIGURE 2 | Intracellular localization of wild-type and mutant C19orf12-mKate2 fusion protein. Representative HeLa cells overexpressing wild-type C19orf12-mKate2 (red signal) or mutant variants G58S and Q96P. C19orf12-mKate2 colocalization with mitochondria (blue signal) or ER (green signal) is represented by two colors image merging of kate2 vs. mitochondrial (magenta signal) or vs. ER (yellow signal). For each merging the relative colocalization scatterplot is inserted as inset on bottom right corner. Analysis of colocalization

is represented by Pearson's coefficient (indicating the correlation between mKate2 and mitochondria or ER signals) and by the Mander's Red coefficient (representing the proportion of mKate2 signal overlapping with mitochondria or ER). Bars: S.E.M., $*p < 0.05$.

Evaluation of Autophagy

In order to understand the nature of the aggregates formed by the wild-type protein, surrounding mitochondria, we performed colocalization study using the specific autophagy marker LC3. Confocal live imaging of LC3 vesicles and C19orf12 displayed that the C19orf12 redistribution induced by oxidative stress inversely correlated. Indeed while H2O2 induced aggregates formation it also reduces the amount of LC3 vescicles (Supplementary Figure 2A). The amount of colocalized dots increased about 50% in response to H_2O_2 exposure (Supplementary Figure 2Aiv). Overall 3D confocal microscopy display that only a minor proportion of LC3- EGFP puncta co-localize with C19orf12-mKate2 aggregates after H_2O_2 exposure (Supplementary Figures 2B). Nonetheless, the effect of C19orf12 on autophagy was evaluated. Coexpression of the autophagic reporter LC3-EGFP and of C19orf12-mKate2 displays a higher amount of EGFP punctae (autophagosomes) compared to cells expressing the autophagic marker with the pmKate2 empty vector (Figure 8A). This data was corroborated by analysis of endogenous LC3 marker. Overexpression of the EGFP tagged wild type C19orf12 induce the conversion of the autophagic marker LC3 heavy form (LC3I) to the light form (LC3II) compared to cells transfected with the empty EGFP vector, indicating the elevation of basal autophagic levels (Figure 8B). In both assays the LC3 conversion was further stimulated when inducing autophagy

by exposing cells to EBSS medium. The promoted conversion of LC3 induced by C19orf12- EGFP overexpression did not appear as a blocked autophagic flux. In fact, overexpression of this plasmid was sufficient to induce a reduction of the autophagic marker p62. This protein is usually required for autophagosome formation and its levels are expected to decrease during autophagy due to degradation of autophagosome content (Klionsky et al., 2012). Indeed treatment with NH4Cl lead to impaired acidification of autophagosomal content and inhibition of autophagosome degradation, with concomitant LC3 conversion and p62 accumulation (Figure 8C). Interestingly, H2O2 treatment inhibits the observed effect on autophagic levels (Figure 9) but caused the relocalization of C19orf12 (Figure 3). In support of this observation, the overexpression of the vectors carrying the mutant forms G58S and Q96P was unable to induce LC3 conversion suggesting a localization dependent role for C19orf12 in regulation of autophagy (**Figure 9**).

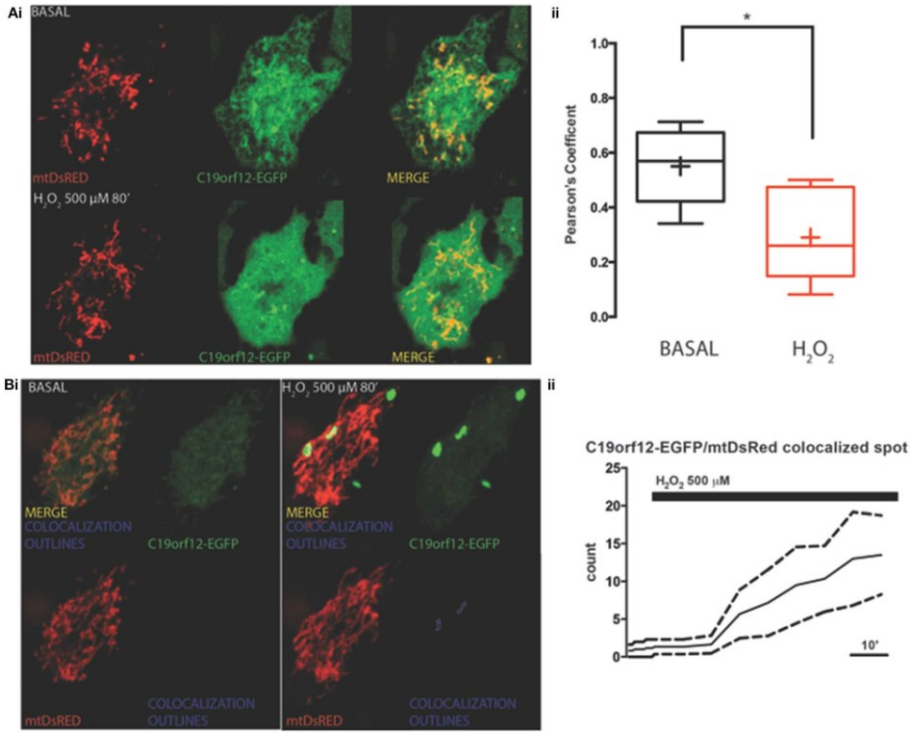

FIGURE 3 | Redistribution of C19orf12 during oxidative stress. (Ai) Representative images of HeLa cells overexpressing the C19orf12-EGFP fusion protein and the mitochondrial marker mtDsRED before (upper panel), and after (lower panel) exposure to H2O2 500 µM. (ii) Quantitative analysis of EGFP and DsRED signal before and after oxidative stress (cross, average; line, median; box, 25 and 75 percentile; bars, max and min value, $n = 8$ *$p > 0.05$). (Bi) Representative distribution of C19orf12-EGFP fusion protein in HeLa cells displayed with low contrast and the mitochondrial marker mtDsRED before (left panel) and after (right panel) exposure to H2O2

500 µM. (ii) Quantitative analysis of C19orf12-EGFP aggregates colocalizing with the mtDsRED signal during challenging with H2O2 500 µM (continuous line, mean; dashed lines, S.E.M., $n = 8$).

In Silico Analyses

We carried out both secondary structure prediction of the full *C19orf12* sequence and modeling of the predicted soluble region (*C19orf12*1−40/81−151) to both understand functional and structural properties of the wild-type protein and the effects of the mutations. C19orf12 was predicted to contains two α-helices located in the trans-membrane (TM) region (Supplementary Figure 3) rich in glycine residues, of which several have been found mutated in MPAN patients: G58S (Panteghini et al., 2012), G53R, G65E, G69R, (Landouré et al., 2013) *C19orf12* contains in the transmembrane helix glycine zipper motifs, (GxxxGxxxG) (Kruer et al., 2014). The most significant glycine zipper patterns in proteins that have been reported so far are (G,A,S)XXXGXXXG and GXXXGXXX(G,S,T) (Kim et al., 2005). The first motif (AXXXGXXXG) corresponding to the sequence 50AFVGGLVGG58 where both G53R and G58S mutations occur is located in close proximity to the first TM α-helix. The second motif 61GLAVGGAVGGLLG73 is longer and contains two of those repeats, with the mutations G65E and G69R. The N- and C-terminal residues (C19orf121−41/77−151) are predicted to rearrange in a soluble three-dimensional (3D) domain homologous to the N-regulatory domain of the bacterial Mg2+ transporters of the MgtE (Maguire, 2006; Payandeh et al., 2013). In the MgtE transporters, this domain forms a right-handed superhelical structure that includes 10 helices per two turns.

Our model does not provide a reliable prediction for the first 14 amino acids of *C19orf12*, which would correspond to the first two helices of the right-handed superhelical motif due to poor sequence similarity

with known structures of MgtE-like transporter. The rest of the domain is well conserved with respect to the bacterial homologs and in this region the Q96P is located in the middle of one of the α helices (corresponding to the α6 of the bacterial N-domain) and well packed within the domain (Figure 10). It is a mutation from a polar residue to a proline, which is a well-known helix-breaker. *FoldX* (Schymkowitz et al., 2005) energy was used to estimate the free-energy changes upon Q96P mutation. In particular, the changes in protein stability upon the mutation were estimated as the difference (66G) between the free energies of unfolding (6G) of the mutant and the wild-type variant. 66G values above 1.6 kcal/mol are expected to significantly affect stability because they correspond to twice the standard deviation of *FoldX* (Schymkowitz et al., 2005) Q96P mutation is predicted to impair protein stability of 5.4 ± 0.3 kcal/mol, (Guerois et al., 2002) suggesting a loss

of protein stability upon this mutation In the model structure,

Gln96 is predicted to be involved in side-chain hydrogen bonds, as the one with Ser124, located in the loop than connect helices α8 and α9 (**Figure 10**). The structural rearrangement caused by Q96P mutation might influence the network of polar interactions mediated by Gln95.

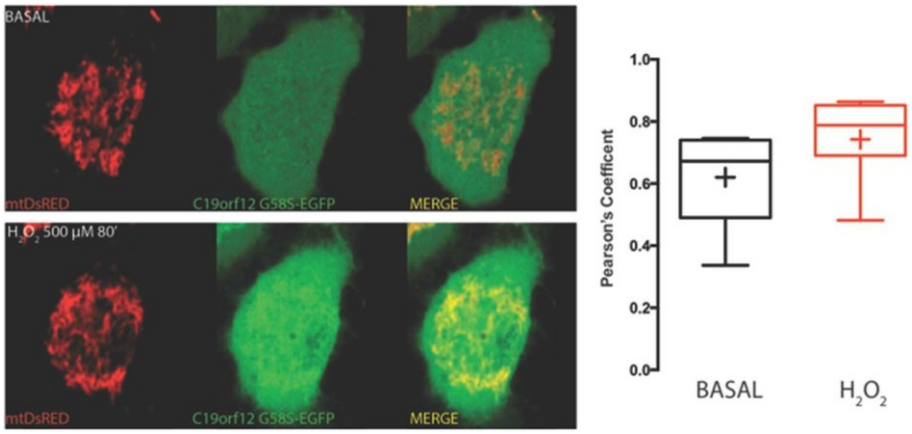

FIGURE 4 | Redistribution of C19orf12 G58S mutant during oxidative stress. Representative HeLa cells overexpressing the C19orf12 G58S-EGFP fusion protein and the mitochondrial marker mtDsRED before (upper panel) and after (lower panel) exposure to
H2O2 500 µM. Quantitative analysis of EGFP and DsRED signal before and after oxidative stress (cross, average; line, median; box,
25 and 75 percentile; bars, max and min value, $n = 8$) is shown on the right

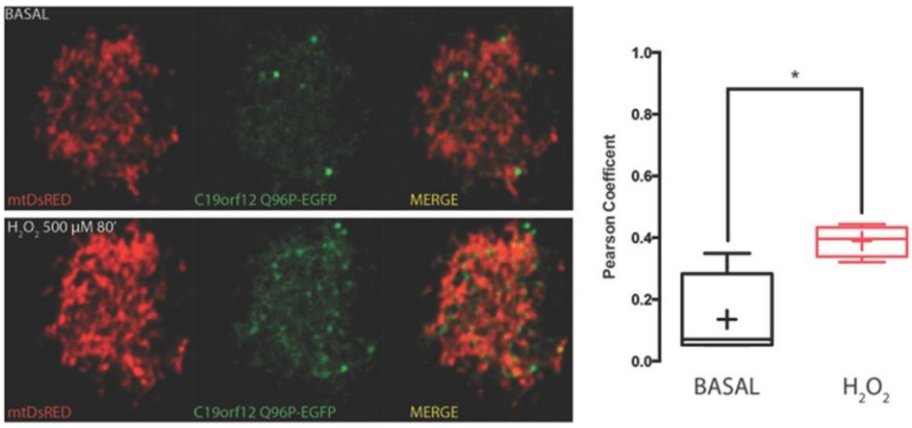

FIGURE 5 | Redistribution of C19orf12 Q96P mutant during oxidative stress. Representative HeLa cells overexpressing the C19orf12 Q96P-EGFP fusion protein and the mitochondrial marker mtDsRED before (upper panel) and after (lower panel) exposure to
H2O2 500 µM. Quantitative analysis of EGFP and DsRed signal before and after oxidative stress (cross, average; line, median; box, 25 and
75 percentile; bars, max and min value, $n = 8$, *, $p > 0.05$) is shown on the right.

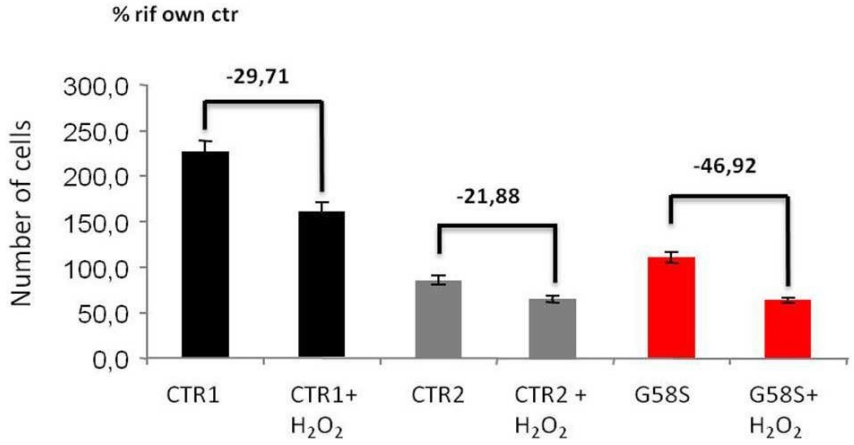

FIGURE 6 | Fibroblasts with C19orf12 mutation are more sensitive to cell death. Human fibroblasts were treated with Hydrogen Peroxide (2 mM H2O2 for 5 h). Apoptosis was evaluated using an automated nuclei count analysis. Numbers above bars indicate the percentage of cell death in the presence of H2O2 as compared to the corresponding untreated sample.

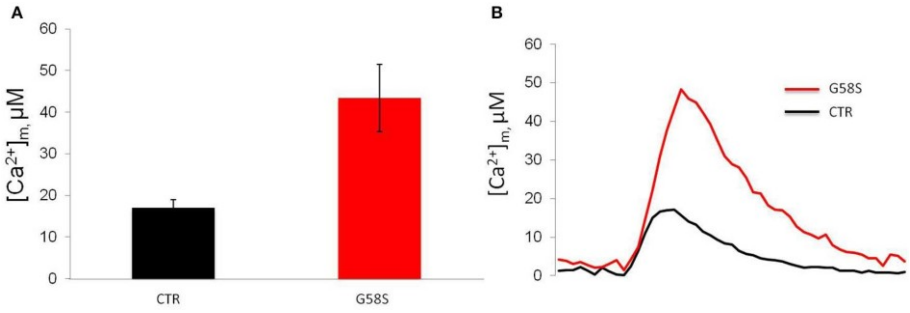

FIGURE 7 | Fibroblasts with C19orf12 mutation displayed increased Ca2+ mobilization. (A) Mitochondrial Ca2+ responses to agonist stimulation (100 µM ATP) measured in human fibroblasts. Graphs show
quantification of mitochondrial Ca2+ from three independent experiments.
(A) Representative traces of Ca2+ responses. CTR [Ca2+]m peak 17. 0 ±1.96 µM; G58S [Ca2+]m peak 43. 4 ± 8.09 µM

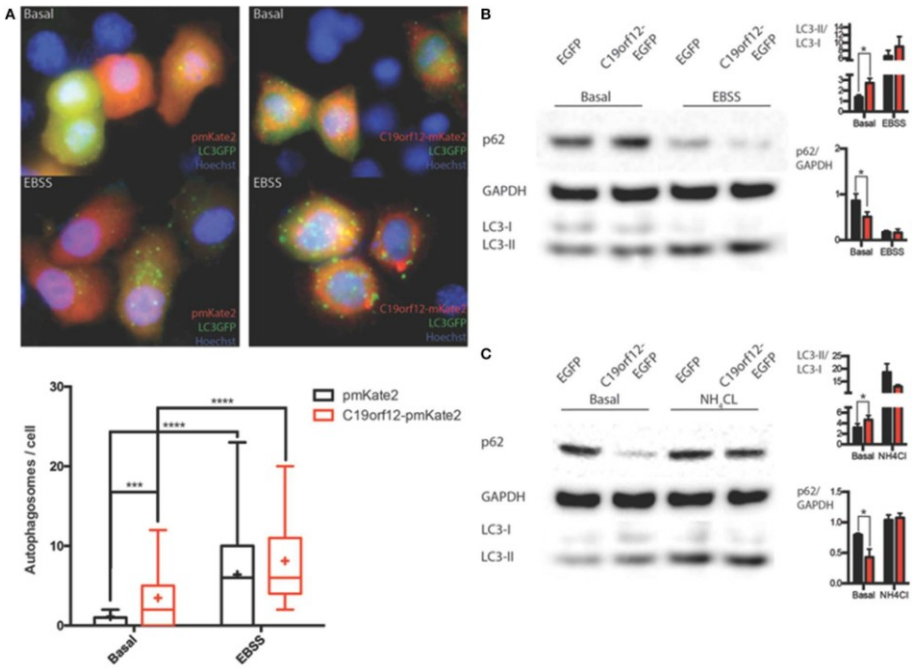

FIGURE 8 | Analysis of autophagy during C19orf12 wild-type overexpression. Representative images of HeLa cells overexpressing C19orf12-mKate2 or empty pmKate2 simultaneously with the autophagic marker LC3-EGFP (A) in basal condition or after exposure to EBSS. In the lower panel quantification of autophagosome counts is displayed (cross, average; line, median; box, 25 and 75 percentile; bars, max and min value, $n = 8$, ***$p > 0.005$, ****$p > 0.001$). (B) Representative western
blot analysis of autophagic markers LC3 and p62 in HeLa cells overexpressing C19orf12-EGFP or EGFP empty vector as control in basal condition or after exposure to EBSS (bars, S.E.M.; $n = 4$; *$p > 0.05$). (C) Representative western blot analysis of autophagic marker LC3 and p62 in HeLa cells overexpressing C19orf12-EGFP or EGFP empty vector as control in basal condition or after exposure to NH4Cl 2mM (bars, S.E.M.; $n = 4$; *$p > 0.05$

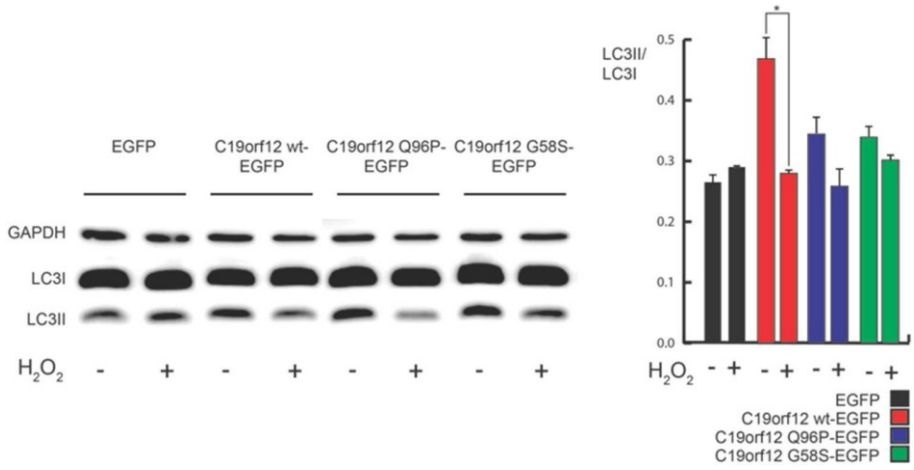

FIGURE 9 | Analysis of autophagy during C19orf12-EGFP wild-type and mutants overexpression. Representative western blot analysis of autophagic marker LC3 in HeLa cells overexpressing C19orf12-EGFP, C19orf12 G58S-EGFP, C19orf12 Q96P-EGFP, or EGFP empty vector as
control (left panel). Densitometry of light LC3 chain (LC3II) bands normalized on heavy LC3 chain (LC3I) bands is shown (right panel). Analysis was performed in basal condition or after stimulation with 500 µM H2O2 for
80 min (bars, S.E.M.; $n = 4$, $*p > 0.05$)

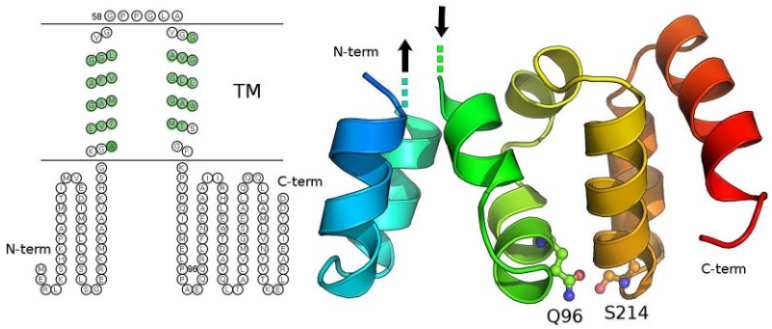

FIGURE 10 | Secondary and tertiary structure of C19orf12. Left panel: The prediction of transmembrane regions carried out with MEMSAT is illustrated and the residues of the transmembrane region, which are predicted in helical structures by PSI-Pred are highlighted in green. Right panel: The three-dimensional (3D) model of the C19orf12 domain homologous to the MgtE N-domain is shown in cartoon. The mutation site Gln96 and the residues Ser214 are shown as sticks and spheres. The protein is shown with shade of colors from blue to red, from the N- to the C-terminal extremity, respectively. The dots and the arrows illustrate the regions that are expected to connect the domain to the membrane. Gly58 is not reported since a reliable 3D model is not available for the transmembrane domain

Discussion

C19orf12 was reported to code for a mitochondrial membrane protein probably involved in lipid metabolism (Hartig et al., 2012). We here demonstrated that C19orf12 protein is not only present in mitochondria but also in ER and MAM. These are zones of close contact between ER and mitochondria, which support communication between the two organelles as concerning lipid transfer and Ca2+ ions exchange. This activity regulates several processes including: ER chaperone- assisted folding of newly synthesized proteins, modulation of mitochondria-localized dehydrogenases involved in ATP-producing Krebs cycle reactions, activation of Calcium- dependent enzymes that execute cell death programs (Berridge, 2002). We observed that the G58S mutant protein was also present into the mitochondrial matrix and we reasoned whether this different sub-cellular localization could also affect its functionality. The C19orf12 protein belongs to the clan of glycine zipper containing membrane domains (Kim et al., 2005). The majority of C19orf12 mutations are clustered in a functional region, which is crucial for this superfamily of proteins and is characterized, in the TM regions, by long and repeated glycine-zipper motifs, generally GxxxGxxxG. This is a common motif in several multimeric known membrane channel structures, where the glycine faces are in direct contacts (Kim et al., 2005). Notably, this pattern is statistically over- represented in membrane proteins in general (Kim et al., 2005). It has been indeed proposed to be the driving force for right-handed packing against a neighboring helix. It has also been suggested to play a crucial role in gating mechanisms (Kim et al.,

2005). The glycine zipper motifs of C19orf12 suggest that they are involved in the interaction between the two TM helices of this protein, even if we cannot rule out also a putative involvement in homo-dimerization. Mutations of the glycines of the glycine-zipper motif to charged or polar residues, as observed in the mutant C19orf12 patients, were likely to impair the correct localization of the protein in the membrane. These bioinformatics predictions fully agreed with the experimental data obtained by western-blot investigation. Indeed, we observed a prevalent cytosolic localization of the mutant G58S protein, while the fraction present in mitochondria was also found in the matrix, indicating that the protein was not tightly bound to the membrane.

Interestingly, glycine zipper motifs have been found in Ap and PrP, which are associated with Alzheimer's and prion diseases. A neuropathological hallmark of both Alzheimer's disease and spongiform encephalopathies includes the formation of deposits in the brain such as amyloid plaques, glial responses and neurofibrillary tangle (Jeffrey, 2013). It is important to notice that histopathological examination of the brain from a single MPAN patient also revealed the presence of Lewy bodies, tangles, spheroids, and tau pathology (Hartig et al., 2012), suggesting a possible common pathological role for the motif in these neurodegenerative disorders We predicted that C19orf12 soluble domain is homologous to the N-terminal regulatory domain of bacterial MgtE transporters. The comparison of the Mg2+-free and –bound structures of a MgtE transporter (Hattori et al., 2007) and NMR experiments (Imai et al., 2012) showed a rearrangement of the N-domain upon Mg2+-interaction. Moreover,

MgtE variants lacking the N-terminal subdomains showed a reduced Mg2+-dependent inhibition and an increased open probability, implicating this subdomain in MgtE function and regulation (Hattori et al., 2009), acting as a sensor of Mg2+ concentration. In eukaryotic organisms, MgtE-like genes belong to the SCL41 family and their precise role is unknown (Fleig et al., 2013; Schweigel- Röntgen and Kolisek, 2014). Interestingly, the N-terminal regulatory domain of bacterial MgtE is missing in SLC41-A1, thus implying that the eukaryotic transporters evolved different mechanisms of regulation (Schweigel-Röntgen and Kolisek2014). The homology of the soluble portion of C19orf12 with this bacterial subdomain, and its localization in membrane, would support a function for C19orf12 as a regulatory domain of eukaryotic MgtE-like proteins, different from SLC41-A1.

In silico investigation of the Q96P predicted for this mutation to cause loss of side-chain mediated hydrogen bonds and to affect the correct architecture of a central α-helix in the 3D structure of the C19orf12 soluble domain homologous to the N-terminal regulatory domain of bacterial MgtE transporters. This suggests a possible role of the α domain in the interaction and regulation of C19orf12 protein with human MgtE-like transporters, acting as a regulatory protein.

Interestingly, deficiency of systemic and intracellular magnesium (Mg) has long been suspected to contribute to the development and progression of Parkinson's and other neurodegenerative diseases, although the molecular mechanism is still unknown (Kolisek et al., 2013).

To gain insight into the pathogenic role of C19orf12 in MPAN we performed *in vitro* investigations by challenging the cells with stressful conditions and by evaluating the response of the wild-type and mutant C19orf12 proteins. We proved that the wild-type C19orf12 protein was able to respond to oxidative stress by enriching its cytoplasmic localization and forming aggregates, which partially co-localized with mitochondria. On the contrary, both C19orf12 mutant proteins were insensitive to oxidative stress and did not form aggregates. In light of the recent observation, that the ER–mitochondria contact sites are important in autophagosome formation (Hamasaki et al., 2013) we proposed a putative role for C19orf12, in control of autophagy. In support of this hypothesis we observed that overexpression of wild-type C19orf12 resulted in conversion of autophagic marker LC3 and reduction of levels of p62. On the contrary, induction of delocalization by oxidative stress results in reduction of autophagy LC3 conversion. Interestingly, the overexpression of mutants, unable to properly gain its intracellular localization, fails to promote autophagy induction and levels of basal autophagy remain unchanged during exposure to oxidative stress.

Live imaging suggested that delocalization of C19orf12 appears related to existence of LC3-vescicles. Indeed the progressive accumulation of C19orf12 in cytoplasm and its accumulations in aggregates were concomitant with the reduction in number of LC3-EGFP vesicles. Furthermore, the amount LC3-EGFP vescicles co-localizing with C19orf12 was extremely low. Since it was reported that the marker LC3- EGFP could produce non-autophagosome related aggregates (Kuma et al., 2007), also C19orf12 aggregates co-

localizing with LC3 puncta have dimension larger then 1.5 μm (average feret 1.98 μm, SEM 0.17, $n = 9$) suggesting that these were not autophagosomes. These results would therefore suggest that the C19orf12 is contemporary able to exert an inhibitory effect on apoptosis induction and a stimulatory effect on autophagy. The loss of autophagy induction observed after mutants overexpression and the increased sensitivity to apoptosis in patients-derived fibroblasts carrying mis-localized mutants, suggests that C19orf12 can induce protective autophagy at the expense of apoptosis and that this effect could be dependent on its intracellular localization.

These results suggest that C19orf12 could be involved in removal of dysfunctional mitochondria by selective autophagy (in a fashion independent on aggregates formation). Considering that MPAN disease mainly affects the brain, it is well possible that neurons carrying C19orf12 mutations, could accumulate altered mitochondria which can't be removed because of the presence of C19orf12 mutations, and could degenerate and/or eventually die. Nonetheless the present results about the role of C19orf12 in regulation of autophagy will require more detailed studies in future.

Finally, we also observed high levels of mitochondrial Ca2+ in fibroblasts derived from patients as compared to control, suggesting that the mutations altering the intracellular distribution of C19orf12 is detrimental for proper mitochondrial function and Ca2+ homeostasis. As a consequence, patient- derived fibroblasts were more sensitive to Ca2+ dependent apoptotic stimuli like H2O2 induced death as compared to control fibroblasts. We here demonstrated that C19orf12 protein involved in NBIA is located in mitochondria and also present

in the ER as previously reported (Landouré et al., 2013), and MAM. Moreover, we proposed a role for this protein as a sensor of mitochondrial damage. We also demonstrated that patients-derived fibroblasts accumulated high levels of mitochondrial Ca^{2+} and were more prone to oxidative stress induced apoptosis. Altogether these data shed new light in the field of NBIA focusing the attention on the role of mitochondria-ER connection in the transfer of essential lipids, in calcium metabolism and in autophagosome formation (Hamasaki et al., 2013), which are fundamental for the maintenance of cellular homeostasis and for determination of cell fate under pathological condition. A role of MAM has been recently proposed in another neurodegenerative disorder that is Alzheimer's disease (Schon and Area-Gomez, 2010) with the demonstration that presenilin 1 and 2 are predominantly located into these specialized structures. It is well possible that proteins such as presenilin 1 and 2 and C19orf12, can shuttle between different sub- cellular compartments depending on the cells status. Moreover, molecular homology modeling suggested a putative role for C19orf12 in regulation of magnesium transport. Magnesium homeostasis is crucial for learning and memory and has a positive effect on synaptic plasticity and density (Barbagallo et al., 2009; Slutsky et al., 2010). Moreover, magnesium and calcium work together to modulate ion channels, which open in response to nerve impulses triggering neurotransmitter release (Slutsky et al., 2004; Bardgett et al., 2005). These observations are particularly relevant in the context of a neurodegenerative disease such as NBIA, but

dedicated experiments are required to further demonstrate this hypothesis.

Acknowledgments

The financial support of Telethon GGP11088 to VT, and GGP11139B to PP, the Italian Association for Cancer Research (IG-14442 to P. and MFAG-13521 to CG); the Italian Ministry of Education, University and Research (COFIN, FIRB, and Futuro in Ricerca) to PP, and TIRCON project of the European Commission's Seventh Framework Programme (FP7/2007-2013, HEALTH-F2-2011, grant agreement No. 277984) to VT and HP are gratefully acknowledged.

Supplementary Material

The Supplementary Material for this article can be found online at: http://journal.frontiersin.org/article/10.3389/fgene.2015.00185/abstract

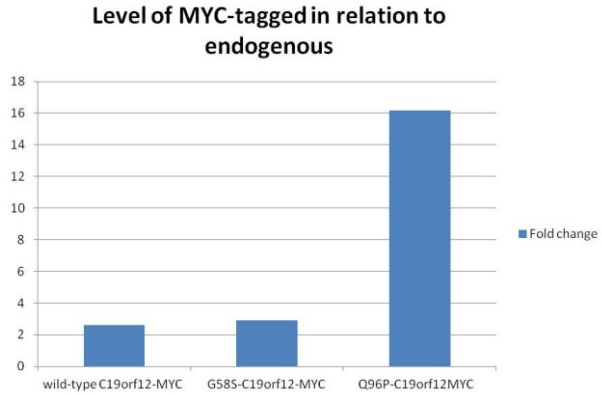

Supplementary Figure 1 | Real-time PCR to evaluate expression level of C19orf12-MYC. Expression level of overexpressed C19orf12-MYC versions (wild-type, G58S, Q96P, respectively) evaluated as fold-change in comparison to endogenous C19orf12.

Figure S2

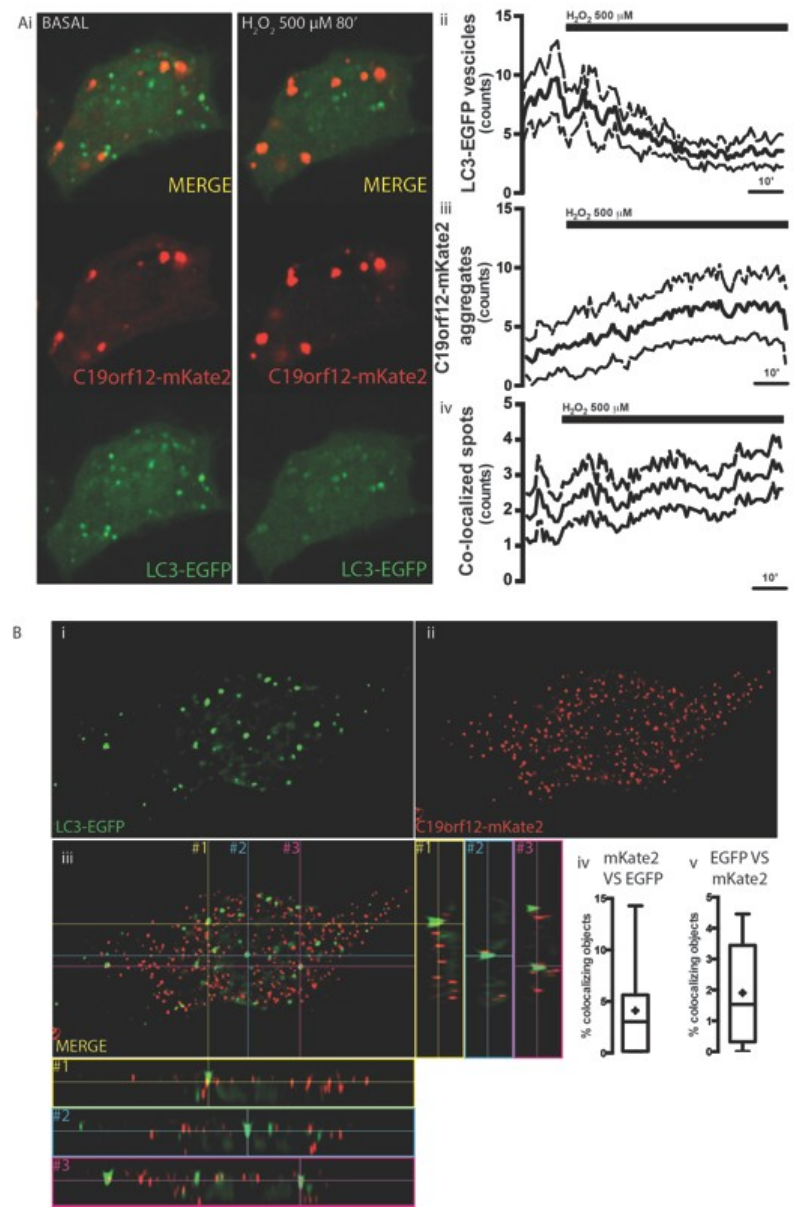

Supplementary Figure 2 | (Ai) Representative behavior of C19orf12-mKate2 aggregates and LC3-EGFP before (left panel) and after (right panel) exposure to H2O2 500 µM. Quantitative analysis of channel independent spot counts:LC3-EGFP vescicles (ii), mkate2 aggregates (iii), and colocalized spot (iv) during challenging with H2O2 500 µM (continuous line: mean, dashed lines: S.E.M., n = 8). (B) Representative 3D images of autophagic vesicles in presence of H2O2 500 µM. (i) LC3-EGFP (green), (ii) C19orf12-mKate aggregates (red), and (iii)

colocalization signal (yellow). Multiple orthogonal view of the merged signal are displayed and marked by sequential numbering. (iv) Percentage of C19orf12-mKate2 aggregates colocalizing with LC3 vescicles (v) LC3 puncta co-localizing with mKate2 aggregates (cross, average; line, median; box, 25 and 75 percentile; bars, max and min value, $n = 12$).

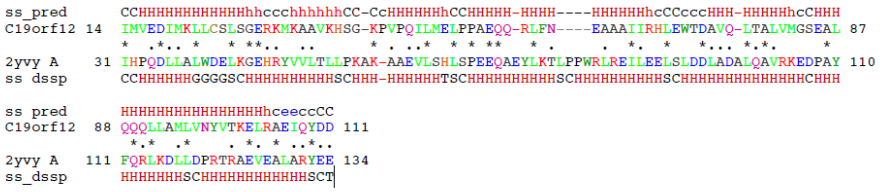

Supplementary Figure 3 | Guide alignment for homology modeling. The sequence alignment between the target (C19orf12) and the template (PDB entry 2yvy, chain A) is shown as derived by the HHPred multiple sequence alignment upon manual correction (see Materials and Methods). "∗" and "." indicates identical and similar residues, respectively.

References

Barbagallo, M., Belvedere, M., and Dominguez, L. J. (2009). Magnesium homeostasis and aging. *Magnes. Res.* 22, 235–246. doi: 10.1684/mrh.2009.0187

Bardgett, M. E., Schultheis, P. J., McGill, D. L., Richmond, R. E., and Wagge, J.R. (2005). Magnesium deficiency impairs fear conditioning in mice. *Brain Res*. 1038, 100–106. doi: 10.1016/j.brainres.2005.01.020

Berridge, M. J. (2002). The endoplasmic reticulum: a multifunctional signaling organelle. *Cell Calcium* 32, 235–249. doi: 10.1016/S0143416002001823

Bolte, S., and Cordelières, F. P. (2006). A guided tour into subcellular colocalization analysis in light microscopy. *J. Microsc*. 224(Pt 3), 213–232. doi: 10.1111/j.1365- 2818.2006.01706.x

Bonora, M., Giorgi, C., Bononi, A., Marchi, S., Patergnani, S., Rimessi, A., et al. (2013). Subcellular calcium measurements in mammalian cells using jellyfish photoprotein aequorin-based probes. *Nat. Protoc.* 8, 2105–2118. doi: 10.1038/nprot.2013.127

Carpenter, A. E., Jones, T. R., Lamprecht, M. R., Clarke, C., Kang, I. H., Friman, O., et al. (2006). CellProfiler: image analysis software for identifying and quantifying cell phenotypes. *Genome Biol*. 7, R100. doi: 10.1186/gb-2006-7-10- r100

Chinnery, P. F., Crompton, D. E., Birchall, D., Jackson, M. J., Coulthard, A., Lombès, A., et al. (2007). Clinical features and natural history of neuroferritinopathy caused by the FTL1460InsA mutation. *Brain* 130(Pt 1), 110–119. doi: 10.1093/brain/awl319

Eswar, N., Webb, B., Marti-Renom, M. A., Madhusudhan, M. S., Eramian, D., Shen, M. Y., et al. (2006). Comparative protein structure modeling with modeller. *Curr. Protoc. Bioinformatics* Chapter 5: Unit 5.6. doi: 10.1002/0471250953.bi0506s15

Fernandez-Vizarra, E., Ferrìn, G., Pèrez-Martos, A., Fernàndez-Silva, P., Zeviani, M., and Enrìquez, J. A. (2010). Isolation of mitochondria for biogenetical studies: an update. *Mitochondrion* 10, 253–262. doi: 10.1016/j.mito.2009. 12.148

Fleig, A., Schweigel-Röntgen, M., and Kolisek, M. (2013). Solute carrier family SLC41, what do we really know about it? *Wiley Interdiscip. Rev. Membr. Transp. Signal*. 2. doi: 10.1002/wmts.95

Guerois, R., Nielsen, J. E., and Serrano, L. (2002). Predicting changes in the stability of proteins and protein complexes: a study of more than 1000 mutations. *J. Mol. Biol*. 320, 369–387. doi: 10.1016/S0022-2836(02)00442-4

Hamasaki, M., Furuta, N., Matsuda, A., Nezu, A., Yamamoto, A., Fujita, N., et al. (2013). Autophagosomes form at ER-mitochondria contact sites. *Nature* 495, 389–393. doi: 10.1038/nature11910

Hartig, M. B., Iuso, A., Haack, T., Kmiec, T., Jurkiewicz, E., Heim, K., et al. (2012). Absence of an orphan mitochondrial protein, c19orf12, causes a distinct clinical subtype of neurodegeneration with brain iron accumulation. *Am. J. Hum. Genet*. 89, 543–550. doi: 10.1016/j.ajhg.2011.09.007

Hattori, M., Iwase, N., Furuya, N., Tanaka, Y., Tsukazaki, T., Ishitani, R., et al. (2009). Mg(2+)-dependent gating of bacterial MgtE channel underlies Mg(2+) homeostasis. *EMBO J.* 28, 3602–3612. doi: 10.1038/emboj.2009.288

Hattori, M., Tanaka, Y., Fukai, S., Ishitani, R., and Nureki, O. (2007). Crystal structure of the MgtE Mg2+ transporter. *Nature* 448, 1072–1075. doi: 10.1038/nature06093

Imai, S., Maruyama, T., Osawa, M., Hattori, M., Ishitani, R., Nureki, O., et al. (2012). Spatial distribution of cytoplasmic domains of the Mg(2+)- transporter MgtE, in a solution lacking Mg(2+), revealed by paramagnetic relaxation enhancement. *Biochim. Biophys. Acta* 1824, 1129–1135. doi: 10.1016/j.bbapap.2012.06.008

Iuso, A., Sibon, O. C., Gorza, M., Heim, K., Organisti, C., Meitinger, T., et al. (2014). Impairment of Drosophila orthologs of the human orphan protein C19orf12 induces bang sensitivity and neurodegeneration. *PLoS ONE* 9:e89439. doi: 10.1371/journal.pone.0089439

Jeffrey, M. (2013). Review: membrane-associated misfolded protein propagation in natural transmissible spongiform encephalopathies (TSEs), synthetic prion diseases and Alzheimer's disease. *Neuropathol. Appl. Neurobiol.* 39, 196-216. doi: 10.1111/nan.12004

Jones, D. T. (2007). Improving the accuracy of transmembrane protein topology prediction using evolutionary information. *Bioinformatics* 23, 538–544. doi: 10.1093/bioinformatics/btl677

Kalman, B., Lautenschlaeger, R., Kohlmayer, F., Büchner, B., Kmiec, T., Klopstock, T., et al. (2012). An international registry for neurodegeneration with brain iron accumulation. *Orphanet J. Rare Dis.* 7:66. doi: 10.1186/1750-1172-7-66

Kim, S., Jeon, T. J., Oberai, A., Yang, D., Schmidt, J. J., and Bowie, J. U. (2005). Transmembrane glycine zippers: physiological and pathological roles in membrane proteins. *Proc. Natl. Acad. Sci. U.S.A.* 102, 14278–14283. doi: 10.1073/pnas.0501234102

Klionsky, D. J., Abdalla, F. C., Abeliovich, H., Abraham, R. T., Acevedo-Arozena, A., et al. (2012). Guidelines for the use and interpretation of assays for monitoring autophagy. *Autophagy* 8, 445–544. doi: 10.4161/auto. 19496

Kolisek, M., Sponder, G., Mastrototaro, L., Smorodchenko, A., Launay, P., Vormann, J., et al. (2013). Substitution p.A350V in Na+/Mg^{2+} exchanger SLC41A1, potentially associated with Parkinsons disease, is a gain-of-function mutation. *PLoS ONE* 8:e71096. doi: 10.1371/journal.pone.0071096

Kruer, M. C., Salih, M. A., Mooney, C., Alzahrani, J., Elmalik, S. A., Kabiraj, M. M., et al. (2014). C19orf12 mutation leads to a pallido-pyramidal syndrome. *Gene* 537, 352–356. doi: 10.1016/j.gene.2013.11.039

Kuma, A., Matsui, M., and Mizushima, N. (2007). LC3, an autophagosome marker, can be incorporated into protein aggregates independent of autophagy: caution in the interpretation of LC3 localization. *Autophagy* 3, 323–328. doi: 10.4161/auto.4012

Landouré, G., Zhu, P. P., Lourenço, C. M., Johnson, J. O., Toro, C., Bricceno, K. V., et al. (2013). Hereditary spastic paraplegia type 43 (SPG43) is caused by mutation in C19orf12. *Hum. Mutat.* 34, 1357–1360. doi: 10.1002/humu. 22378

Maguire, M. E. (2006). Magnesium transporters: properties, regulation and structure. *Front. Biosci.* 11, 3149–3163. doi: 10.2741/2039

Marchi, S., Patergnani, S., and Pinton, P. (2014). The endoplasmic reticulum-mitochondria connection: one touch, multiple functions. *Biochim. Biophys. Acta* 1837, 461–469. doi: 10.1016/j.bbabio.2013.10.015

McGuffin, L. J., Bryson, K., and Jones, D. T. (2000). The PSIPRED protein structure prediction server. *Bioinformatics* 16, 404–405. doi: 10.1093/bioinformatics/16.4.404

McNeill, A., Pandolfo, M., Kuhn, J., Shang, H., and Miyajima, H. (2008). The neurological presentation of ceruloplasmin gene mutations. *Eur. Neurol*. 60, 200–205. doi: 10.1159/000148691

Mereghetti, P., Ganadu, M. L., Papaleo, E., Fantucci, P., and De Gioia, L. (2008). Validation of protein models by a neural network approach. *BMC Bioinformatics* 9:66. doi: 10.1186/1471-2105-9-66

Panteghini, C., Zorzi, G., Venco, P., Dusi, S., Reale, C., Brunetti, D., et al. (2012). C19orf12 and FA2H mutations are rare in Italian patients with neurodegeneration with brain iron accumulation. *Semin. Pediatr. Neurol.* 19, 75–81. doi: 10.1016/j.spen.2012.03.006

Patergnani, S., Suski, J. M., Agnoletto, C., Bononi, A., Bonora, M., De Marchi, E., et al. (2011). Calcium signaling around Mitochondria Associated Membranes (MAMs). *Cell Commun. Signal.* 9:19. doi: 10.1186/1478-811X-9-19

Payandeh, J., Pfoh, R., and Pai, E. F. (2013). The structure and regulation of magnesium selective ion channels. *Biochim. Biophys. Acta* 1828, 2778–2792. doi: 10.1016/j.bbamem.2013.08.002

Rouault, T. A. (2013). Iron metabolism in the CNS: implications for neurodegenerative diseases. *Nat. Rev. Neurosci*. 14, 551–564. doi: 10.1038/nrn3453

Sambrook, J., and Russell, D. W. (2006). Calcium-phosphate-mediated Transfection of Eukaryotic Cells with Plasmid DNAs. *CSH Protoc*. 2006. doi: 10.1101/pdb.prot3871

Schon, E. A., and Area-Gomez, E. (2010). Is Alzheimers disease a disorder of mitochondria-associated membranes? *J. Alzheimers Dis*. 20(Suppl. 2), S281–S292. doi: 10.3233/JAD-2010-100495

Schweigel-Röntgen, M., and Kolisek, M. (2014). SLC41 transporters-molecular identification and functional role. *Curr. Top. Membr*. 73, 383–410. doi: 10.1016/B978-0-12-800223-0.00011-6

Schymkowitz, J., Borg, J., Stricher, F., Nys, R., Rousseau, F., and Serrano, L. (2005). The FoldX web server: an online force field. *Nucleic Acids Res*. 33, W382-W388. doi: 10.1093/nar/gki387

Slutsky, I., Abumaria, N., Wu, L. J., Huang, C., Zhang, L., Li, B., et al. (2010). Enhancement of learning and memory by elevating brain magnesium. *Neuron* 65, 165–177. doi: 10.1016/j.neuron.2009.12.026

Slutsky, I., Sadeghpour, S., Li, B., and Liu, G. (2004). Enhancement of synaptic plasticity through chronically reduced Ca2+ flux during uncorrelated activity. *Neuron* 44, 835–849. doi: 10.1016/j.neuron.2004.11.013

Söding, J., Biegert, A., and Lupas, A. N. (2005). The HHpred interactive server for protein homology detection and structure prediction. *Nucleic Acids Res.* 33, W244-W248. doi: 10.1093/nar/gki408

Tiranti, V., DAdamo, P., Briem, E., Ferrari, G., Mineri, R., Lamantea, E., et al. (2004). Ethylmalonic encephalopathy is caused by mutations in ETHE1, a gene encoding a mitochondrial matrix protein. *Am. J. Hum. Genet.* 74, 239–252. doi: 10.1086/381653

Tiranti, V., Galimberti, C., Nijtmans, L., Bovolenta, S., Perini, M. P., and Zeviani, M. (1999). Characterization of SURF-1 expression and Surf-1p function in normal and disease conditions. *Hum. Mol. Genet.* 8, 2533–2540 doi: 10.1093/hmg/8. 13.2533

Wieckowski, M. R., Giorgi, C., Lebiedzinska, M., Duszynski, J., and Pinton, P. (2009). Isolation of mitochondria-associated membranes and mitochondria from animal tissues and cells. *Nat. Protoc*. 4, 1582–1590. doi: 10.1038/nprot.2009.151

Conflict of Interest Statement: The authors declare that the research was conducted in the absence of any commercial or financial relationships that could be construed as a potential conflict of interest.

Copyright © 2015 Venco, Bonora, Giorgi, Papaleo, Iuso, Prokisch, Pinton and Tiranti. This is an open-access article distributed under the terms of the Creative Commons Attribution License (CC BY). The use, distribution or reproduction in other forums is permitted, provided the original author(s) or licensor are credited and that the original publication in this journal is cited, in accordance with accepted academic practice. No use, distribution or reproduction is permitted which does not comply with these terms

CHAPTER 3

Exome Sequence Reveals Mutations in CoA Synthase as a Cause of Neurodegeneration with Brain Iron Accumulation

Sabrina Dusi 1, Lorella Valletta 1, Tobias B. Haack 2,3, Yugo Tsuchiya 4, Paola Venco 1, Sebastiano Pasqualato 5, Paola Goffrini 6, Marco Tigano 6, Nikita Demchenko 4, Thomas Wieland 3, Thomas Schwarzmayr 3, Tim M. Strom 2,3, Federica Invernizzi 1, Barbara Garavaglia 1, Allison Gregory 7, Lynn Sanford 7, Jeffrey Hamada 7, Conceicao Bettencourt 8, Henry Houlden 8, Luisa Chiapparini 9, Giovanna Zorzi 10, Manju A. Kurian 11,12, Nardo Nardocci 10, Holger Prokisch 2,3, Susan Hayflick 7, Ivan Gout 4, and Valeria Tiranti 1

1Unit of Molecular Neurogenetics –, IRCCS Foundation Neuro- logical Institute ‘‘C. Besta,’’ 20126 Milan, Italy; 2Institute of Human Genetics, Technische Universita¨t Mu¨nchen, 81675 Munich, Germany; 3Institute of Human Genetics, Helmholtz Zentrum Mu¨nchen, 85764 Munich, Germany; 4Institute of Structural and Molecular Biology, University College London, London WC1E 6BT, UK; 5Crystallography Unit, Department of Experimental Oncology, European Institute of Oncology, IFOM-IEO Campus, 20139 Milan, Italy; 6Department of Life Sciences, University of Parma, 43124 Parma, Italy; 7Department of Molecular & Medical Genetics, Oregon Health & Science University, Portland, OR 97329, USA; 8UCL Institute of Neurology and The National Hospital for Neurology and Neurosurgery, Queen Square, London WC1N 3BG, UK; 9Unit of Neuroradiology, IRCCS Foundation Neurological Institute ‘‘C. Besta,’’ 20133 Milan, Italy; 10Unit of Child Neurology, IRCCS Foundation Neurological Institute ‘‘C. Besta,’’ 20133 Milan, Italy; 11Neurosciences Unit, UCL-Institute of Child Health, Great Ormond Street Hospital, London WC1N 3JH, UK; 12Department of Neurology, Great Ormond Street Hospital, London WC1N 3JH, UK

Am J Hum Genet. 2014 Jan 2;94(1):11-22. doi: 10.1016/j.ajhg.2013.11.008. Epub 2013 Dec 19.

Abstract

Neurodegeneration with brain iron accumulation (NBIA) comprises a clinically and genetically heterogeneous group of disorders with progressive extrapyramidal signs and neurological deterioration, characterized by iron accumulation in the basal ganglia. Exome sequencing revealed the presence of recessive missense mutations in COASY, encoding coenzyme A (CoA) synthase in one NBIA-affected subject. A second unrelated individual carrying mutations in COASY was identified by Sanger sequence analysis. CoA synthase is a bifunctional enzyme catalyzing the final steps of CoA biosynthesis by coupling phosphopantetheine with ATP to form dephospho-CoA and its subsequent phosphorylation to generate CoA. We demonstrate alterations in RNA and protein expression levels of CoA synthase, as well as CoA amount, in fibroblasts derived from the two clinical cases and in yeast. This is the second inborn error of coenzyme A biosynthesis to be implicated in NBIA.

Introduction

The common pathological feature of a group of genetic disorders termed ‘‘neurodegeneration with brain iron accumulation’’ (NBIA) is brain iron overload.1 Distinct subclasses of early-onset neurodegeneration with autosomal-recessive transmission are defined by mutations in specific genes: PANK2 (MIM 606157) causes pantothenate kinase-associated neurodegeneration (PKAN);2,3 PLA2G6 (MIM 256600) causes phospholipase A2-

associated neuro- degeneration (PLAN, also known as INAD);4 FA2H (MIM 611026) causes fatty acid hydroxylase-associated neurodegeneration (FAHN);5 and C19orf12 (MIM 614297) causes mitochondrial membrane protein-associated neurodegeneration (MPAN).6,7 More recently, a distinctive form of NBIA with X-linked dominant de novo mutations in WDR45 (MIM 300894), coding for a protein with a putative role in autophagy, was reported.8,9

These genes account for ~70% of subjects with NBIA, leaving a significant fraction without an identified genetic defect. For this reason we performed exome sequence investigation in one individual with clinical presentation and neuroimaging suggestive of NBIA but without mutations in previously associated genes. By applying this approach we identified a homozygous missense mutation in COASY, coding for CoA synthase. We then performed traditional Sanger sequence analysis of a larger cohort of idiopathic NBIA cases, and we found a second individual harboring mutations in the same gene. CoA synthase is a bifunctional enzyme possessing 40PP adenyltransferase (PPAT) and dephospho-CoA kinase (DPCK) activities, catalyzing the last two steps in the CoA biosynthetic pathway.10 The enzyme is encoded by a single gene in mammals and Drosophila,11,12 although two different genes code for PPAT and DPCK activities in yeast and bacteria.13 In human there are three splice variants: COASY alpha is ubiquitously expressed and has a molecular weight of 60 kDa; COASY beta is predominantly expressed in the brain and possesses a 29 aa extension at the N terminus;14 and

COASY gamma is predicted to code for C-terminal region of CoA synthase corresponding to DPCK domain. Several studies have investigated the subcellular compartmentalization of the CoA biosynthetic pathway and have demonstrated that both PANK2, defective in the most common NBIA disorder, and CoA synthase alpha and beta are mitochondrial enzymes. PANK2 is mainly located in the intermembrane space2,15,16 whereas CoA synthase alpha and beta are anchored to the outer mitochondrial membrane by the N-terminal region17 or localized within the mitochondrial matrix.18 We here demonstrate that COASY is mainly located in the mitochondrial matrix and that the identified amino acid substitution causes instability of the protein with altered function of its enzymatic activity.

Methods

Exome and Sanger Sequencing

Informed consent for participation in this study was obtained from all individuals involved and from their parents, in agreement with the Declaration of Helsinki, approved by the ethics committee of the Fondazione IRCCS (Istituto di Ricovero e Cura a Carattere Scientifico) Istituto Neurologico C. Besta (Milan, Italy) and by the ethics committees of the other institutes participating in the screening (Germany, UK, USA).

Exome sequencing and variant filtering was performed as described previously.8 In brief, exonic DNA fragments were enriched with the SureSelect 50 Mb kit from Agilent and

sequenced as 100 bp paired-end reads on a HiSeq 2500 system from Illumina. For sequencing statistics details see Table S1 avail- able online. We predicted that causal mutations would be very rare and would alter the protein. We therefore searched for nonsynonymous variants with a frequency <0.1% in 2,700 control exomes analyzed in Munich and public databases that, given the reported consanguinity of the parents, were anticipated to be homozygous. This analysis left a total of 12 candidate genes (Table S2). The detailed list of these 12 genes is reported in Table S3. We first excluded the following genes because of the presence of additional subjects with compound heterozygous or homozygous mutations related with different clinical phenotypes: HRNR, ADAM8, BZRAP1, C17orf47, LRP1B, EVC2, KIAA1797, and CACNB1. Moreover, variants in HRNR, CACNB1, C17orf47, and KIAA1797 were predicted to be benign by PolyPhen. Four remaining genes (GUCA2A, FBXO47, COASY, and IFNW1) were potentially good candidates carrying deleterious mutations.

By performing segregation analysis of the c.265G>T homozygous variant in GUCA2A, we found that also the healthy mother (subject I-2 of family 1) and one of the healthy sisters (subject II-4 of family 1) carried this variant.

Segregation analysis of c.490A>G in IFNW1 showed that this change was present in homozygous state in the healthy mother (subject I-2 of family 1) and in two healthy sisters (subjects II-4 and II-5 in family 1). Altogether, this observation excluded both

GUCA2A and IFNW1 as potential candidate genes (see also Table S3).

FBXO47 was mainly expressed in kidney, liver, and pancreas and it was suggested to act as a tumor-suppressor gene in renal carcinoma and possibly other malignancies.19 However, because this gene carries a splice site mutation, we decided to perform sequence analysis in a subgroup of 56 NBIA-affected individuals. We did not identify any pathogenic mutation in this cohort of subjects.

Based on these data and because COASY coded for an enzyme involved in Coenzyme A biosynthesis as PANK2, we concentrated our efforts on the analysis of this gene.

RNA Extraction and Real-Time PCR

Total RNA was isolated from fibroblasts (80% confluence) with the RNeasy Mini Kit (QIAGEN). RNA quantity was measured with the Nanodrop instrument (Nanodrop Technologies). RNA was used as a template to generate complementary DNA (cDNA) by GoScript Reverse Transcriptase protocol (Promega). Reverse transcriptase products were used in real-time PCR to evaluate the expression level of COASY with the Power SYBR Green PCR Master Mix (Applied Biosystems) system. The housekeeping gene used for data normalization was GAPDH. Primer sequences are as follows: COASY, forward 5'-AGTTGCGGTTTCTCCGTTAG-3' and reverse 5'-ATCCTGGGAGGGGGAAAT-3'; GAPDH, forward 5'-

CTCTGCTCCTCCTGTTCGAC-3' and reverse 5'-ACGACCAAATCCGTTGA-3'.

Expression and Purification of Recombinant hDPCK in Bacteria

mRNA coding for human DPCK domain (COASY amino acid sequence from 355 to 564) was expressed with the N-terminal histidine-tag from pET30-a(þ) (Novagen) at 37○C in E. coli strain BL21 (DE3), after induction with 0.2 mM IPTG.

Cells were lysed by a French press in 50 mM Tris-HCl (pH 8), 0.5 M NaCl, 1% Triton X-100, 20 mM imidazole, 1 mM phenylmethylsulfonyl fluoride (PMSF), 10 mM bmercaptoethanol, and Roche Complete EDTA-free protease inhibitor cocktail. After clearing, the lysate was loaded on a Ni-NTA beads (QIAGEN) column. Bound proteins were eluted with an imidazole gradient. Fractions containing His-hDPCK were pooled, desalted, and loaded onto an anion-exchange (AE) Resource-S column (GE Healthcare) equilibrated in 50 mM Tris-HCl (pH 7.4), 2.5% glyc- erol, 20 mM bmercaptoethanol. The protein was eluted with a NaCl gradient, concentrated by ultrafiltration, and further separated by size exclusion chromatography (SEC) on a Superdex-200 column (GE Healthcare) equilibrated in 10 mM Tris-HCl (pH 7.4), 0.15 M NaCl, 2.5% glycerol, 0.1 mM EDTA, and 1 mM DTT. The entire purification scheme was carried out at 4○C.

Mitochondria and Mitoplast Isolation from Cultured Cells

Isolated mitochondria from cultured cells were obtained according to the protocol described by Fernandez-Vizarra.20

For mitoplast purification, mitochondria were dissolved in 1 ml Buffer A (MOPS 20 mM, sucrose 0.25 M [pH 7.4]). A total of 1 ml of 200 mg/ml digitonin in Buffer A was added to each sample. Samples were mixed and incubated on ice 5 min, then centrifuged 3 min at 8,000 rpm at 4○C. Supernatant was discarded and pellet dissolved in 1 ml Buffer B (MOPS 20 mM, sucrose 0.25 M, EDTA Na4 1 mM [pH 7.4]). Samples were incubated on ice for 5 min, then centrifuged at 12,000 rpm at 4○C for 3 min. Separate fractions of mitochondria and mitoplasts were also treated with 0.04 mg of proteinase K (PK) for 15 min at 4○C or 37○C; PK digestion was blocked with PMSF. In some samples of mitochondria and mitoplasts, 0.1% Triton X-100 was added followed by incubation for 15 min at 37°C.

Immunoblot Analysis

Approximately 1 3 106 fibroblasts, grown in DMEM (EuroClone) were trypsinized, centrifuged at 1,200 rpm for 3 min, and solubilized in 200 ml of RIPA buffer (50 mM Tris-HCl [pH 7.5], 150 mM NaCl, 1% NP40, 0.5% NaDOC, 5 mM EDTA) with 13 Complete Mini Protease Inhibitor Cocktail Tablets (Roche) for 40 min at 4°C. 30 mg of proteins were used for each sample in denaturing sodium-dodecyl sulfate polyacrylamide gel electrophoresis (SDS-PAGE). Immunoblot analysis was

performed as described21 with the ECL-chemiluminescence kit (Amersham).

Antibodies

A rabbit monoclonal anti-COASY antibody was used at 1:1,000 dilution (EPR8246-Abcam). A mouse monoclonal anti-b-TUBULIN antibody was used at a final concentration of 1 mg/ml (Sigma- Aldrich). Secondary anti-rabbit and anti-mouse antibodies were used at 1:2,000 and 1:7,000 dilution, respectively.

HPLC Analysis of Dephospho-CoA, CoA, and AcetylCoA

HPLC analysis was performed on recombinant wild-type and mutant DPCK proteins, on fibroblast lysates derived from control and subjects carrying COASY variants, and on isolated yeast mitochondria.

The method employed a column (Kinetex 5u C18 100A New Column 250 x 4.6 mm from Phenomenex) eluted with 100 mmol/l NaH2PO4 and 75 mmol/l CH3COONa (pH was adjusted to 4.6 by the addition of concentrated H3PO4)-acetonitrile (94:6, v/v) at a flow rate of 1.0 ml/min. The ultraviolet (UV) detector was set at 259 nm. To obtain standard solutions of 5 mM, dephospho-CoA and CoA were dissolved in 50 mmol/l KH2PO4-K2HPO4 buffer (pH 7.0). CoA and dephospho-CoA standards were eluted at approximately 4.5 and 8 min, respectively, and CoA compounds were quantified by comparison of peak areas with those of authentic standards.

In Vitro DPCK Activity

1 mg of purified wild-type or mutant protein was incubated for 2 hr at 37○C in 50 ml of reaction mixture containing 50 mM Tris-HCl (pH 8), 5 mM MgCl2, 1 mM ATP, and 0.1 mM dephospho-CoA. After incubation, sample was treated with perchloric acid (PCA) 3%, vortexed, and centrifuged at 13,000 rpm at 4○C. Trietanol- amine was added to the supernatant to a final concentration of 100 mM, and then the sample was neutralized with 5 M K2CO3.

Fibroblast Analysis

Fibroblasts, grown on 10 cm plates (approx. 80%–90% confluent), were washed with PBS and collected by trypsinization. 40 ml of ice- cold PCA (5%) was added to cells and samples were vortexed and centrifuged at 18,000 3 g for 5 min at 4○C. The supernatant was collected and triethanolamine was added to a final concentration of 100 mM. The pH was adjusted to 6.5 with 5 M K2CO3 before centrifuging again at 18,000 3 g for 3 min at 4○C to remove potassium perchlorate. Neutralized PCA extract was made up to 100 ml with Na2H2PO4 (150 mM), Tris-(2-carboxyethyl) phosphine hydrochloride (TCEP) (10 mM), EDTA (5 mM), and methanol (9%) and filtered through a 0.2 mm PVDF filter, and 50 ml was injected for HPLC analysis of CoA compounds.

In Vitro PPAT/DPCK Assay of Cell Homogenates

Fibroblasts grown on 10 cm plates (approx. 80%–90% confluent) were washed with PBS and collected by trypsinization. Cells were homogenized in 150 ml buffer containing 50 mM Tris/HCl

(pH 7.5), 150 mM NaCl, 10 mM 2-glycerophosphate, 1 mM EDTA, 0.5 mM TCEP, and protease inhibitor cocktail (Roche). Total protein concentration in the homogenate was measured by Bradford assay. 65 mg of homogenate protein was incubated with 2 mM ATP, 5 mM MgCl2, and 5 mM 4-phosphopantetheine in a total volume of 50 ml at 30○C for 1 hr. 4-phosphopantetheine was prepared by phosphorylating pantetheine with bacterially expressed pantothenate kinase 1b. For control incubation, ATP and MgCl2 were added to homogenate, but 4-phospho-pantetheine was omitted. After the incubation, PCA (3.5% final) was added to the reaction mixtures before centrifugation at 18,000 3 g for 5 min at 4○C. The pH of the PCA-soluble fraction was adjusted to 6.5 with TEA/K2CO3 and CoA compounds formed were analyzed by HPLC as described above.

Yeast Mitochondria Analysis

Mitochondrial suspensions were diluted to obtain about 0.5 mg/ml in a final volume of 150 ml of 5% 5-sulfosalicylic acid containing 50 mmole/l DTT and vortexed. The homogenates were centrifuged at 12,000 3 g for 10 min at 4○C. The supernatant was passed through a 0.45 mm filter (Millipore) and the filtrate (40 ml) was injected directly into the HPLC system. We loaded equal amount of yeast mitochondrial proteins (40 mg) and we performed CoA quantification by evaluating peak's areas as compared to known concentration of internal standard

Yeast Strains and Media

Yeast strains used in this study were W303-1B (MATaade2-1 leu2- 3,112 ura3-1 his3-11,15 trp1-1 can1-100) ade2-1 leu2-3,112 ura3-1 trp1-1 his3-11,15, its isogenic strain cab5::KanMx4 that harbors plasmid pFl38-CAB5 or pFl39-CAB5, and the strain cab5::KanMx4 that harbors plasmid pYEX-BX-COASY (see below). Cells were cultured in minimal medium 40 supplemented with appropriate amino acids and bases for auxotrophy as previously described.22 To obtain medium lacking pantothenate (40-Pan), a mixture of vitamins without pantothenate was prepared. Various carbon sources (Carlo Erba Reagents) were added at the indicated con- centration. YP medium contained 1% Bacto-yeast extract and 2% Bacto-peptone (ForMedium). Media were solidified with 20 g/l agar (ForMedium) and strains were incubated at 23○C, 30○C, or 37○C.

Cloning Procedures and Plasmid Vectors

pFL38-CAB5 was obtained by PCR amplification of CAB5, including the upstream and the downstream regions, from genomic DNA of strain W303-1B with primers as follows.

For CAB5 (forward 5'-GGGGGGATCCCCATTGCTTAGAA TGGGCGG-3' and reverse 5'-CCGCGGTACCGAGAACCCATAGAATTCGAC-3'), the oligos were modified at 5' end in order to insert restriction sites for cloning in the centromeric plasmid pFL38 carrying the URA3 marker.23 pFL39-CAB5 was obtained by subcloning CAB5 into pFL39 vector carrying the TRP1 marker.23 Human COASY and

human COASY^{Arg499Cys} were amplified by PCR from pcDNA3.1 constructs, containing wild-type and mutant cDNA, respectively, with primers described below.

For COASY (forward 5'-GGGGGGATCCATGGCCGTATT CCGGTCG-3' and reverse 5'-CCGCGTCGACTCAGTCGAGGGCCTGATGAGTC-3'), the oligonucleotides contained appropriate restriction sites to allow cloning in the BamHI-SalI-digested pYEX plasmid under the control of CUP1 promoter. All cloned fragments were sequenced to check the absence of mutations. Restriction-enzyme digestions, Escherichia coli transformation, and plasmid extractions were performed with standard methods.24

Site-Directed Mutagenesis and Generation of Yeast cab5 Strains

The conserved human arginine 499 residue (RefSeq accession number NM_025233.6), which is replaced by a cysteine in human COASY, corresponds to arginine 146 (RefSeq NM_001180504.3) in the yeast protein. The CAB5 mutant allele was obtained by site- directed mutagenesis (QuikChange II Site-Directed Mutagenesis Kit Stratagene) by introducing an AGA>TGT codon substitution, resulting in p.Arg146Cys amino acid change. The corresponding modified primers used to generate mutated allele are as follows.

For COASY^{Arg146Cys} (forward 5'-CGCAAGAATTGCAACTAGAATGTTTAATGACAAGAAAT CCTG-3' and reverse 5'-

CAGGATTTCTTGTCATTAAACATTCTAGTTGCAATTCTT GCG-3'), mutagenized insert was verified by sequencing of both strands.

The pFL38 plasmid-borne CAB5 was transformed in the W303-1B by the lithium-acetate method25 to allow cell viability and the resident CAB5 was deleted with the KanMX4 cassette amplified from plasmid pCXJKan by primers described below.

For CAB5-*Kan* (forward 5'-CAGATAGCCACAATTAAAATATGCTGGTAGTGGGATTG ACAGGTCGTACGCTGCAGGTCGAC-3' and reverse 5'-GTAATTATAAGATATCAACCTTATACCCGCTGAAGACTT TTTATTTTGAAGATCGATGAATTGAGCTCG-3'), both of them contained a 50 complementary stretch for an internal sequence of CAB5 ORF and a 30 complementary stretch (underlined in the sequences) for the extremities of the *KanMX4* cassette. Strains with engineered *CAB5* were selected on YP supplemented with 200 mg/ml geneticin and gene rearrangement was confirmed by PCR. Transformation of *cab5::Kan^{R}/pFLl38CAB5* strain with pfl39-CAB5 and pFL39-CAB5^{Arg146Cys} constructs and plasmid shuffling on media supplemented with 5-FOA in order to select spontaneous events of Uraþ constructs loss were finally per- formed. Similarly, cab5::Kan^{R}/pFL39CAB5 strain was transformed with pYEX-BX-COASY and pYEX-BX-COASYArg499Cys constructs; loss of Trpþ plasmids was induced by growing the transformants with tryptophan in the medium.

Yeast Mitochondria Isolation

Mitochondria were purified as previously reported.26 In brief, cells cultured at 28○C in the 40 medium supplemented with 0.6% glucose were collected and washed. Spheroplasts were obtained after Zymoliase20T digestion (Nacalai Tesque) and disrupted with a glass-teflon potter homogenizer. Mitochondria were purified by differential centrifugation. Total protein concentrations were quantified according to Bradford (Bio-rad).

Results

Molecular and Biochemical Investigations

Exome-NGS analysis of one individual (subject II-3, family 1, Figure 1) affected by idiopathic NBIA resulted in the identification of 12 genes (Table S3) that carried variants potentially relevant for the disease. However, as described in detail in the Subjects and Methods section, several of these genes were not investigated further because (1) the identified variants were present in additional individuals and associated with other clinical phenotypes; (2) genetic segregation analysis was not compatible with clinical presentation of the subjects of family 1; or (3) gene function and tissue-specific expression could hardly explain the neurological presentation. The homozygous mutation in COASY, coding for a bifunctional enzyme converting 40-phosphopantetheine into dephospho-CoA and then to Coenzyme A, was considered as potentially relevant for the disease and further investigated. By Sanger sequencing we confirmed the

presence of the homozygous missense COASY mutation in the affected individual (Figure 1: sub- ject II-3, family 1). The family had no history of neurological disorders and this subject was the youngest and the only affected of five siblings. She was born to consanguineous parents after an uneventful pregnancy and normal delivery. Birth weight was 3,850 g. There was no history of perinatal complications and she attained normal early developmental milestones. From 24 months of age, parents reported gait difficulties and persistent toe walking. At age 6, when she started primary school, she showed poor academic ability. At age 15, general physical examination was normal. Neurological evaluation showed mild oro-mandibular dystonia with dysarthria and also spastic dystonic paraparesis, but she was still able to walk unaided. Neuropsychological evaluation demonstrated cognitive impairment (total IQ = 49). The disease continued to prog- ress slowly and at the age of 20 she became unable to ambulate independently. During the most recent examination at age 25, the clinical picture was dominated by a severe spastic bradykinetic-rigid syndrome associated with mild dystonia and with distal areflexia in the lower limbs. There were no clinical or psychometric data suggesting mental deterioration but behavioral disturbances with obsessive-compulsive symptoms and depression was evident. Funduscopic examination and visual evoked potential studies were normal and on electroretinogram there were no signs of retinopathy. Electromyographic and nerve conduction studies were consistent with a mild motor axonal neuropathy. Serial brain MRI showed bilateral hypointensity in

the globi pallidi associated with a central region of hyperintensity in the anteromedial portion (Figure 1).

Identification of one Italian subject carrying COASY mutation prompted us to analyze the nine exons of this gene in a cohort of 280 NBIA-affected individuals of different ethnicity by using polymerase chain reaction and direct Sanger sequencing. Primer sequences and PCR conditions are described in Table S4. By this analysis we identified a second Italian case carrying COASY mutations (Figure 1: subject II-2, family 2). He is 20 years old and he was born at term of uneventful pregnancy from healthy nonconsanguineous parents. Psychomotor development was normal in the first year of life, but he was delayed in walking as a result of instability and toe walking. At age 3 the neurological picture was characterized by spastic tetra- paresis with moderate mental and language impairment. The disease was progressive, with worsening of the motor signs in the lower limbs and progressive involvement of the upper limbs and oro-mandibular region. He lost independent ambulation at age 15. At age 17, the neurological examination showed mild oro-mandibular dystonia with dysarthria, spastic-dystonic tetraparesis with prevalent involvement of lower limbs, and parkinsonian features (rigidity and abnormal postural reflexes). Distal amyo- trophia and areflexia with pes cavus were also evident. Cognitive impairment was severe (total IQ < 40) with obsessive-compulsive behavior and complex motor tics. On follow-up, 2 years later, the neurological picture was unchanged. Nerve conduction study and

electromyography detected a motor axonal neuropathy more prominent in the lower limbs.

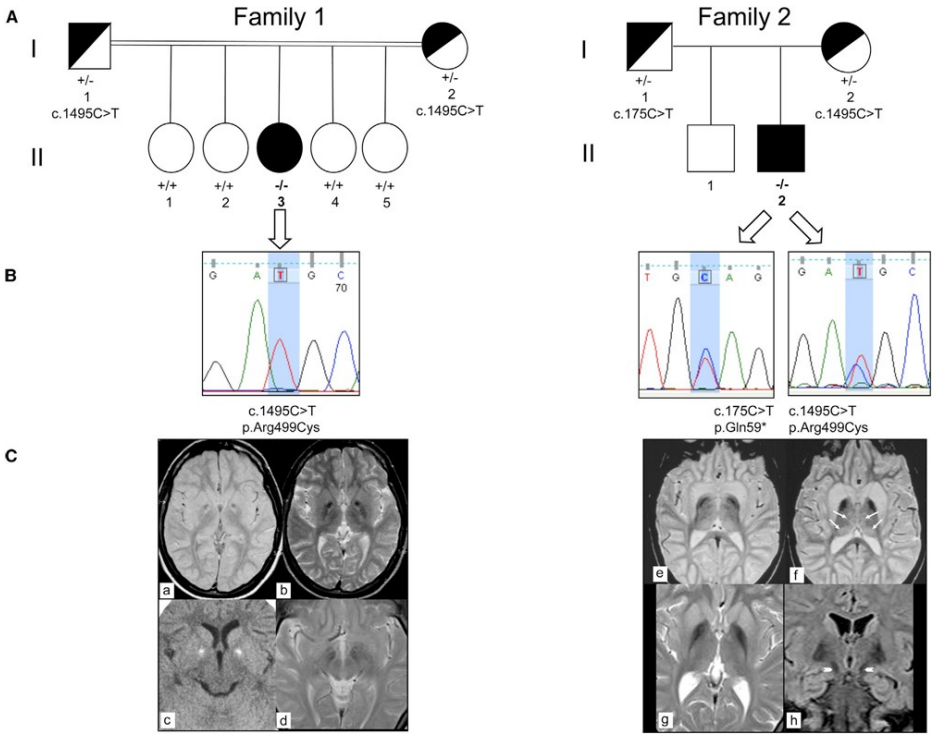

Figure 1. Genetics and MRI of Subjects Carrying COASY Mutations

(A) Pedigrees of family 1 (left) and family 2 (right). II-3, affected individual in family 1; II-2, affected individual in family 2. The presence of homozygous or compound heterozygous mutation is indicated by —/—; wild-type sequence by þ/þ; heterozygous mutation by þ/—.

(B) Electropherograms show sequence variations in individual II-3 of family 1 (left) and in individual II-2 of family 2 (right).

(C) Left: MRI of individual II-3 of family 1 at 11 years of age (a–c). Axial MR (1.5 T) proton density and T2-weighted images (a, b) show bilateral low signal intensity in the globi pallidi (clearly visible in b) with a central region of high signal intensity located in the anteromedial portion of the nuclei (‘‘eye-of-the-tiger’’ sign) and with a large central spot of low signal intensity. Axial CT (c) shows bilateral hyperdensities consistent with calcifications and corresponding to the central spot visble on MRI. Six years later (d), no changes were found.

The hypointensity in the medial portion of the substantia nigra was also unchanged. Right: MRI of individual II-2 of family 2 at 9 years of age (e, f) and at age 19 (g, h). Axial T2-weighted 1.5 T MR images (e, f) reveal hypointensity in the pallida. Both caudate nuclei and putamina are swollen and hyperintense. Slight hyperintensity is also present in both medial and posterior thalami (arrows). Axial T2-weighted MR image (g) confirms bilateral symmetric low signal intensity and atrophy in the pallida. Both putamina and caudate nuclei are still slightly hyperintense with minimal swelling. Coronal FLAIR image (h) demonstrates low signal in both pallida and in the medial portion of the substantia nigra (arrowheads).

There was no retinal or optic nerve involvement, as demonstrated by normal funduscopic and evoked potential studies.

The first brain MRI performed at age 5 demonstrated hyperintensity and swelling of both caudate nuclei and putamina and mild hyperintensity in both thalami. Globi pallidi were normal. At ages 9 and 19, hypointensity in the globi pallidi was evident and no significant changes were found in the caudate nuclei, putamina, and thalami (Figure 1).

Subject II-3 of family 1 (Figure 1) carried a homozygous missense mutation, a c.1495C>T transition causing an amino acid change p.Arg499Cys (referral sequence NM_025233.6; numbering starts from the first methio- nine). Segregation analysis performed in family 1 indicated heterozygous state in the parents (Figure 1), and the four healthy sisters showed wild-type sequence (Figure 1).

Subject II-2 of family 2 (Figure 1) turned out to be a com- pound heterozygote for the same mutation, c.1495C>T (p.Arg499Cys), identified in subject II-3, and for a c.175C>T transition, resulting

in a premature p.Gln59* stop codon in the N-terminal regulatory region of the protein. Segregation analysis in the parents demonstrated that the two mutations were on different alleles: one in- herited from the mother and one from the father (Figure 1). The healthy brother was not available for genetic testing. The missense substitution affected an amino acid residue Arg499, which is highly conserved in all available animal, plant, and yeast species, including S. cerevisiae, and is localized in the nucleotide-binding site of the DPCK domain (Figure 2). Furthermore, mutational analysis of Arg140, equivalent to Arg499, in the mycobacterial dephospho-CoA kinase (CoaE) revealed the importance of this residue in ATP binding and phosphotransfer reaction.27,28

The substitution was predicted to be pathogenic by in silico analysis according to Polyphen2 (p = 1) and MutPred (p = 0.909). Frequency of the mutation derived from the Exome Variant Server and calculated on European, American, and African population was 1 out of 13,005 analyzed cases.

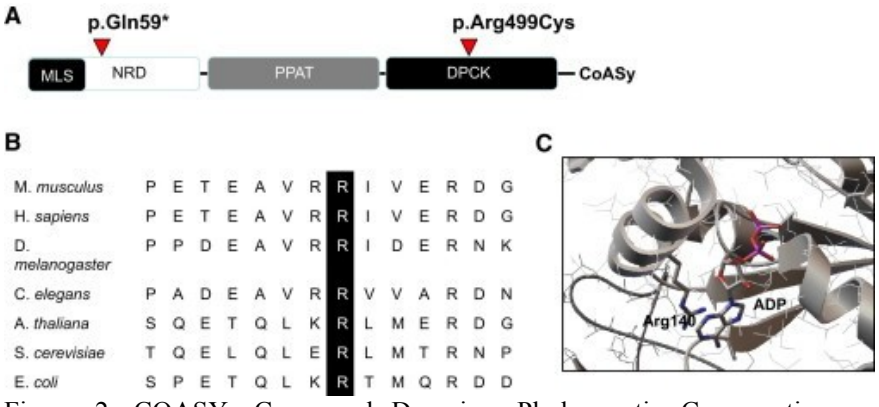

Figure 2. COASY: Conserved Domains, Phylogenetic Conservation, and Crystal Structure

(A) Schematic domain organization of human CoA synthase and location of point mutations. Abbreviations are as follows: MLS, mitochondrial localization signal; NRD, N terminus regulatory domain; PPAT, 40PP adenylyltransferase domain; DPCK, dephospho-CoA kinase domain.
(B) Amino acid sequence alignment showing conservation of Arg499 across species.
(C) Crystal structure of E. coli DPCK (CoaE) (PDB ID 1VHL) showing the position of Arg140 (equivalent to Arg499 in human DPCK) in the nucleotide-binding site.

To evaluate the impact of the two mutations on the stability of the transcript, we extracted mRNA from fibroblasts of subjects II-3 (family 1) and II-2 (family 2) and reverse transcribed it into cDNA. Quantitative real-time PCR showed that although in individual II-3 the amount of mutant COASY transcript was similar to that of the control sample (Figure 3A), it was reduced to 50% in individual II-2, suggesting RNA decay.

Next, we analyzed COASY level in total cell lysates obtained from both mutants and control fibroblasts by using a monoclonal anti-COASY antibody. We first tested the antibody specificity by verifying its cross-reactivity with the 62 kDa COASY alpha in vitro translation product (Figure 3B).

Immunoblot analysis revealed the presence of a normal protein content in three different control fibroblasts whereas a significant reduction of the protein amount was detected in fibroblasts of subject II-2 (family 2) carrying the premature stop codon and the missense p.Arg499Cys (Figure 3B). Interestingly, we also observed a minimally detectable immunoreactive band corresponding to COASY in subject II-3 (family 1) carrying the

homozygous p.Arg499Cys substitution (Figure 3B). This suggests that the p.Arg499Cys change is associated with instability or accelerated degradation of the protein. Immunoblot analysis of fibroblasts derived from subject I-2 of family 1 and from both parents of family 2 (Figure 3B) showed a partial reduction of the protein level. As reported in Figure 3C, protein amount quantified by densitometry analysis with three different controls as standard resulted to be around 50% in subject I-2 of family 1 and in the parents of family 2 and less than 5% in both affected individuals.

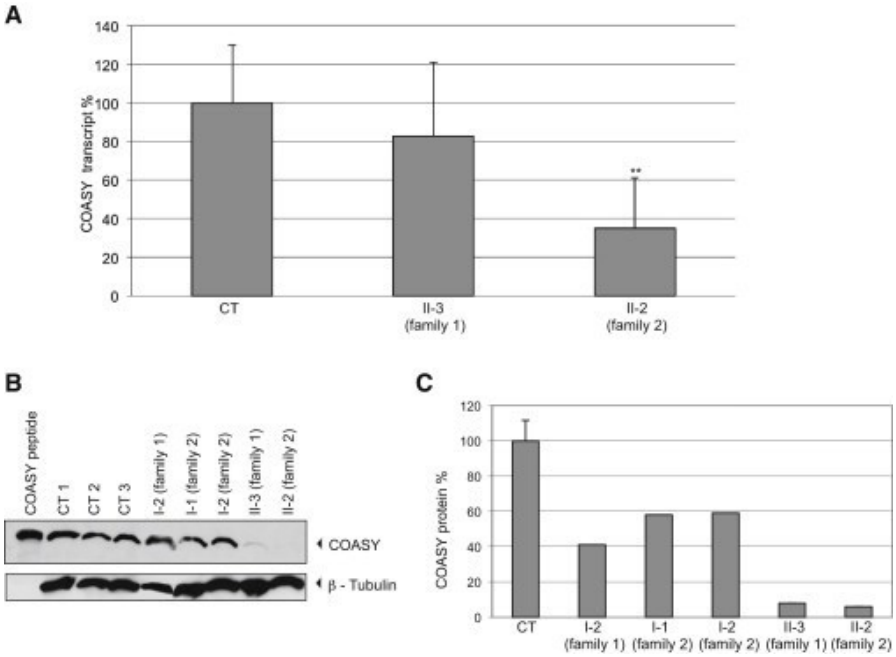

Figure 3. COASY mRNA Expression and Protein Accumulation in Skin Fibroblasts

(A) Quantification of COASY mRNA levels by real-time PCR in fibroblasts of subject II-3 and II-2 relative to the expression of glyceraldehyde 3-phosphate dehydrogenase (GAPDH). The amount of COASY transcript is reduced in subject II-2 versus control samples (CT), indicating mRNA decay. Data are represented as mean ± SD. Statistically significant differences with CT were determined by the Student's t test; $**p < 0.02$.

(B) Immunoblot analysis of COASY in fibroblasts derived from three healthy subjects (CT 1, CT 2, CT 3), individual I-2 (family 1), individuals I-1 and I-2 (family 2), and affected subjects (II-3 and II-2). The same amount of protein (30 μg) was loaded. β-tubulin was used as a loading control. As a control, COASY in vitro translation product (COASY peptide) was loaded.
(C) Relative quantification of the protein amount: mean ± SD of three controls (CT); of individual I-2 (family 1); of individuals I-1 and I-2 (family 2); and of affected subjects II-3 and II-2. Histogram shows COASY amount quantified by densitometry and normalized on β-tubulin level

Studies in Yeast Saccharomyces cerevisiae

To further test the pathogenic role of the COASY missense mutation, we used the yeast Saccharomyces cerevisiae. Biosynthesis of CoA in S. cerevisiae follows the same pathway described for mammalian cells: pantothenate, formed de novo from several amino acids or taken up from outside the cell, is converted in CoA in five reactions

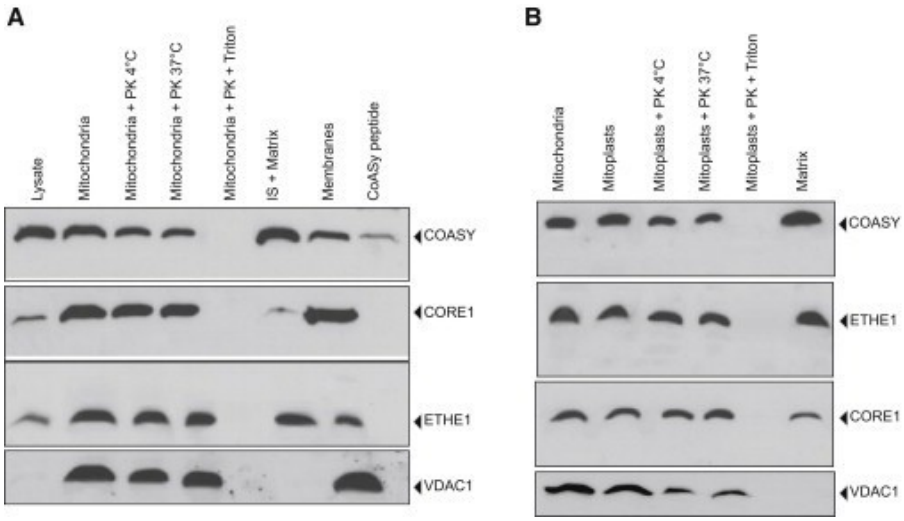

Figure 4. Mitochondrial Localization of COASY

(A) Immunoblot analysis on mitochondria and different submitochondrial fractions derived from HeLa cells. Mitochondria were treated for 15 min at

4°C or 37°C with proteinase K (PK) in presence or absence of triton. The filter was incubated with anti-COASY, anti-CORE1, anti-ETHE1, and anti-VDAC1 antibodies. As a control, COASY in vitro translation product (COASY peptide) was loaded.

(B) Immunoblot analysis on mitoplasts, matrix, and inner membrane isolated from HeLa cells. Mitoplasts were treated for 15 min at 4°C or 37°C with PK in presence or absence of triton. The filter was sequentially incubated with anti-COASY, anti-ETHE1, anti-CORE1, and anti-VDAC antibodies.

catalyzed by enzymes encoded by CAB1 through CAB5.29 With the exception of CAB1, the other genes of the pathway have been identified because of sequence similarity and their function in CoA biosynthesis assessed by heterologous complementation with bacterial genes. The only difference with human is that in yeast, as in E. coli, the PPAT and DPCK activities reside on different proteins encoded by CAB4 and CAB5 genes, respectively. Deletion of each CAB gene results in a lethal phenotype, indicating an essential role for this pathway in yeast.

Sequence analysis indicated that Arg499 is highly conserved from yeast to human and corresponds to Arg146 in the yeast Cab5p (see also Figure 2). By using the plasmid shuffling method, deletion strains expressing either the mutant alleles cab5^{Arg146Cys} and COASY^{Arg499Cys} or the CAB5 and COASY wild-type genes were generated. The Dcab5 lethal phenotype was rescued by the re-expression of either human COASY wild-type or human COASY^{Arg499Cys} and yeast cab5^{Arg146Cys}. No major defects of growth on different substrates or at different temperatures were observed (data not shown).

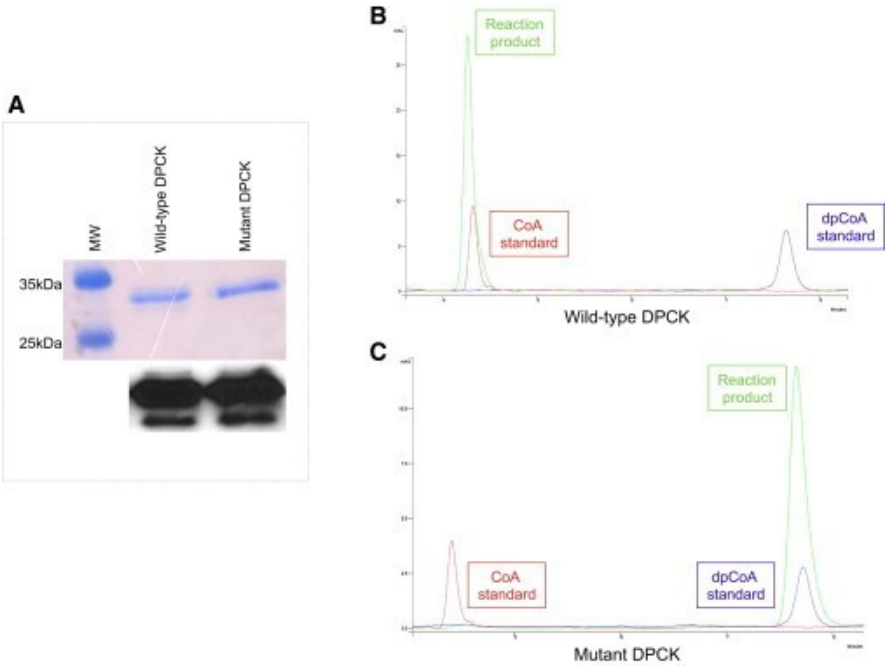

Figure 5. HPLC Analysis of CoA Production by Wild-Type and Mutant DPCK Recombinant Proteins

(A) Top: equal amount of purified wild-type and mutant DPCK proteins were loaded on a 12% SDS page and stained with Coomassie blue. Bottom: immunoblot analysis on the same gel showing that anti-COASY antibody is able to recognize both the wild-type and the mutant protein.

(B) Chromatogram showing the peak corresponding to the reaction product (green) obtained from incubation of wild-type DPCK recombinant protein with ATP and dephospho-CoA.

(C) Chromatogram showing the peak corresponding to the reaction product (green) obtained from incubation of mutant DPCK-Arg499Cys recombinant protein with ATP and dephospho-CoA. Red peak, CoA standard; blue peak, dephospho-CoA standard.

However, we noticed that the mutant cab5Arg146Cys as well as the strain expressing COASYArg499Cys became auxotrophic for pantothenate and showed growth reduc- tion. In fact, wild-type yeast can form colonies regardless of the presence of pantothenate at all tested temperatures (Figure 7A); by contrast, in the absence of pantothenate both mutants cab5Arg146Cys and COASYArg499Cys failed to form colonies at 37○C and a significant impairment of growth was observed at both 23○C and 28○C when compared with that of the strain expressing the wild-type alleles (Figure 7B). This result supports the pathoge- nicity of the substitution p.Arg499Cys and suggests that the mutant enzyme requires a higher concentration of pantothenate to produce enough CoA to sustain yeast growth.

Because Cab5p as COASY is located into the mitochon- dria,30 we measured the level of CoA in mitochondria isolated from wild-type, COASYArg499Cys, and cab5Arg146Cys transformed yeasts grown in complete medium at 28○C with 0.6% glucose. We first verified, by immunoblot analysis, that $COASY^{Arg499Cys}$ was expressed in yeast at a comparable level as in the wild-type enzyme (not shown). We could not verify $cab5^{Arg146Cys}$ expression because the available antibody did not cross-react with the yeast protein. We observed that the level of CoA was reduced to 40% in yeast transformed with both the human COASYArg499Cys and yeast $cab5^{Arg146Cys}$ mutant versions as compared to wild-type (Figure 8).

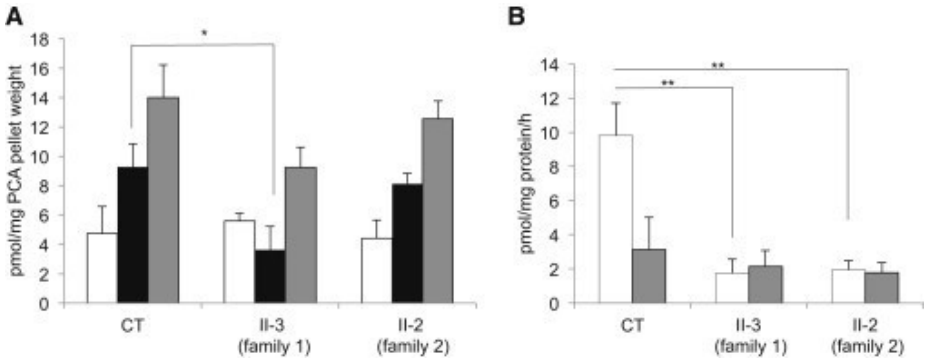

Figure 6. HPLC Analysis of CoA and CoA Derivatives in Fibroblasts

(A) CoA (white bar), acetyl-CoA (black bar), and total CoA (gray bar) levels in primary skin fibroblasts derived from a healthy control (CT) and from the two affected individuals (II-3, family 1; II-2, family 2). Results shown are mean ± SEM of four independent experiments. Statistically significant differences in acetyl-CoA amount between CT and subject II-3 (family 1) were determined by the Student's t test; $*p < 0.05$. This subject also shows a reduction in acetyl-CoA, which is not statistically significant. A reduction of total CoA was observed in both affected individuals, although not statistically significant.

(B) De novo synthesis of CoA and dephosphoCoA (dpCoA) in primary skin fibroblasts derived from a healthy control (CT) and from the two affected individuals (II-3, family 1; II-2, family 2). CoA (white bar) and dpCoA (gray bar) produced from 4′PP as substrate were quantified by HPLC after deproteinization of reaction mixture with PCA (3% final). Results shown are mean ± SEM of values from three independent experiments. Statistically significant differences with CT were determined by the Student's t test; $**p < 0.02$.

Discussion

We here report the second inborn error of CoA synthesis leading to a neurodegenerative disorder. The first defect discovered was

due to PANK2 mutations, causing the most prevalent NBIA subtype, PKAN.2

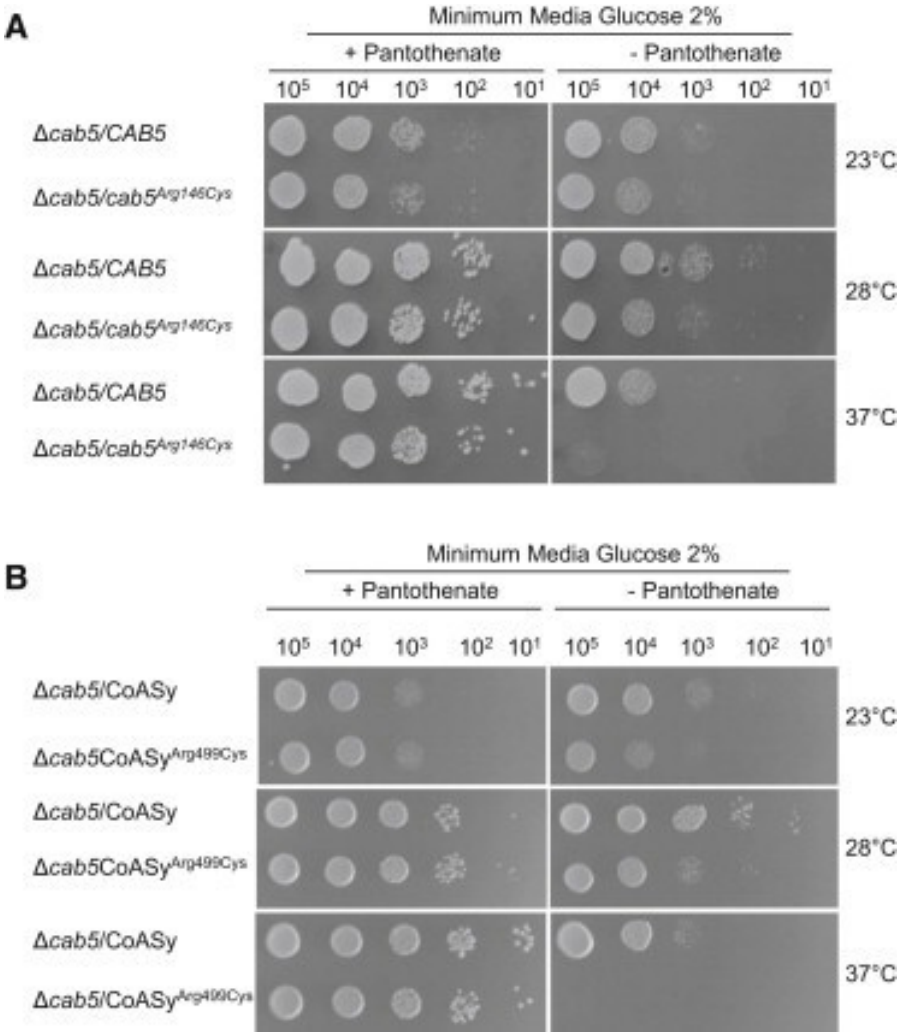

Figure 7. Growth of Yeast Strains in Presence or Absence of Pantothenate

The strain Δcab5 was transformed with pFL39 plasmid carrying the wild-type CAB5 and the mutant allele cab5Arg146Cys (A) or with pYEX-BX plasmid carrying COASY and COASYArg499Cys (B). Equal amounts of serial dilutions of cells from exponentially grown cultures (105, 104, 103, 102, 101 cells) were spotted onto minimum medium 40 plus 2% glucose, with or

without pantothenate 1 mg l−1. The growth was scored after 3 days of incubation at 23°C, 28°C, or 37°C. Each experiment of serial dilution grow test was done in triplicate starting from independent yeast cultures.

Coenzyme A (CoA) is a crucial cofactor in all living organisms and is involved in several enzymatic reactions. It is a key molecule for the metabolism of fatty acids, carbohydrates, amino acids, and ketone bodies. Its biosyn- thesis proceeds through a pathway conserved from prokaryotes to eukaryotes, involving five enzymatic steps, which utilize pantothenate (vitamin B5), ATP, and cysteine.

In the first step, catalyzed by pantothenate kinase, the product of PANK2, pantothenic acid is phosphorylated to generate 40-phosphopantothenic acid. Then, this inter- mediat is converted into 40-phosphopantothenoyl- cysteine, which is subsequently decarboxylated to 40-phosphopantetheine. The last two steps are carried out by the bifunctional enzyme CoA synthase, which converts 40-phosphopantetheine into dephospho-CoA and then CoA.31

We have identified mutations in the COASY in two subjects with clinical and MRI features typical of NBIA. They displayed a strikingly similar phenotype, more severe in subject II-2 of family 2, presenting with early-onset spastic-dystonic paraparesis with a later appearance of parkinsonian features, cognitive impairment, and pronounced obsessive-compulsive disorder. The disease was slowly progressive with loss of ambulation during adolescence and adulthood.

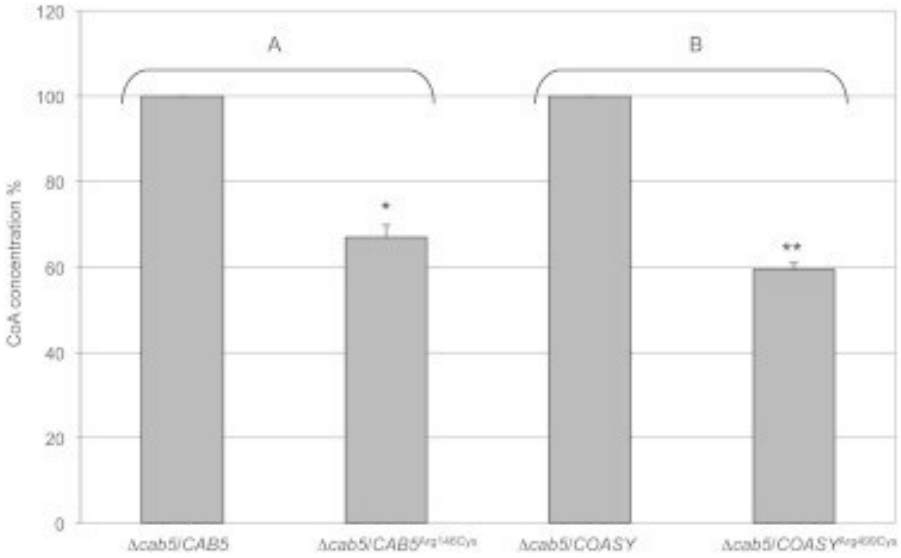

Figure 8. HPLC Analysis of CoA in Yeast Mitochondria

CoA level in mitochondria isolated from Δcab5 yeast transformed with wild-type (WT) or mutant (p.Arg146Cys) yeast CAB5 (A), and with wild-type or mutant (p.Arg499Cys) human COASY (B). Equal amount of mitochondrial proteins (40 μg) were used in each assay. Results shown are mean ± SD of values from three independent experiments. Values of mutant samples are expressed as percentage of values obtained in wild-type samples taken as 100%. Statistically significant differences were determined by the Student's t test; $*p < 0.05$; $**p < 0.02$.

This phenotype overlaps with other NBIA disorders, including the presence of an axonal neuropathy, which is commonly reported in phospholi- pase A2-associated neurodegeneration (PLAN) and also in mitochondrial membrane protein-associated neurodegen-eration (MPAN) cases.32

In subject II-3 of family 1, MR images are reminiscent of the ''eye-of-the-tiger'' sign even if with subtle features, which differentiate it from the typical appearance present in

PKAN.33,34 In subject II-2 of family 2, an isolated involvement of neostriatum, which usually hallmarks a metabolic rather than degenerative disorder, preceded the evidence of the typical increase of pallida iron content. Such features have not been previously reported, expanding the MR spectrum of NBIA disorders.

Both individuals presented with a severe neurological disorder but they have survived up to the third decade of life, suggesting the presence of residual amount of CoA as observed in cultured fibroblasts. The complete absence of CoA would be probably incompatible with life, and organisms have developed alternative strategies to counteract deleterious effects of mutations in CoA enzymatic pathway. For instance, mammals possess four closely related PANK isoforms,2 1a, 1b, 2, and 3, which exhibit a tissue-specific pattern of expression. This redundancy could explain why PKAN patients can survive into the first or second decade of life. Probably, the different isoforms can compensate each other to maintain adequate CoA level. This was clearly demonstrated in mice by the simultaneous knockout of two different Pank genes.35

COASY has been reported to code for three transcript variants resulting in tissue-specific isoforms.14 The existence and functional significance of these variants are presently unknown but both mutations found in this study affect the protein sequence common to isoforms alpha and beta, predicting overall impairment of COASY function. Considering the ubiquitous presence of the enzymatic COASY activity, it remains

unexplained why only the brain is affected and other organs are preserved. It is possible that a more severe impairment of CoA levels occurs in this organ, thus explaining the prevalence of neurological symptoms. At the cellular level CoA concentration is regulated by numerous factors, including hormones, glucocorticoids, nutrients, and cellular metabolites,36,37 and a link between the complex signaling mTOR pathway, which is implicated in numerous metabolic and signaling processes, and CoA biosynthesis has been proposed.38 Moreover, it is relevant to notice that the mutations targeted genes coding for pantothenate kinase39 and PPAT activity of CoA synthase36 are the two rate- limiting steps in CoA biosynthesis. All together these factors could contribute to modulate the clinical presentation of individuals carrying COASY mutations.

It is still unknown how mutations in genes involved in Coenzyme A enzymatic pathway cause neurodegeneration with iron accumulation in specific areas of the brain but whereas for PANK2 it was hypothesized that cysteine accumulation may chelate iron and catalyze free radical forma- tion,40 a different mechanism could be involved in case of COASY mutations.

In Drosophila it has been demonstrated that abolishing the different genes of CoA biosynthetic pathway including the fumble/PANK2 and PPAT-DPCK activities causes a neurological phenotype characterized by brain vacuolization without iron accumulation.12

Identification of mutations in CoA synthase strongly reinforces the essential role of CoA biosynthetic pathway for the

development and functioning of the nervous system. This also underlines the importance of further investigations on different subcellular pools of CoA avail- able, because a specific mitochondrial pathway could exist considering that both PANK2 and CoA synthase are mitochondrial enzymes.16–18 At present it is not understood whether CoA can pass from cytosol to mitochondria, even if a CoA-specific carrier has been identified in the inner mitochondrial membrane.41 Moreover, it is not clear whether the regulation of the different pools is coordinated and whether the utilization could be modulated in response to different physiological or pathological conditions.

In conclusion, we have demonstrated that COASY mutations cause a distinctive NBIA subtype. This finding will require further investigation to understand the connection linking CoA metabolism to neurodegeneration, iron accumulation, and mitochondrial bioenergetics. We propose CoPAN, standing for COASY protein-associated neurodegeneration, as the acronym for NBIA caused by CoA synthase mutations to conform with the current nomenclature in use to classify these disorders.

Supplemental Data

Supplemental Data include four tables and can be found with this article online at http://www.cell.com/AJHG/

Acknowledgments

We would like to thank Mario Savoiardo and Federica Zibordi for helpful neuroradiological and clinical support and Fabrizio Villa for experimental advice. The financial support of Telethon GGP11088 to V.T. is gratefully acknowledged. This work was sup- ported by TIRCON project of the European Commission's Seventh Framework Programme (FP7/2007-2013, HEALTH-F2-2011, grant agreement no. 277984). We thank the Cell line and DNA bank of paediatric movement disorders of the Telethon Genetic Biobank Network (project no. GTB07001) and the Bank for the Diagnosis and Research of Movement Disorders (MDB) of the EuroBiobank. The financial support of Mariani Foundation of Milan is gratefully acknowledged. T.B.H. and S.H. were supported by the NBIA Disor- ders Association. M.A.K. is a Wellcome Trust Intermediate Clinical Fellow. H.H. and C.B. are grateful to the MRC UK (grant number G0802870) and Backman-Strauss Foundation.

References

1. Gregory A., Hayflick S.J. Genetics of neurodegeneration with brain iron accumulation. Curr. Neurol. Neurosci. Rep. 2011;11:254–261. [PubMed]

2. Zhou B., Westaway S.K., Levinson B., Johnson M.A., Gitschier J., Hayflick S.J. A novel pantothenate kinase gene (PANK2) is defective in Hallervorden-Spatz syndrome. Nat. Genet. 2001;28:345–349. [PubMed]

3. Hörtnagel K., Prokisch H., Meitinger T. An isoform of hPANK2, deficient in pantothenate kinase-associated neurodegeneration, localizes to mitochondria. Hum. Mol. Genet. 2003;12:321–327. [PubMed]

4. Morgan N.V., Westaway S.K., Morton J.E., Gregory A., Gissen P., Sonek S., Cangul H., Coryell J., Canham N., Nardocci N. PLA2G6, encoding a phospholipase A2, is mutated in neurodegenerative disorders with high brain iron. Nat. Genet. 2006;38:752–754. [PubMed]

5. Kruer M.C., Paisán-Ruiz C., Boddaert N., Yoon M.Y., Hama H., Gregory A., Malandrini A., Woltjer R.L., Munnich A., Gobin S. Defective FA2H leads to a novel form of neurodegeneration with brain iron accumulation (NBIA) Ann. Neurol. 2010;68:611–618. [PubMed]

6. Hartig M.B., Iuso A., Haack T., Kmiec T., Jurkiewicz E., Heim K., Roeber S., Tarabin V., Dusi S., Krajewska-Walasek M. Absence of an orphan mitochondrial protein, c19orf12, causes a distinct clinical subtype of neurodegeneration with brain iron accumulation. Am. J. Hum. Genet. 2011;89:543–550. [PubMed]

7. Panteghini C., Zorzi G., Venco P., Dusi S., Reale C., Brunetti D., Chiapparini L., Zibordi F., Siegel B., Garavaglia B. C19orf12 and FA2H mutations are rare in Italian patients with neurodegeneration with brain iron accumulation. Semin. Pediatr. Neurol. 2012;19:75–81. [PubMed]

8. Haack T.B., Hogarth P., Kruer M.C., Gregory A., Wieland T., Schwarzmayr T., Graf E., Sanford L., Meyer E., Kara E. Exome sequencing reveals de novo WDR45 mutations causing a phenotypically distinct, X-linked dominant form of NBIA. Am. J. Hum. Genet. 2012;91:1144–1149. [PubMed]

9. Saitsu H., Nishimura T., Muramatsu K., Kodera H., Kumada S., Sugai K., Kasai-Yoshida E., Sawaura N., Nishida H., Hoshino A. De novo mutations in the autophagy gene WDR45 cause static encephalopathy of childhood with neurodegeneration in adulthood. Nat. Genet. 2013;45:445–449. e1. [PubMed]

10. Aghajanian S., Worrall D.M. Identification and characterization of the gene encoding the human phosphopantetheine adenylyltransferase and dephospho-CoA kinase bifunctional enzyme (CoA synthase) Biochem. J. 2002;365:13–18. [PubMed]

11. Bosveld F., Rana A., Lemstra W., Kampinga H.H., Sibon O.C. Drosophila phosphopantothenoylcysteine synthetase is required for tissue morphogenesis during oogenesis. BMC Res. Notes. 2008;1:75. [PubMed]

12. Bosveld F., Rana A., van der Wouden P.E., Lemstra W., Ritsema M., Kampinga H.H., Sibon O.C. De novo CoA biosynthesis is required to maintain DNA integrity during development of the Drosophila nervous system. Hum. Mol. Genet. 2008;17:2058–2069. [PubMed]

13. Daugherty M., Polanuyer B., Farrell M., Scholle M., Lykidis A., de Crécy-Lagard V., Osterman A. Complete reconstitution of the human coenzyme A biosynthetic pathway via comparative genomics. J. Biol. Chem. 2002;277:21431–21439. [PubMed]

14. Nemazanyy I., Panasyuk G., Breus O., Zhyvoloup A., Filonenko V., Gout I.T. Identification of a novel CoA synthase isoform, which is primarily expressed in the brain. Biochem. Biophys. Res. Commun. 2006;341:995–1000. [PubMed]

15. Johnson M.A., Kuo Y.M., Westaway S.K., Parker S.M., Ching K.H., Gitschier J., Hayflick S.J. Mitochondrial localization of human PANK2 and hypotheses of secondary iron accumulation in pantothenate kinase-associated neurodegeneration. Ann. N Y Acad. Sci. 2004;1012:282–298. [PubMed]

16. Alfonso-Pecchio A., Garcia M., Leonardi R., Jackowski S. Compartmentalization of mammalian pantothenate kinases. PLoS ONE. 2012;7:e49509. [PubMed]

17. Zhyvoloup A., Nemazanyy I., Panasyuk G., Valovka T., Fenton T., Rebholz H., Wang M.L., Foxon R., Lyzogubov V., Usenko V. Subcellular localization and regulation of coenzyme A synthase. J. Biol. Chem. 2003;278:50316–50321. [PubMed]

18. Rhee H.W., Zou P., Udeshi N.D., Martell J.D., Mootha V.K., Carr S.A., Ting A.Y. Proteomic mapping of mitochondria in living cells via spatially restricted enzymatic tagging. Science. 2013;339:1328–1331. [PubMed]

19. Simon-Kayser B., Scoul C., Renaudin K., Jezequel P., Bouchot O., Rigaud J., Bezieau S. Molecular cloning and characterization of FBXO47, a novel gene containing an F-box domain, located in the 17q12 band deleted in papillary renal cell carcinoma. Genes Chromosomes Cancer. 2005;43:83–94. [PubMed]

20. Fernández-Vizarra E., Ferrín G., Pérez-Martos A., Fernández-Silva P., Zeviani M., Enríquez J.A. Isolation of mitochondria for biogenetical studies: An update. Mitochondrion. 2010;10:253–262. [PubMed]

21. Tiranti V., Galimberti C., Nijtmans L., Bovolenta S., Perini M.P., Zeviani M. Characterization of SURF-1 expression and Surf-1p function in normal and disease conditions. Hum. Mol. Genet. 1999;8:2533–2540. [PubMed]

22. Magni G.E., Von Borstel R.C. Different rates of spontaneous mutation during mitosis and meiosis in yeast. Genetics. 1962;47:1097–1108. [PubMed]

23. Bonneaud N., Ozier-Kalogeropoulos O., Li G.Y., Labouesse M., Minvielle-Sebastia L., Lacroute F. A family of low and high copy replicative, integrative and single-stranded *S. cerevisiae/E. coli* shuttle vectors. Yeast. 1991;7:609–615. [PubMed]

24. Sambrook J., Russel D.W. Cold Spring Harbor Laboratory Press; Cold Spring Harbor: 2001. Molecular Cloning: A Laboratory Manual.

25. Gietz R.D., Schiestl R.H. Quick and easy yeast transformation using the LiAc/SS carrier DNA/PEG method. Nat. Protoc. 2007;2:35–37. [PubMed]

26. Glick B.S., Pon L.A. Isolation of highly purified mitochondria from *Saccharomyces cerevisiae*. Methods Enzymol. 1995;260:213–223. [PubMed]

27. Walia G., Gajendar K., Surolia A. Identification of critical residues of the mycobacterial dephosphocoenzyme a kinase by site-directed mutagenesis. PLoS ONE. 2011;6:e15228. [PubMed]

28. Walia G., Surolia A. Insights into the regulatory characteristics of the mycobacterial dephosphocoenzyme A kinase: implications for the universal CoA biosynthesis pathway. PLoS ONE. 2011;6:e21390. [PubMed]

29. Olzhausen J., Schübbe S., Schüller H.J. Genetic analysis of coenzyme A biosynthesis in the yeast *Saccharomyces cerevisiae*: identification of a conditional mutation in the pantothenate kinase gene *CAB1*. Curr. Genet. 2009;55:163–173. [PubMed]

30. Reinders J., Zahedi R.P., Pfanner N., Meisinger C., Sickmann A. Toward the complete yeast mitochondrial proteome: multidimensional separation techniques for mitochondrial proteomics. J. Proteome Res. 2006;5:1543–1554. [PubMed]

31. Leonardi R., Zhang Y.M., Rock C.O., Jackowski S. Coenzyme A: back in action. Prog. Lipid Res. 2005;44:125–153. [PubMed]

32. Hogarth P., Gregory A., Kruer M.C., Sanford L., Wagoner W., Natowicz M.R., Egel R.T., Subramony S.H., Goldman J.G., Berry-Kravis E. New NBIA subtype: genetic, clinical, pathologic, and radiographic features of MPAN. Neurology. 2013;80:268–275. [PubMed]

33. Hayflick S.J., Westaway S.K., Levinson B., Zhou B., Johnson M.A., Ching K.H., Gitschier J. Genetic, clinical, and radiographic delineation of Hallervorden-Spatz syndrome. N. Engl. J. Med. 2003;348:33–40. [PubMed]

34. Kruer M.C., Boddaert N., Schneider S.A., Houlden H., Bhatia K.P., Gregory A., Anderson J.C., Rooney W.D., Hogarth P., Hayflick S.J. Neuroimaging features of neurodegeneration with brain iron accumulation. AJNR Am. J. Neuroradiol. 2012;33:407–414. [PubMed]

35. Garcia M., Leonardi R., Zhang Y.M., Rehg J.E., Jackowski S. Germline deletion of pantothenate kinases 1 and 2 reveals the key roles for CoA in postnatal metabolism. PLoS ONE. 2012;7:e40871. [PubMed]

36. Tahiliani A.G., Beinlich C.J. Pantothenic acid in health and disease. Vitam. Horm. 1991;46:165–228. [PubMed]

37. Smith C.M., Savage C.R., Jr. Regulation of coenzyme A biosynthesis by glucagon and glucocorticoid in adult rat liver parenchymal cells. Biochem. J. 1980;188:175–184. [PubMed]

38. Nemazanyy I., Panasyuk G., Zhyvoloup A., Panayotou G., Gout I.T., Filonenko V. Specific interaction between S6K1 and CoA synthase: a potential link between the mTOR/S6K pathway, CoA biosynthesis and energy metabolism. FEBS Lett. 2004;578:357–362. [PubMed]

39. Rock C.O., Calder R.B., Karim M.A., Jackowski S. Pantothenate kinase regulation of the intracellular concentration of coenzyme A. J. Biol. Chem. 2000;275:1377–1383. [PubMed]

40. Gregory A., Hayflick S.J. Neurodegeneration with brain iron accumulation. Folia Neuropathol. 2005;43:286–296. [PubMed]

41. Fiermonte G., Paradies E., Todisco S., Marobbio C.M., Palmieri F. A novel member of solute carrier family 25 (SLC25A42) is a transporter of coenzyme A and adenosine 3′,5′-diphosphate in human mitochondria. J. Biol. Chem. 2009;284:18152–18159. [PubMed]

CHAPTER 4

Coenzyme A corrects pathological defects in human neurons of *PANK2* associated neurodegeneration.

Daniel I. Orellana1§, Paolo Santambrogio1§, Alicia Rubio2, Latefa Yekhlef3, Cinzia Cancellieri2, Sabrina Dusi4, Serena Gea Giannelli2, Paola Venco4, Pietro Giuseppe Mazzara2, Anna Cozzi1, Maurizio Ferrari5,6, Barbara Garavaglia4, Stefano Taverna3, Valeria Tiranti4, Vania Broccoli2,7,$ and Sonia Levi1,7,$*

1Proteomic of Iron Metabolism Unit, Division of Neuroscience, 20132 Milano, Italy.2Stem Cells and Neurogenesis Unit, Division of Neuroscience, San Raffaele Scientific Institute, 20132 Milano, Italy. 3Neuroimmunology Unit, Division of Neuroscience, San Raffaele Scientific Institute, 20132 Milano, Italy.4 Molecular Neurogenetics Unit, Foundation IRCCS-Neurological Institute "Carlo Besta," Milano, Italy. 5Genomic Unit for the Diagnosis of Human Pathologies, Division of Genetics and Cell Biology, San Raffaele Scientific Institute, Milano, Italy. 6Vita-Salute San Raffaele University, 20132 Milano, Italy.7Institute of Neuroscience, National Research Council, 20129 Milano, Italy.

Submitted

Abstract

Panthothenate kinase-associated neurodegeneration (PKAN) is an early- onset and severe disabling neurodegenerative disease for which no therapy is available. PKAN is caused by mutations in *PANK2*, which encodes for the mitochondrial enzyme pantothenate kinase 2. Its function is to catalyse the first limiting step of Coenzyme A (CoA) biosynthesis. We generated induced pluripotent stem cells from PKAN patients and showed that their derived neurons exhibited premature death, increased ROS production, aberrant mitochondria, impairment of respiratory capacity and major membrane excitability defects. Futhermore, PKAN neurons showed a significant iron mishandling that led to deficiency in heme synthesis and aconitase enzymatic activities, suggesting alterations of cellular iron homeostatic control. CoA supplementation prevented neuronal death and ROS formation, restoring mitochondrial and neuronal functionality. Our findings provide direct evidence that PANK2 malfunctioning is responsible for abnormal phenotypes in human neuronal cells and indicate CoA treatment as a possible therapeutic intervention.

Introduction

PKAN (OMIM *606157) is an autosomal recessive movement disorder caused by mutations in Pank2 (Zhou et al, 2001). It belongs to a heterogeneous group of neurodegenerative diseases, collectively known as neurodegeneration with brain iron accumulation (NBIA), which are characterized by severe iron overload in specific brain regions, neurodegeneration and extrapyramidal dysfunction (Hayflick et al, 2006; Levi & Finazzi, 2014). Mutations in *PANK2* approximately account for 50% of NBIA cases in Caucasian population (Colombelli et al, 2015). PKAN usually manifests in early childhood with gait disturbances and rapidly progresses to a severe movement deficit with dystonia, dysarthria and dysphagia (Hartig et al, 2012). A distinguished feature of this disease is the presence of the eye-of- the-tiger sign in the globus pallidus on T2*-weighted magnetic resonance imaging which reflects the focal accumulation of iron in this area (Zorzi et al).

PANK2-mediated CoA biosynthetic pathway takes place in mitochondria and cytosol. It involves five consecutive enzymatic steps highly conserved in animal evolution, starting from pantothenate (vitamin B5), ATP, and cysteine (Leonardi et al, 2005; Srinivasan et al, 2015). The recent identification of Coenzyme A synthase (COASY, the enzyme catalyzing the last two steps of CoA biosynthesis) as causative of a subtype of NBIA (Dusi et al, 2014), strongly reinforces the essential role of CoA in the correct functioning of the neural cells. In fact, CoA is a key molecule involved in more than 100 metabolic processes, among which CoA derivatives are

crucial substrates for ATP-generation via the tricarboxylic acid cycle, fatty acid metabolism, cholesterol and ketone body biosynthesis, and histone and non- histone protein acetylation (Akram, 2014; Siudeja et al, 2011). Although these processes are vital for any cell type, it remains unexplained why the disease affects primarily the central nervous system.

Animal models for PKAN, despite being informative for studying pathological mechanisms, share only few neuropathological signs with milder severity compared to those associated with the human disorder, limiting their impact for predicting novel therapeutics (Brunetti et al, 2012; Garcia et al, 2012; Kuo et al, 2005; Rana et al, 2010). In fact, whereas presenting some levels of neurodegeneration, these models lack any evidence of brain iron mishandling, preventing any insight on the causative link between PANK2 deficiency and brain iron deposition (Levi & Finazzi, 2014). *In vitro* studies of PKAN patients' fibroblasts have been instrumental to reveal some defects in mitochondrial activity and iron metabolism associated with *PANK2* deficiency, but their specific contribute to the pathological neurodegenerative processes cannot be appreciated in these cells (Campanella et al, 2012; Santambrogio et al, 2015).

Experiments in cell cultures have revealed that, in addition to vitamin B5, pantetheine can also be phosphorylated, and its product, 4-phosphopantetheine, can function as a precursor for CoA (Srinivasan et al, 2015). Interestingly, food supplemented with pantetheine was shown to partially revert the neuronal defects in mutant flies, fishes, and mice (Brunetti et al, 2014; Rana et al, 2010; Zizioli et al, 2015).

However, pantetheine-mediated rescuing effects were particularly limited in the mouse model, since this molecule is highly unstable in serum and is rapidly converted into vitamin B5 and cysteamine by pantetheinases (Brunetti et al, 2014). Recently, an alternative mechanism of CoA delivery to the cells has been described, consisting in extracellular CoA conversion into 4'- phosphopantetheine, which in turn passively crosses membranes and is converted back to CoA by COASY (Srinivasan et al, 2015). Notably, neurodegeneration in dPank deficient mutant flies and fishes was rescued by CoA administration by raising the levels of total intracellular CoA ((Srinivasan, 2015 #13;(Zizioli et al, 2015). However, it remains unknown whether exogenous CoA administration can be by any means efficacious in more complex animal models or in patients' human cells.

Considering the aforementioned limitations in the existing cellular and animal models, we took advantage of the human induced pluripotent stem cell (hiPSC) reprogramming technology to establish cultures of faithful human neuronal cells starting from patients' fibroblasts (Amamoto & Arlotta, 2014; Marchetto et al, 2011; Peitz et al, 2013; Tiscornia et al, 2011).

Here, we demonstrate that PKAN hiPSC-derived neurons exhibited severe functional impairments such as alteration of the oxidative status and mitochondrial dysfunctions, including impaired energy production, Iron Sulfur Cluster (ISC) and heme biosynthesis, with consequent cellular iron imbalance. Strikingly, supplementation of CoA in the neuronal growth medium was sufficient to restore the majority of these functional defective phenotypes.

Results

Generation and characterization of PKAN and normal donor hiPSC- derived neurons

To obtain a human PKAN neuronal model, we established multiple lines of transgene-free hiPSCs by reprogramming fibroblasts of three patients and three neonatal normal donors by Sendai virus mediated expression of the four Yamanaka's factors (see Material and Methods). One patient carried the c.569insA mutation, causing the premature stop codon p.Y190X, while two siblings were carrying the same mutation c.1259delG causing a frameshift p.F419fsX472 (here referred to as p.F419fsX472a and b). These mutations lead to the complete lack of PANK2 protein in fibroblasts (Santambrogio et al, 2015). Independent hiPSC clones for each individual were generated and fully characterized. In particular, we selected 3 clones from normal donors and 3 for both patients p.F419fsX472a and b, and 1 for patient p.Y190X.

The expression of master regulators of pluripotent stem cells and associated markers assessed by RT-PCR (*SOX2*, *OCT4*, *KLF4*, *REX1*, *GDF3*, *FGF4*, *DPPA-2, DPPA-4, TDGF, TERT*) and immunofluorescence analysis (OCT4, SOX2, NANOG, TRA1-60, SSEA-1) confirmed the stem cell pluripotency state of the hiPSC lines (Fig. EV 1A, B). Additionally, in all clones Nanog expression was detected at high levels by qRT-PCR (Fig. EV 1C).

Furthermore, pluripotency of hiPSC lines was functionally demonstrated by their effective differentiation into cells of the three different germ layers expressing endodermal, mesodermal, and

ectodermal markers (Fig. EV 1D). The presence of the original *PANK2* mutations was verified by direct sequence analysis of each hiPSC clone (Fig. EV 2A). All the selected hiPSCs were regularly assessed for the maintenance of correct karyotype content during cell expansion *in vitro* (Fig. EV 2B).

We then differentiated control and PKAN hiPSCs into a pure and stable population of self-renewable neuronal precursor cells (NPCs). To this end, hiPSCs were differentiated into EBs in the presence of strong inhibitors of the SMAD signaling until the emergence of neural-like rosettes composed of radially organized Nestin+/Pax6+ neural progenitors in both control and PKAN hiPSCs (Fig. EV 3A, B) (Marchetto et al, 2010). At day 21, neural rosettes were isolated, disaggregated, and transferred in N2/B27-based medium supplemented with the growth factor FGF2 (Marchetto et al, 2010). In these conditions, NPCs acquired the expression of the forebrain-specific marker FoxG1 and gave rise to expandable populations of highly proliferative cells. Stable NPC cultures were established with equal efficiency from all controls and PKAN hiPSCs (Fig. EV 3C) and were competent to differentiate into neurons and astrocytes (Fig. EV 3D).

Effective *in vitro* modeling of disease relies on generation of human neurons with substantial functional activity. To this end, we opted to overexpress the neurogenin-2 (Ngn2) neurogenic factor, which was shown to dramatically accelerate neuronal maturation *in vitro* and generate a large amount of enriched glutamatergic neurons (Zhang et al, 2013). Thus, after verifying the absence of PANK2 in NPCs (Fig. 1A), they were transduced with a lentivirus co-expressing both Ngn2

and the puromycin resistance gene to select only for the transgene-expressing cells. Neuronal differentiation was promoted in B27 serum-free medium supplemented with BDNF. Two weeks after Ngn2 expression, control and PKAN neurons appeared to have developed complex morphology, organized in a dense network and expressing crucial neuronal markers like Tuj1, MAP2, and NeuN (Fig. 1B).

Immunofluorescence analysis revealed also that hiPSC-derived neurons expressed the voltage-gated Na+ channels (panNav) and the vesicular glutamate transporter 1 (VGlut1) (Fig. 1B). These data suggested that the majority of the neurons generated were glutamatergic, as previously shown (Broccoli et al, 2015; Zhang et al, 2013). The absence of the PANK2 protein was confirmed by immunoblotting in PKAN mutant neurons only (Fig. 1C). Morphological inspection did not reveal any difference in either total dendritic length or branching complexity when comparing control and PKAN neurons (Fig. 1D).

In order to evaluate neuronal firing properties, we performed electrophysiological recordings at 4-20 weeks from initial differentiation. To obtain comparable growth conditions and to minimize interferences, control and PKAN neurons were co-cultured in the same culture dish and were distinguishable by expressing either the GFP (control) or the tdTomato (PKAN) fluorescent proteins (Fig. 1E). Individual cells were first recorded incurrent-clamp mode to detect intrinsic properties and action potential firing activity. The majority of control cells (20 out of 32, 63%) responded to injection of suprathreshold current steps (10-100 pA, 1s) with trains of overshooting action potentials at variable frequencies (5-15 Hz).

Conversely, the majority of PKAN neurons (14 out of 23, 61%) responded to similar current injection protocols with an anomalous firing activity consisting of brief series of spikes (often no more than 2-3 action potentials with strongly decremental amplitudes) followed by a plateau potential superimposed with irregular oscillations (Fig. 1F). The average maximal firing rate was 13 ± 1Hz in 14 control and 3 ± 2Hz in 13 PKAN human neurons, respectively ($p<0.001$, unpaired t-test), while the mean resting membrane potential was -48 ± 3 mV in control vs. -37 ± 2 mV in PKAN human neurons ($p<0.001$, unpaired t-test). Conversely, the input resistance was not significantly different in the two groups (ctrl: 507±78MΩ, PKAN human neurons: 677 ± 151 MΩ; $p>0.05$, unpaired t-test). In addition, peak amplitudes of voltage-dependent sodium currents (INa) were significantly larger in control cells than in PKAN neurons (1970 ± 464 pA *vs.* 849 ± 207 pA, respectively, $p<0.05$, Mann-Whitney rank sum test; Fig. 4F). . These data suggest that human PKAN neurons displayed aberrant electrophysiological properties as compared to neurons from normal donors (Fig. 1G). Specifically, PKAN neuronal cells showed significantly reduced peak Na+ currents and were unable to respond to current stimulation with appropriate trains of repetitive spikes.

PANK2-deficiency leads to mitochondrial dysfunction in PKAN human neurons.

To address whether the affected functionality of PKAN neurons was associated to mitochondrial dysfunction, we first evaluated the integrity of mitochondrial membrane potential using the mitochondria-specific fluorescent probe tetramethylrhodamine-methyl-ester (TMRM) (Cozzi et al, 2013). At 3 weeks from differentiation, the fluorescence associated to the neuronal cells, as recognized by the neuronal specific anti-NCAM staining, was sampled by the IN-Cell Analyzer system across the entire neuronal culture, thus avoiding limitations with the manual inspection (Fig. 2A). Results were plotted relatively to the mean of control fluorescence intensity showing that PKAN neurons exhibited a statistically significant reduction (about 20% lower) in TMRM incorporation respect to control neurons (Fig. 2A). Ultrastructural analysis revealed evident morphological alterations of mitochondria in PKAN neurons, which appear aberrant, enlarged, and swollen with damaged cristae, often strictly packed against the outer membrane with vacuolization of the matrix (Fig. 2B). By measuring the longer diameter perpendicular to the longitudinal axis of mitochondria (n= 200), we revealed a difference in the distribution of diameter length, which suggests that a higher proportion of altered mitochondria is present in PKAN compared to control neurons (Fig. 2C).

Next, we investigated respiratory activity as a critical parameter of mitochondrial function. Respiration was quantified by microscale oxygraphy allowing the real-time measurement of the global oxygen consumption rate (OCR) (Fig. 2D). Oligomycin and FCCP treatment

were also performed in order to measure ATPase inhibition and the uncoupled stimulated respiration. The values obtained in PKAN were significantly lower than those obtained in control neurons for each of the respiratory conditions. This reduced respiratory capacity is in agreement with the presence of mitochondrial dysfunctions.

PANK2-deficiency alters the oxidative status of PKAN neurons.

One of the downstream effects of impaired respiration is the increase of Radical Oxygen Species (ROS). Thus, we monitored ROS levels in basal conditions using the fluorescent ROS-sensitive dichlorofluorescein (DCF) on 3-weeks differentiated NCAM-positive neurons (Fig. 3A). Interestingly, ROS levels were strongly enhanced in the PKAN compared to control neurons (Fig. 3A). In addition, we measured the reduced form of glutathione using the ThiolTracker Violet probe in NCAM-positive neurons (Fig. 3B). In line with heightened ROS levels, significant lower levels of reduced glutathione were detected in PKAN compared to control neurons (Fig. 3B). To confirm that this altered oxidative status is directly related to PANK2 deficiency, we reintroduced in PKAN NPCs a functional copy of *PANK2* by lentiviral transduction (PANK2-LV) before the induction of differentiation. As expected, PANK2 re-expression, confirmed by immunoblotting (Fig. 3C), was sufficient to reduce ROS levels in PKAN neurons (Fig. 3C).

PANK2-deficiency altered mitochondrial iron-dependent biosynthetic pathway and cytosolic iron homeostasis

In mitochondria, iron is converted into its biological active form through two iron-dependent biosynthetic pathways: ISC and heme. To verify if PANK2- deficiency leads to impairment of these mitochondrial pathways we investigated the activity of two ISC-containing enzymes and heme content in hiPSC-derived neurons. In-gel activities of mitochondrial and cytosolic aconitases (mAco and cAco) were measured in 3 weeks differentiated neurons (Fig. 4A, upper panel). A significant reduction in activity of both aconitases was detected in PKAN compared to control neurons (Fig. 4A, lower panel). This decrease was not due to reduced protein levels since comparable amounts of mAco and cAco were revealed in western-blot analysis (Fig. 4B).

Heme quantification was performed on NPCs and not in neurons due to the low sensitivity of the method, which required a substantial amount of cells. The spectroscopic quantification revealed a significant reduction of heme in PKAN as compared to control NPC (Fig. 4C). Concomitant decrease in both ISC and heme content might represent a signal for the cell to enhance iron incorporation through the activation of the mRNA-binding activity of the ISC- deprived form of cAco (apo-cAco), which controls the translation of mRNAs of several iron-related proteins (IRP1/IRE machinery) (Muckenthaler et al, 2008). We tested this hypothesis by measuring the level of two iron proteins responsible for either cellular iron uptake (Transferrin receptor1, TfR1) or iron storage (ferritin). As expected by the increase amount of the apo-cAco form, the level of TfR1 was increased (~1.8

fold) while ferritin was reduced (~3 fold) in PKAN compared to control neurons (Fig. 4D). These results provide evidence that iron metabolism is impaired in PKAN neurons, which exhibit a manifested cellular iron deficient phenotype

Exogenous CoA can rescue the deficits in PKAN neurons

The evidence that cells can use external CoA as a source for internal CoA biosynthesis (Srinivasan et al, 2015) prompted us to verify the effect of its addition to the neuronal culture medium. In a first instance, we monitored the vitality of PKAN and control neuronal co-cultures over time after differentiation. Analysis was performed by counting the number of either tdTomato+-PKAN or GFP+-control neurons as shown in Fig. 8a. No difference between the two neuronal populations was detected after 1 day of differentiation. In contrast, at day 150, the number of PKAN neurons dropped to about 20% while control neurons were only slightly reduced (Fig. 5A). This might well be caused by the severe impairment of PKAN neurons in acquiring functional properties, which promote neuronal survival. In contrast, neuronal growth medium supplemented with 25□M CoA (at day 120) strongly reduced PKAN neuronal loss at day 150, promoting a 3-fold increase in survived neurons (Fig. 5A). In addition, patch-clamp experiments revealed a significant recovery of functional properties in the PKAN neurons (Fig. 5B). Indeed, the rate of PKAN neurons with mature firing increased from 38% (8 out of 21 cells) in untreated conditions compared to 79% (11 out of 14 cells, $p<0.05$, z- test) after CoA treatment. Conversely, the rate of control neurons with mature functionality was not different in CoA vs.

untreated conditions (7 out of 12 cells, 58% and 14 out of 20 cells, 70%, respectively, $p>0.05$, z-test; not shown) Next, we examined whether the addition of CoA starting from day 1 onwards during differentiation could restrain the heightened oxidative status in PKAN neurons. Indeed, in the presence of CoA the ROS levels were comparable between PKAN and control neurons indicating that CoA could effectively restrain the disease-associated ROS overproduction (Fig. 5C). Notably, the presence of CoA restored to control levels the mitochondria respiratory activity in PKAN neurons from patient F419fsX472a (Fig. 5D). To check the beneficial effect of CoA treatment on iron dependent mitochondrial biosynthesis we quantified the amount of heme that resulted recovered in PKAN NPC (Fig. 5E).

Discussion

Our previous results on PKAN from fibroblasts and neurons obtained by direct conversion of fibroblast suggested that neuronal impairment was mainly caused by alteration of mitochondria functionality and oxidative status (Santambrogio et al, 2015). However, these two models presented some limitations as concerning the opportunity to clarify the relationship between iron dys-regulation and neuronal death. This is essentially due to the cell specific iron metabolism requirement in fibroblasts, which is different from that in neurons, and to poor efficiency (about 5%) of direct conversion of fibroblasts into neurons, that hampers any functional electrophysiological and biochemical investigation (Santambrogio et al, 2015).

Herein, we have established hiPSC-derived neuronal cultures with high efficiency from PANK2 defective patients, providing an in depth molecular and biochemical characterization of their metabolic and functional alterations that allowed us to exhaustively define the neuronal phenotype. In addition and more significantly, we demonstrated, for the first time, the therapeutic effect of exogenous CoA administration in reverting pathological phenotypes in neurons. PKAN is a devastating infantile disorder for which only symptomatic treatments are currently available. The cascade of pathophysiological events caused by defective CoA biosynthesis as well as the association between mitochondrial dysfunction and brain iron accumulation are far to be clear. One prevailing hypothesis proposes that the imbalance of CoA pool could impair lipid homeostasis, thus resulting in membrane dysfunction and mitochondrial alteration including energetic deficiency and impairment of oxidative status and iron metabolism. Indeed, recent data obtained by microarray and whole-transcriptome gene expression assays indicated the interconnection between NBIA genes and iron-related genes. These genes might be implicated in synapse and lipid metabolism related pathways (Bettencourt et al, 2015; Heidari et al, 2016). The first result of our work is the successful generation of PKAN hiPSCs and their neuronal derivatives, suggesting that PANK2 deficiency does not affect the neuronal fate commitment and differentiation of these cells, as would be expected considering that the patients have a normal brain development.

We also provided evidence that PKAN neurons display profound alterations of mitochondrial morphology and energetic capacity,

which are probably responsible for the loss of fully functional neurons. Indeed, most PKAN neurons were impaired in their ability of firing repetitive trains of action potentials in response to depolarizing current injection, a defect that may derive either from the inability of neuronal precursors to mature into functional neurons or from a dissipation of energy-dependent transmembrane ionic gradients, which in normal conditions ensure the appropriate flux of ion currents through membrane channels.

In addition, we attributed the alteration of iron homeostasis to defective mitochondrial iron-dependent pathways: ISC and heme biosynthesis. ISC are prosthetic groups of numerous mitochondrial and cytosolic enzymes (respiratory complexes, ferrochelatase, aconitases, lipoate synthase, DNA helicases and others) (Lill et al, 2014). Thus, their deficiency may affect many biosynthetic pathways and trigger neurodegeneration. Similar neurodegenerative events have been described to occur in Friedreich's ataxia (Pandolfo, 2003), where deficiency of the ISC-iron-chaperon frataxin causes the shortages of the ISC dependent-respiratory complexes that lead to energy deficiency (Hick et al, 2013; Lodi et al, 1999). This deficit is responsible for a decrease in antioxidant capacity and accumulation of iron in mitochondria due to its inefficient utilization. The consequent damage is primarily caused by iron-generated free radicals that may inflict further injury to ISC-proteins (Lu & Cortopassi, 2007). Interestingly, our results highlighted a comparable pathological association between ISC defects and energy deficiency, suggesting that these factors are common features in triggering neuronal death. Although further analysis are necessary to clarify the association

between ISC defect and energy deficiency, this ineffective mitochondrial iron utilization might be the signal that promotes iron import into the cells and, with time, leads to iron accumulation. This is in agreement with previous studies (Bettencourt et al, 2015; Heidari et al, 2016), which postulated that disturbances in NBIA gene networks could contribute to dysregulation of iron metabolism and, in turn, progressive increase in brain iron levels aggravates the disruption of these NBIA genes. Nonetheless, we have not detected any frank iron deposition in PKAN neurons yet. Two different reasons might account for this result. On one hand, the period of time where human neurons in culture were observed might not be long enough considering that iron deposition is detectable in patients only few or more years after birth. On the other hand, iron accumulation in patients is restricted to pallidal GABAergic and, less frequently, dopaminergic neurons of substantia nigra. We favored to conduct our study on forebrain-specific glutamatergic excitatory neurons since this system is among the fewest that can be derived from hiPSCs providing a homogeneous neuronal network with robust functional activities. Given the pan-neuronal deficits occurring in this disorder, this cellular model is perfectly suited for investigating the pathophysiological roots at the base of this neuropathology including the initial steps of the iron mishandling phenotype. Furthermore, we proved that CoA administration to human neurons restores PANK neuron functionality, inhibits neuronal cell death, prevents the development of harmful ROS, and rescues heme biosynthesis and respiratory activity, establishing a strong proof of principle for the use of this compound as a therapeutic agent. This is further corroborated

by previous *in vivo* data on fly and zebrafish PKAN models (Srinivasan et al, 2015);(Zizioli et al, 2015), which clearly established the efficacy of CoA treatment in preventing or ameliorating the pathologic events.

Overall, these data indicate that this new human neuronal model represents a powerful platform for investigating pathogenic mechanism of disease and testing the efficacy of therapeutic compounds. Our observations pave the way for CoA treatment not exclusively for PKAN disease but also for CoA deficiency related disorders.

Material and Methods

Plasmid constructions

Construction of the TetO-Ngn2-p2a-hPANK2-2HA-t2a-Puromycin viral vector: in brief, the TetO-Ngn2-t2a-Puro (kindly provided by T. C. Sudhof) was modified in order to insert in the Xba site p2a peptide in frame with the existing t2a peptide and complete of MCS (created by oligonucleotide annealing, Suppl. Table I). The human PANK2 coding sequence followed by a HA tag was PCR amplified from the pCDNA3.1-hPANK2-HA construct (primers in Suppl. Table I) in order to provide it with AgeI and XbaI respectively at its 5' and 3'. They were used to insert the coding region in frame with the Ngn2 and puromycin cassette in the intermediate described above.

Fibroblasts culture and hiPSC generation

Skin biopsies were obtained from patients coming from the Movement Disorders Bio-Bank available at the Neurogenetics Unit of the Neurological Institute 'Carlo Besta' (INCB), Milan, Italy. Two PKAN patients are siblings carrying the mutation c.1259delG causing a frameshift p.F419fsX472 (here referred as PKAN(F419fsX472a) and b) (Campanella et al, 2012; Santambrogio et al, 2015). The third patient carries the c.569insA mutation, causing a premature stop codon p.Y190X (Hartig et al, 2006). All subjects gave their written consent for the skin biopsy procedure and for the use of the sample material for research purposes. Fibroblasts were cultured in DMEM high glucose (Life Technologies), 10% FBS (Life Technologies), 2 mM L- Glutamine (Sigma-Aldrich), and 1% penicillin/streptomycin (100U Pen- 100□g/ml Strep). Fibroblasts were reprogrammed into hiPSCs with the CytoTune-iPS 2.0 Sendai reprogramming kit (Life Technologies) according to manufacturer's instruction. Mutations were corroborated by sequence analysis on hiPSC clones. Colonies started to appear 30 days later, and at around day 40, they were selected according to their morphology and transferred to a new feeder layer with the same culture conditions (DMEM/F12 (Sigma-Aldrich), 20% Knockout serum replacement- KSR (Life Technologies), 1% P/S, 2 mM L-Glutamine, 1% non-essential amino acids MEM NEAA (Life Technologies), 1mM NaPyr (Sigma-Aldrich), 0.1mM beta-mercaptothanol (Life Technologies) and 10 □g/ml FGF2 (Life Technologies)). Subsequently, hiPSC clones were passed into feeder free conditions on matrigel hESC-qualified coated plates (Corning) gradually increasing the percentage of mTeSR-1 medium (Stemcell

Technologies). hiPSCs were passaged every 5–7 days with ReLeSR (Stemcell Technologies) on matrigel coated wells. Fibroblast and iPSCs were periodically tested for mycoplasma contamination by PCR.

***In vitro* three germ layers differentiation**

Feeder-free hiPSCs were treated with accutase (Sigma-Aldrich) for 5 min, washed with mTeSR-1 medium and centrifuged. Cells were then resuspended in DMEM-20%FBS-1%P/S and maintained in the same medium for 20 days. Medium was changed every 2 days.

Karyotype analysis

Metaphase chromosome preparation was obtained from hiPSCs as follow. Cells were grown on a well dish until they reached an 80-90% confluence. Then colcemid (1:100, Sigma-Aldrich) was added to the cells for 3hr and incubated at 37°C. Cells were then trypsinized, treated for 30 min using standard hypotonic solution and fixed (3:1, methanol:acetic-acid) for 30 min. Chromosome were spread on a coverslip and stained with Quinacrine (Sigma- Aldrich) mounted in McIlvaine buffer. Fluorescence was analyzed in a fluorescent microscope. Images were obtained in blind conditions to the examiner.

RT-PCR analysis

RNA was extracted using Trizol reagent (Sigma-Aldrich) and then, retrotranscribed using iScript Super Mix (Biorad). In quantitative real time PCR, Titan HotTaq EvaGreen qPCR mix (BioAtlas) was used

and expression levels were normalized respect to □-actin. Primers used to amplify cDNA samples are listed in Suppl. Table II.

Generation of human neuronal precursors cells and neurons

To obtain NPCs, EBs were formed by dissociation of hiPSC colonies with passaging solution (Miltenyi Biotec) and plating onto low-adherence dishes in mTeSR medium for 10 days supplemented with Noggin (0.5 □g/mL)(R&D System), SB431542 (5 □M) (Sigma-Aldrich); N2 (1:200)(Life Technologies); and 1%P/S. In order to obtain rosettes, EBs were plated onto matrigel growth factor reduced (Corning)-coated dishes in DMEM/F12 (Sigma-Aldrich) plus N2 (1:200); 1% NEAA (Life Technologies) and 1% P/S. After 10 days rosettes were dissociated with accutase and plated again onto matrigel-coated dishes with NPC medium (DMEM/F12; N2(1:200); B27(1:100, Life Technologies); 1%P/S and FGF2 (20ng/ml)). Homogeneous populations of NPCs were achieved after 3-5 passages with accutase in the same conditions.

Neurons were obtained as previously described (Zhang et al, 2013) with few modifications. NPCs were transduced with a lentivirus expressing Ngn2 cDNA under the control of a tetracycline-responsive promoter and a LV expressing rtTA. Lentivirus were produced as previously described (Indrigo et al, 2010). NPCs were seeded on matrigel-coated wells and differentiated in medium containing Neurobasal (Life Technologies), BDNF (10ng/ml, Peprotech), NT-3 (10ng/ml, Peprotech), B27, P/S and doxycycline (2□g/ml, Sigma-Aldrich). NT-3 was present in the medium just the first week of differentiation and doxycycline just for three weeks. Half of the

medium was changed every 2 days. For co-cultures experiments 6x104 cells (half GFP controls and half tdTomato patients) were seeded on matrigel-coated covers. After 5 days, 2x104 cortical mice neurons were added to improve differentiation and electrophysiological activity.

Immunoblotting

1x105 cells were seeded on 6 well matrigel-coated plates and differentiated to neurons. Soluble cellular extracts for immunoblotting were obtained by lysing cells in 20 mM Tris–HCl, pH 7.4, 1% Triton X-100, and protease inhibitor cocktail (Roche) followed by centrifugation at 16000 g for 10 min. Twentyfive micrograms of total proteins were separated by sodium dodecyl sulfate–12 % polyacrylamide gel electrophoresis (SDS–PAGE), and immunoblotting was performed using specific antibodies followed by peroxidase-labelled secondary antibodies (Sigma-Aldrich). Signal was revealed by the ECL- chemiluminescence kit (GE Healthcare). Total protein contents were measured using the BCA protein assay calibrated with bovine serum albumin (Thermo Fisher Scientific). Antibodies used are listed in Suppl. Table III.

Immunofluorescence

8x104 cells were seeded on matrigel-coated covers and differentiated to human neurons. Cells were fixed in 4% paraformaldehyde and processed as previously described (Cozzi et al, 2013).

Determination of aconitase activity

Aconitase activity was in-gel assayed as described in (Tong & Rouault, 2006). The patient and controls neurons were grown in differentiation medium, harvested, washed in PBS and lysed in 20 mM Tris-HCl buffer, pH 7.4, 1% Triton X-100, protease inhibitor cocktail, 2 mM citrate, 0.6 mM MnCl2, and 40 mM KCl. Soluble extracts (40 □g) in 25 mM Tris-HCl, pH 8.0, 10% glycerol, bromophenol blue, were loaded on PAGE gels containing 8% acrylamide, 132 mM Tris base, 132 mM borate, and 3.6 mM citrate in the separating gel; and 4% acrylamide, 67 mM Tris base, 67 mM borate, 3.6 mM citrate in the stacking gel. The run was performed at 180 V for 2.5 h at 4°C. Aconitase activity was determined in the dark at 37°C by incubating the gel in 100 mM Tris-HCl, pH 8.0, 1 mM NADP, 2.5 mM cis-aconitic acid, 5 mM MgCl2, 1.2 mM MTT, 0.3 mM phenazine methosulfate, and 5 U/ml isocitrate dehydrogenase. The quantification of the signal was performed using the NIH image software ImageJ.

Determination of mitochondrial membrane potential

Human neurons were incubated with Alexa Fluor 488 mouse anti–human CD 56 (anti-NCAM; BD Biosciences) for 1 hour, with 20 □M of TMRM (Molecular Probes) for 15 min, and with 2 □g/ml of Hoechst 33342 for 2 min. All of these incubations were performed at 37°C. The cells were washed and randomly analyzed by IN-Cell Analyzer 1000 system (GE Healthcare). The fluorescence of TMRM from NCAM–positive cells was collected to compare the relative mitochondrial membrane potential. A minimum of 100 neurons for

each patient or control was analyzed in at least three independent experiments for each sample.

Determination of heme content

Heme content was measured in NPCs from patients and controls as previously described (Santambrogio et al, 2011). Briefly, the cells were washed with phosphate-buffered saline and dissolved in 0.25 mL of 98% formic acid and incubated for 15 min. The heme content was evaluated by analysing the clear supernatant at 400 nm, with an extinction coefficient of 1.56x105x M-1 x cm-1. The data were normalized to protein content as determined by the BioRad Protein Assay (BioRad).

Glutathione measurement

Patients and controls human neurons were incubated with 20 □M ThiolTracker Violet (Invitrogen) for 30 min at 37°C, washed with PBS and fixed in 4% paraformaldehyde in PBS for 20 min at room temperature. The cells were then permeabilized for 3 min in PBS containing 0.1% Triton X100, 10% normal goat serum. Next, the cells were incubated with Alexa Fluor 647 mouse anti-human CD56 (anti-NCAM, BD Biosciences, diluted 1:40) for 1 hour at 37°C, and with 2 □g/ml Hoechst for 2 min. After washing, the cells were randomly analyzed by IN Cell Analyzer 1000 system (GE Healthcare). The ThiolTracker Violet fluorescence in NCAM-positive cells was collected to compare relative glutathione contents. The quantification of the signal was performed using the NIH image software ImageJ.

A minimum of 100 neurons for each patient or control was analyzed in at least three independent experiments for each sample

Determination of ROS

Human neurons were incubated with Alexa Fluor 647 mouse anti-human CD56 (anti-NCAM, BD Biosciences, diluted 1:40) for 1 hour, with 20 □M of 2',7'-dichlorodihydrofluorescein diacetate (H2DCFDA; Molecular Probes) for 15 min, and with 2 □g/ml of Hoechst 33342 for 2 min. All of these incubations were performed at 37°C. The cells were washed and randomly analyzed using an IN-Cell Analyzer 1000 system (GE Healthcare). The fluorescence of DCF from NCAM–positive cells was collected to compare the relative ROS contents. The quantification of the signal was performed using the NIH image software ImageJ. A minimum of 100 neurons for each patient or control was analyzed in at least three independent experiments for each sample.

Electron microscopy

Human neurons were fixed in 4% paraformaldehyde and 2.5% glutaraldehyde, post fixed with 2% OsO4, washed, dehydrated and embedded in Epon812. Thin sections were stained with uranyl acetate and lead citrate and examined in a Leo912 electron microscope (Zeiss). Images were randomly obtained in blind conditions to the examiner.

Measurement of dendritic arborization

Labeled neurons were randomly chosen for quantification with a total of 38 dendritic arborizations analized in at least three independent experiments for each sample. Morphometric measurements were made using NeuronStudio image analysis software (http://research.mssm.edu/cnic/tools-ns.html). Individual dendrites were selected randomly and traced manually. The maximum length and branching points were measured and archived automatically.

Patch-clamp electrophysiology

Individual slides containing co-cultured PKAN and control neurons were transferred in a recording chamber mounted on the stage of an upright BX51WI microscope (Olympus, Japan) equipped with differential interference contrast optics (DIC) and an optical filter set for the detection of GFP and tdTomato fluorescence (Semrock, Rochester, NY, USA). Cells were perfused with artificial cerebrospinal fluid (ACSF) containing (in mM): 125 NaCl, 3.5 KCl, 1.25 NaH2PO4, 2 CaCl2, 25 NaHCO3, 1 MgCl2, and 11 D-glucose, saturated with 95% O2 5% CO2 (pH 7.3). The ACSF was continuously flowing at a rate of 2-3 ml/min at room temperature. Whole-cell patch-clamp recordings were performed using pipettes filled with a solution containing the following (in mM): 10 NaCl, 124 KH2PO4, 10 HEPES, 0.5 EGTA, 2 MgCl2, 2Na2-ATP, 0.02 Na-GTP, (pH 7.2, adjusted with KOH; tip resistance: 4-6 MΩ).

All recordings were performed using a MultiClamp 700B amplifier interfaced with a PC through a Digidata 1440A (Molecular Devices).

Data were acquired using pClamp10 software (Molecular Devices) and analyzed with GraphPad Prism 5 and SigmaStat 3.5 (Systat Software Inc.). Voltage- and current-clamp traces were sampled at a frequency of 10 kHz and low-pass filtered at 2 kHz. The input resistance (Rin) was calculated by dividing the steady-state voltage response to a negative current step (-10 to -50 pA, 1s) by the amplitude of the injected current. Labeled GFP or tdTomato neurons were randomly chosen for measurement and no blind experiments were done for electrophysiology studies.

Determination of respiratory activity

Oxygen consumption rate (OCR) was measured in PKAN and control neurons with a XF96 Extracellular Flux Analyzer (Seahorse Bioscience, Billerica, MA, USA). Each control and PKAN-NPCs was seeded on a XF 96-well cell culture microplate (Seahorse Bioscience) at a density of 15–20×103 cells/well and differentiated as previously described. After replacing the growth medium with 180 □L of bicarbonate-free DMEM pre-warmed at 37°C, cells were incubated at 37°C without CO2 for 1 hour before starting the assay procedure. Then, baseline measurements of OCR, after addition of 1 □M oligomycin and of 2,1 □M carbonyl cyanide 4-(trifluoromethoxy) phenylhydrazone (FCCP) were measured using an already established protocol (Invernizzi et al, 2012). Data were expressed as pmol of O2 per minute and normalized by cell number measured by the CyQUANT Cell proliferation kit (Invitrogen), which is based on a fluorochrome binding to nucleic acids. Fluorescence was measured in a microplate luminometer with

excitation wavelength at 485 ± 10 nm and emission detection wavelength at 530 ± 12.5 nm. All determinations were performed in 9 replicates for each sample. At least three different experiments were carried out in different days. Experiments were carried out in blind conditions to the examiner.

Statistical analyses

Statistical methods were not employed to predetermine sample size in the *in vitro* and *in vivo* experiments. All the experiments were performed at least in triplicate; data was analyzed using GraphPad Prism. In general, for normally distributed data two tailed unpaired Student's t-test and one- or two-way ANOVA followed by Bonferroni post test was used. For non-normally distributed data, Mann-Whitney rank sum test was used. The data are reported as the mean +/- s.e.m. *, ** and *** indicate $p<0.05$, $p<0.01$ and $p<0.001$, respectively. A p value <0.05 was considered statistically significant

Acknowledgments

The financial support from Telethon-Italia (Grants no. GGP11088 to SL and VT), AISNAF (to SL), European Research Council (AdERC #340527 to V.B.), TIRCON project (FP7/2007-2013, HEALTH-F2-2011, # 277984 to VT),

Mariani Foundation of Milan is gratefully acknowledged. Part of this work was carried out in ALEMBIC, an advanced microscopy laboratory established by the San Raffaele Scientific Institute and the Vita-Salute San Raffaele University. We thank the Cell line and DNA bank of pediatric movement disorders and mitochondrial diseases of

the Telethon Genetic Biobank Network (project no. GTB07001) and the Bank for the Diagnosis and Research of Movement Disorders (MDB) of the EuroBiobank. The authors declare no competing financial interests

Author Contributions

DO and AR developed the neuronal models; PS and DO performed analysis on neurons; LY performed electrophysiological recordings; SGG generated and produced PANK2 expressing lentiviruses; CC and PGM established and maintained hiPSCs; MF provided the genetic analysis of hiPSC; AC performed biochemical experiments on neurons, SD and PV performed genetic and microscale-oxygraphy analysis; BG provided fibroblasts from the biobank; ST analyzed electrophysiological data and wrote the manuscript; SL, VB, VT conceived the study and wrote the manuscript

Conflict of Interests

The authors declare no competing financial interests.

Figure Legends

Fig. 1 Development and characterization of hiPSC-derived neurons from normal donor (control) and PKAN patients. **A** Representative IF image of NPCs from a control and a PKAN patient. NPC were stained for Nestin, FoxG1 and Pank2. **B** NPCs from a control and PKAN patient were differentiated into neurons by overexpressing Ngn2 (one representative experiment is shown). Two weeks after the infection differentiated NPC were positive for neuronal markers □III-tubulin (Tuj1), Map2, NeuN and human nuclei (hNu) and synaptic markers, the voltage-gated Na+ channels (PanNav)and the vesicular glutamate transporter 1 (VGlut1). **C** Western blot of soluble cell homogenates from human neurons probed with the indicated antibodies. Asterisk indicates nonspecific band and arrows point to PANK2 and β-actin. Data are presented as one example of three independent experiments. **D** Plots showing the total dendritic length and branching points between control and PKAN patients. Data presented as mean and ± SEM from at least three independent experiments. A total of 38 neurons were counted for each sample. Statistics were determined by the Student ' s t-test, n.s.= not significant, $p>0.05$. **E** Representative example of a co-culture containing control (*green*) and PKAN (*red*) human neurons. Control and PKAN NPCs were infected with GFP-LV and tdT-LV expressing vectors, respectively, and differentiated for 8 weeks. *Scale bars* 20 □m. **F** Examples of electrophysiological properties of human neurons obtained from a control individual (*top*) and a PKAN patient (*bottom*). Traces on the *left* represent trains of action potentials induced by injection of a suprathreshold current step

through the patch electrode in current-clamp mode. *Middle* traces show Na+and K+ currents (down- and upward-deflecting from baseline, respectively) in response to a 60 mV step from a holding voltage of -70 mV in voltage-clamp mode. Insets on the *right* display enlarged portions of the traces to magnify fast Na+ currents. **G** Summary histogram with percentages of recorded cells showing repetitively firing in control vs. PKAN human neurons (*p<0.05).

Fig. 2 Mitochondrial membrane potential and morphology resulted affected in PKAN human neurons. **A** Representative images of human neurons cells stained with the mitochondrial membrane potential sensible fluorescent probe TMRM, the neuronal specific anti-NCAM antibody and the nuclear staining Hoechst. *Scale bar* 20 □m. Plot showing the quantification of TMRM fluorescence signal from NCAM+. Data presented as means + SEM of at least three independent experiments; statistically significant differences were determined by the Student's t-test, *p<0.05. B Representative images of the ultrastructural analysis of fixed human neurons cells examined with electron microscope. *Scale bar* 500nm. C Mitochondrial size was measured at level of

the larger diameter along the perpendicular axis for all the mitochondria in >30 field (200 mitochondria in total) for each sample. ***p<0.001, Student t-test. **d** OCR normalization to cell number. OCR was measured in basal conditions, and after oligomycin and FCCP addiction. Bars indicate means + SEM of three independent experiments; ** p=0.01; ***p<0.001 (unpaired, two-tailed Student's t test).

Fig. 3 PKAN human neurons show altered oxidative status. **A** An example of human neurons stained with the ROS sensible fluorescent probe DCF and the nuclei dye Hoechst. Anti-NCAM was used to detect neurons neuronal specific anti-NCAM antibody. *Scale bar* 20 □m. Plots of the DCF fluorescence signal from NCAM positive controls- and PKAN human neurons, infected or not with Ngn2-PANK2-LV. Data presented as means + SEM of at least three independent experiments; statistically significant differences were determined by the Student's t-test, *p<0.05, **p<0.01. **B** Representative images of human neurons stained with ThiolTracker Violet and the anti Tuj1. *Scale bar* 20 □m. ThiolTracker Violet fluorescence signal from Tuj1 positive human neurons were quantified and shown in the plots. Data presented as means + SEM of at least three independent experiments; statistically significant differences were determined by the Anova test, *p<0.05, **p<0.01. **C** Western blot of soluble cell homogenates from patients human neurons overexpressing PANK2. Proteins were separated on 12% SDS- PAGE gels probed with the indicated antibodies. Asterisk indicates nonspecific band and arrows point to PANK2
and β -actin. Data are presented as one example of three independent experiments.

Fig. 4 PKAN human neurons show impaired iron dependent mitochondrial biosynthesis. **A** *Upper panel*: In-gel enzymatic activity of mitochondrial and cytosolic aconitase (mAco and cAco, respectively). The protein band stained with Coomassie blue was used for loading control (Loading). *Lower panel*: quantification of mAco

and cAco enzymatic activity by densitometry. **B** Western blot analysis of mitochondrial and cytosolic aconitases. **C** Heme quantification by absorbance at 400 nm of the soluble cell lysates. **D** *Upper panel*: western blot analysis of transferrin receptor (TfR1) and ferritin (FtH). Lower panel: quantification of TfR1 or FtH normalized on actin by densitometry. All the data are presented as means + SEM of at least three independent experiments; statistically significant differences were determined by Student's t-test or oneway Anova test. *p<0.05, **p<0.01, ***p<0.001.

Fig. 5 CoA treatment recovers PKAN human neurons abnormal phenotype and functionality. **A** Representative images of co-cultures of control and PKAN NPC infected with GFP-LV and tdT-LV expressing vectors, respectively, at the beginning (Day1) and after 150 days of differentiation (Day150). *Scale bar* 20
□m. Plots show the number of *green* and *red* human neurons counted at different time points. **B** Example of electrophysiological properties of cultured PKAN human neurons with or without CoA incubation for 30 days. Repetitive firing activity (*left*) and relatively large Na+ and K+ currents (*right*) were restored by CoA. The histogram on the *right* shows fractions of repetitively firing cells recorded in untreated vs. CoA-treated human neurons from control and PKAN patients (*p<0.05). **C** An example of human neurons stained with the ROS sensible fluorescent probe DCF and the nuclei dye Hoechst. Anti-NCAM antibody was used to detect neurons. *Scale bar* 20 □m. Plots of the DCF fluorescence signal from NCAM+ controls- and PKAN human neurons, differentiated or not in the presence of CoA (25 □M)

in the medium for 3 weeks. All data are presented as means + SEM of at least three independent

experiments; statistically significant differences were determined by one way Anova test. *p<0.05, **p<0.01, ***p<0.001. **D** Oxygen consumption rate (OCR) with and without CoA. Basal and uncoupled (FCCP) respiration increased after CoA supplementation. Data presented as means + SEM of nine independent replicates for each condition; statistically significant differences were determined by the Student's t-test, *p<0.05, ***p<0.001. **E** Heme quantification by absorbance at 400 nm of the soluble NPC cell lysates. All data are presented as means + SEM of at least three independent experiments; statistically significant differences were determined by one way Anova test. **p<0.01

Expanded View Figure Legends

Fig. EV 1 Characterization of hiPSC clones obtained from fibroblasts of controls and PKAN patients. **A** RT-PCR analysis of the indicated pluripotency markers expressed by hiPSC clones. Fgf4: fibroblast growth factor 4; Gdf3: Growth differentiation factor-3; Rex1: Reduced expression 1; Tert: telomerase reverse transcriptase; Klf4: Kruppel-like factor 4; Sox2: sex determining region Y-box 2; c-myc: Myc proto-oncogene protein; Dppa2/4: developmental pluripotency-associated 2/4; Oct4: octamer-binding transcription factor 4; Tdgf: teratocarcinoma derived growth factor; Gapdh: Glyceraldhyde 3-phosphate dehydrogenase. **B** Representative images of control and three PKAN iPSC colonies immunostained with the pluripotency

markers Oct4, SSEA-1, Nanog, Tra-1-60, Sox2. Nuclei stained with Hoechst. *Scale bar* 100

□m. **C** Levels of Nanog expression analysed by qRT-PCR in PKAN and control iPSCs. All clones obtained in the study expressed high levels of Nanog. **D** Representative image of control and PKAN iPSCs differentiated in vitro into all three germ layers (endoderm, FoxA2; mesoderm, SMA; ectoderm, Tuj1). Hoechst dye was used to stain nuclei. *Scale bar* 20 □m.

Fig. EV 2 Characterization of hiPSC clones obtained from fibroblasts of PKAN patients and healthy controls. **A** DNA sequence analysis of the hiPSC clones confirmed the presence of the indicated mutation in *PANK2*. **B** Karyotype analysis of generated hiPSC lines for a control and the three PKAN patients. All hiPSC lines displayed a normal karyotype.

Fig. EV 3 Generation and differentiation of NPC from hiPSC of controls and PKAN patients. **A** Representative images of embryoid bodies (EBs) at 10 days obtained from control and PKAN patient hiPSC. *Scale bar* 100 □m. **B** Representative IF images for rosettes at 10 days obtained from the EBs. Neural rosettes clusters express the typical markers (FoxG1, Nestin, Pax6, zo1, ki67, DCX). Hoechst dye was used to stain nuclei. *Scale bar* 100 □m. **C** Representative IF images of NPC obtained from neural rosette differentiated from control and PKAN patient. NPCs express the markers (Nestin, FoxG1, Sox2, ki67, Pax6, Tuj1, DCX and Otx2). Hoechst dye was used to stain nuclei. *Scale bar* 20 □m. **D** NPCs obtained from hiPSC lines can potentially be differentiated into neurons (Map2) and astrocytes (GFAP). *Scale bar* 20 □m

Supplementary Table I. Oligonucleotides used to clone the PANK2 into Ngn2 lentiviral construct.

TetO-Ngn2-t2a-Puro modification.	CTAGCGGCAGCGGCGCCACCAACTTCAGCCTGC TGAAGCAGG CCGGCGACGTGGAGGAGAACCCCGGCCCCACCG GTGTTAACT; CTAGAGTTAACACCGGTGGGGCCGGGGTTCTCCT CCACGTCGC CGGCCTGCTTCAGCAGGCTGAAGTTGGTGGCGC CGCTGCCG
hPKAN primers	ccgACCGGTATGAGGAGGCTCGGGCCCTTCC; tgcTCTAGAGGCGTAGTCGGGCACGTCGTAG

Supplementary Table II. Primers used to characterized iPSC.

Gene	**Forward**	**Reverse**
KLF4	TTATTCTCTCCAATTCGCTG	GGACTCCCTGCCATAG
SOX	CAAGCTCCTTCAACTGGTT	CTTAGAATGATGCAAG
OCT	AGAAAGCGAACCAGTATC	CTCAAAATCCTCTCGT
TER	ACCAAGAAGTTCATCTCCC	AAAGAAAGACCTGAG
GDF	AAAGGGAACAGTTGACAT	AGCTACATCCAGCAG
DPP	GATGCAAAATACCAGCCCT	CGTTTCCTCGAACATC
FGF4	CTACAACGCCTACGAGTCC	GTTGCACCAGAAAAG
REX	CAGATCCTAAACAGCTCGC	GCGTACGCAAATTAA
CMY	CTGGACACGCTGACGAAA	TTCAGCACGCTTCTCC
TDG	TTTGCTCGTCCATCTCGGG	GCTCCTTACTGTGCTG
DPP	GACCTCCACAGAGAAGTC	AGGTGGCAGTTTAGA
GAD	CAAGATCATCAGCAATGCC	GCCTGCTTCACCACCT
NAN	CCTCCATGGATCTGCTTAT	ATCTGCTGGAGGCTGA
ACT	ACCCCAGCCATGTACGTT	GGTGAGGATCTTCATG

PAN	GGGCAGAGGCATGCACAA	GCACCAACGAGGGAC
PAN	GGTTCATAAATGTTAACTT	GATCTGCCCATCTCGG

Supplementary Table III. Antibodies used in the study.

Antibody	**Manufacturer**	**Application**	**Dilution**
Alexa Fluor 488 anti-	BD	IF	1:80
Alexa Fluor 647 anti-	BD	IF	1:80
Oct4	Abcam	IF	1:250
SSEA-1	Immuno Sci	IF	1:250
NANOG	Abcam	IF	1:250
TRA-1-6	Millipore	IF	1:250
SOX2	Abcam	IF	1:250
FoxA2	Abcam	IF	1:250
Anti-SMA	Sigma-Aldrich	IF	1:500
βIII-tubulin/Tuj1	Covance	IF	1:500
FoxG1	Abcam	IF	1:200
Anti human Nestin	Millipore	IF	1:500
Pax6	Covance	IF	1:200
FITC-anti-zo1	Zymed	IF	1:200
DCX	Millipore	IF	1:200
Ki67	Immunological	IF	1:200
Otx2	R&D	IF	1:200
Map2	Immunological	IF	1:400
GFAP	Millipore	IF	1:200
hNu	Millipore	IF	1:200
NeuN	Millipore	IF	1:200
Pank2	Origen Tech	IF/WB	1:200/1:300
PanNav	Sigma-Aldrich	IF	1:100
Vglut1	Synaptic	IF	1:200
mAco	Antibody	WB	1 g/ml
cAco	Home made	WB	1:500
TfR1	Zymed	WB	1:2000
FtH	Home made	WB	1:2000
Actin	Sigma-Aldrich	WB	1:6000
Anti-mouse HRP	Sigma-Aldrich	WB	1:100000
Anti-rabbit HRP	Sigma-Aldrich	WB	1:50000
Anti-mouse-546	Immunological	IF	1:800
Anti-rabbit-488	Immunological	IF	1:800

Figure EV 1

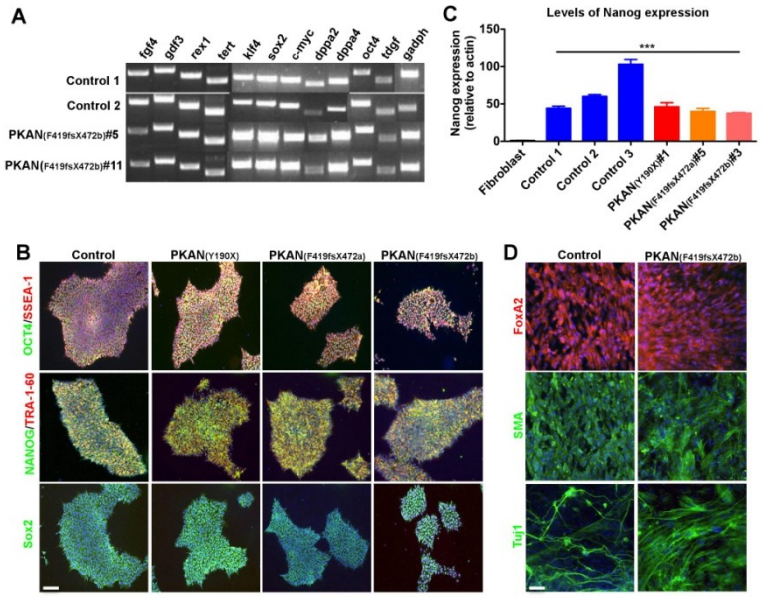

Figure EV 2

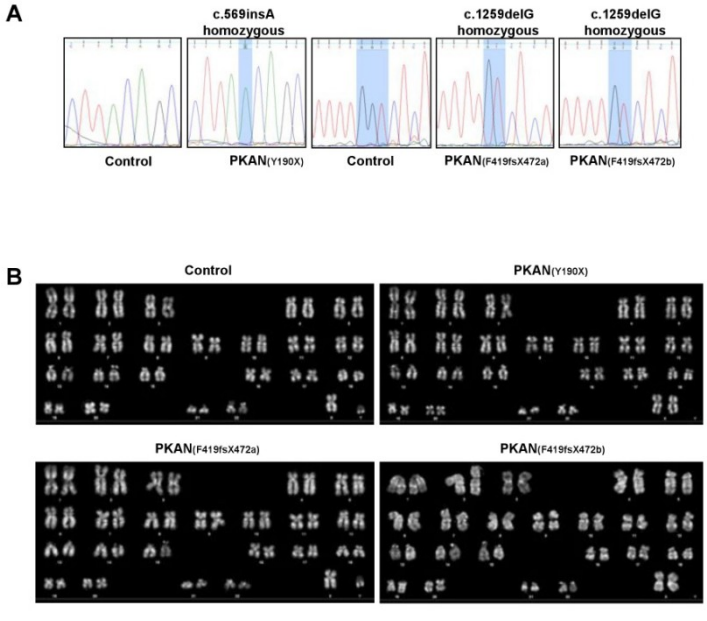

Figure EV 3

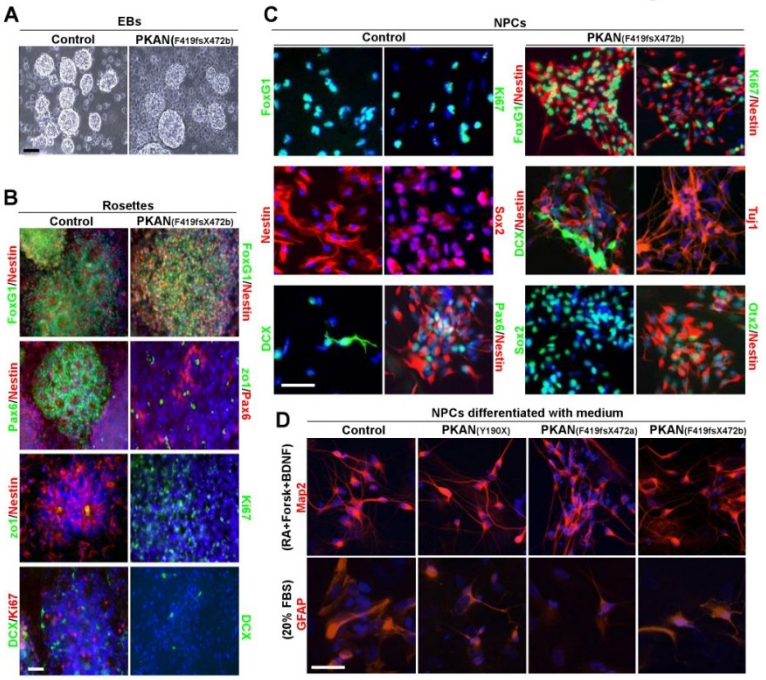
A
EBs
Control
PKAN(F419fsX472b)
B
Rosettes
Control
PKAN(F419fsX472b)
FoxG1/Nestin
FoxG1/Nestin
Pax6/Nestin
zo1/Pax6
zo1/Nestin
Ki67
DCX/Ki67
DCX
C
NPCs
Control
PKAN(F419fsX472b)
FoxG1
Ki67
FoxG1/Nestin
Ki67/Nestin
Nestin
Sox2
DCX/Nestin
Tuj1
DCX
Pax6/Nestin
Sox2
Otx2/Nestin
D
NPCs differentiated with medium
Control
PKAN(Y190X)
PKAN(F419fsX472a)
PKAN(F419fsX472b)
(RA+Forsk+BDNF)
Map2
(20% FBS)
GFAP

Figure 1

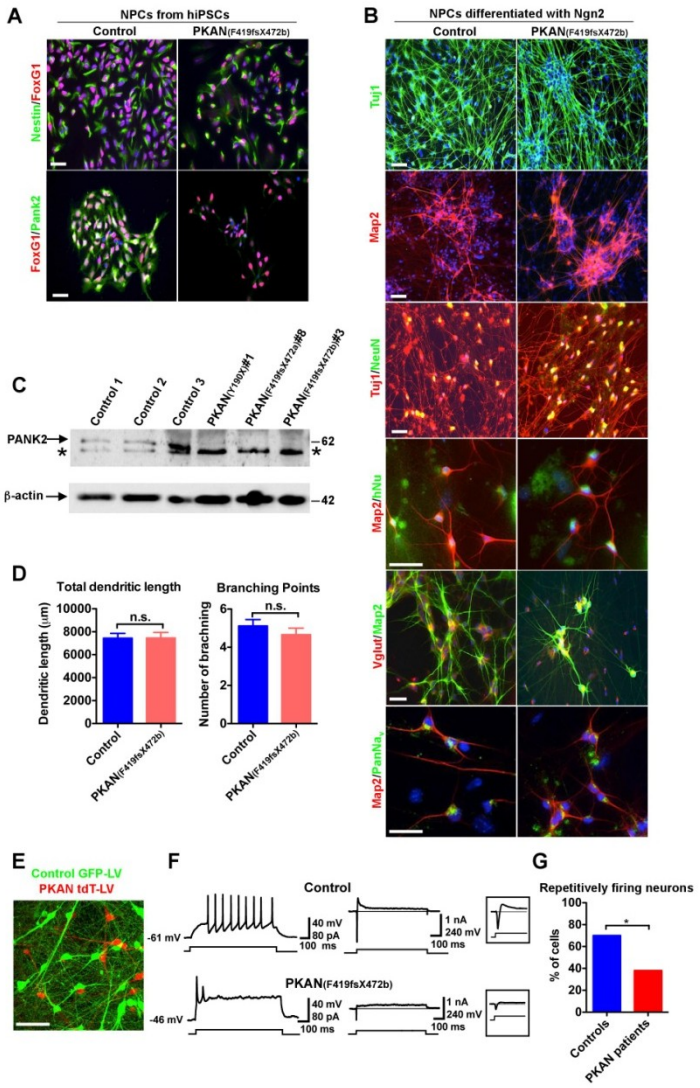
A
NPCs from hiPSCs
Control
PKAN(F419fsX472b)
Nestin/FoxG1
FoxG1/Pank2
B
NPCs differentiated with Ngn2
Control
PKAN(F419fsX472b)
Tuj1
Map2
Tuj1/NeuN
Map2/hNu
Vglut/Map2
Map2/PanNa
C
Control 1
Control 2
Control 3
PKAN(Y190X)#1
PKAN(F419fsX472a)#8
PKAN(F419fsX472b)#3
PANK2
β-actin
62
42
D
Total dendritic length
Dendritic length (µm)
n.s.
Control
PKAN(F419fsX472b)
Branching Points
Number of brachning
n.s.
Control
PKAN(F419fsX472b)
E
Control GFP-LV
PKAN tdT-LV
F
Control
-61 mV
40 mV
80 pA
100 ms
1 nA
240 mV
100 ms
PKAN(F419fsX472b)
-46 mV
40 mV
80 pA
100 ms
1 nA
240 mV
100 ms
G
Repetitively firing neurons
% of cells
*
Controls
PKAN patients

Figure 2

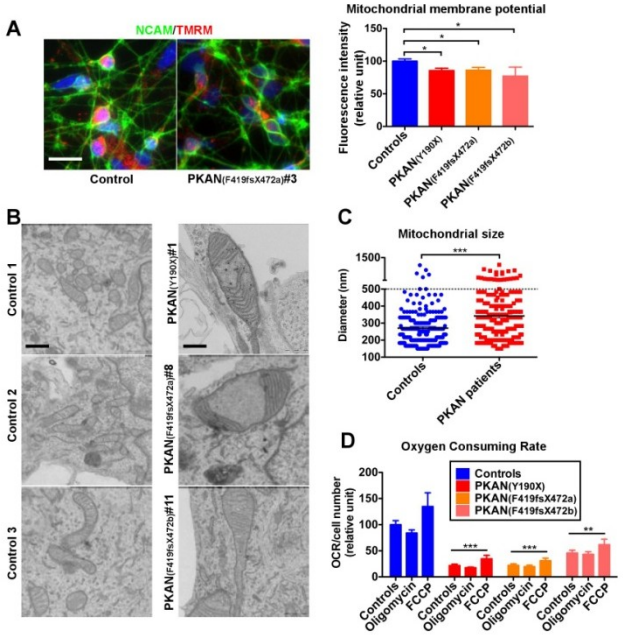

Figure 3

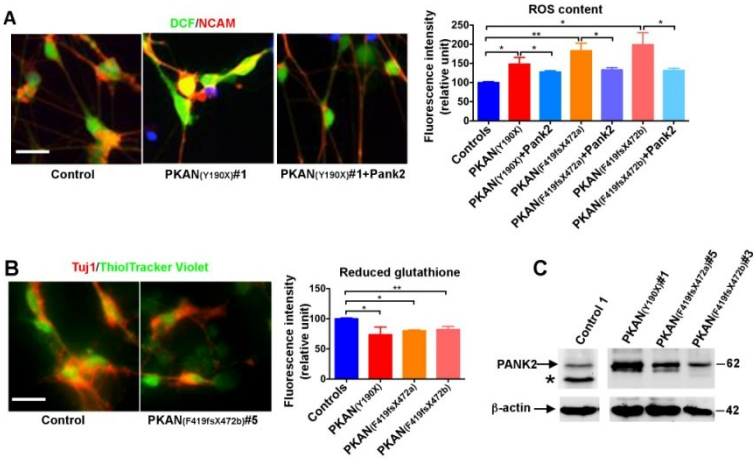

Figure 4

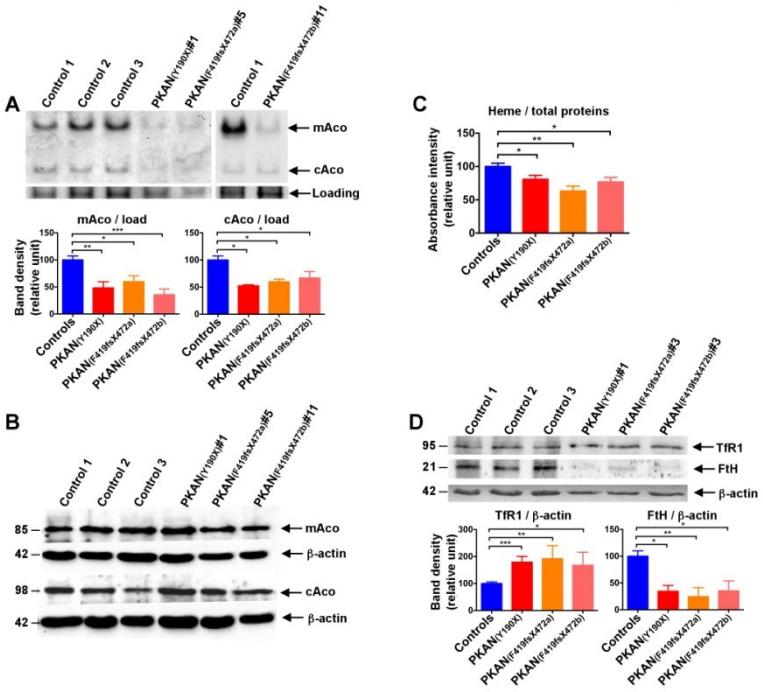
A
Control 1
Control 2
Control 3
PKAN(Y190X)#1
PKAN(F419fsX472a/b)#5
Control 1
PKAN(F419fsX472a/b)#11
mAco
cAco
Loading
mAco / load
cAco / load
Band density (relative unit)
Controls
PKAN(Y190X)
PKAN(F419fsX472a)
PKAN(F419fsX472b)
B
Control 1
Control 2
Control 3
PKAN(Y190X)#1
PKAN(F419fsX472a/b)#5
PKAN(F419fsX472a/b)#11
85
42
98
42
mAco
β-actin
cAco
β-actin
C
Heme / total proteins
Absorbance intensity (relative unit)
Controls
PKAN(Y190X)
PKAN(F419fsX472a)
PKAN(F419fsX472b)
D
Control 1
Control 2
Control 3
PKAN(Y190X)#1
PKAN(F419fsX472a/b)#3
PKAN(F419fsX472a/b)#3
95
21
42
TfR1
FtH
β-actin
TfR1 / β-actin
FtH / β-actin
Band density (relative unit)
Controls
PKAN(Y190X)
PKAN(F419fsX472a)
PKAN(F419fsX472b)

Figure 5

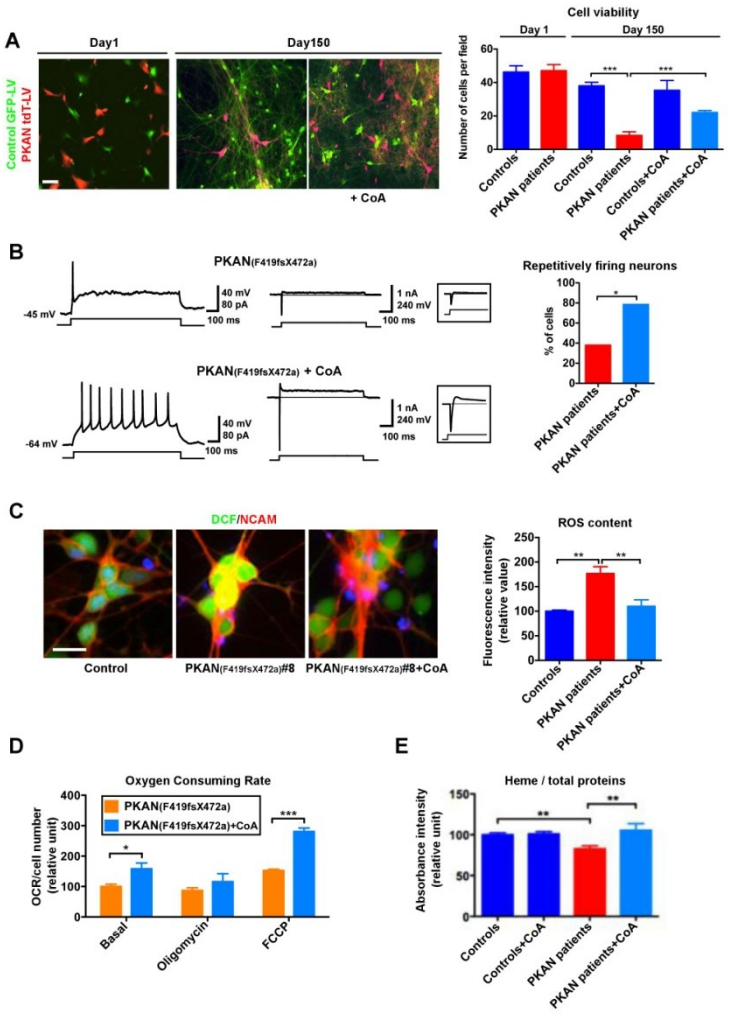
A
Day1
Day150
Control GFP-LV
PKAN tdT-LV
+ CoA
Cell viability
Day 1
Day 150
Number of cells per field
Controls
PKAN patients
Controls
PKAN patients
Controls+CoA
PKAN patients+CoA
B
PKAN(F419fsX472a)
-45 mV
40 mV
80 pA
100 ms
1 nA
240 mV
100 ms
PKAN(F419fsX472a) + CoA
-64 mV
Repetitively firing neurons
% of cells
PKAN patients
PKAN patients+CoA
C
DCF/NCAM
Control
PKAN(F419fsX472a)#8
PKAN(F419fsX472a)#8+CoA
ROS content
Fluorescence intensity (relative value)
Controls
PKAN patients
PKAN patients+CoA
D
Oxygen Consuming Rate
PKAN(F419fsX472a)
PKAN(F419fsX472a)+CoA
OCR/cell number (relative unit)
Basal
Oligomycin
FCCP
E
Heme / total proteins
Absorbance intensity (relative unit)
Controls
Controls+CoA
PKAN patients
PKAN patients+CoA

References

Akram M (2014) Citric acid cycle and role of its intermediates in metabolism.*Cell Biochem Biophys* 68**:** 475-478

Amamoto R, Arlotta P (2014) Development-inspired reprogramming of the mammalian central nervous system. *Science* 343**:** 1239882

Bettencourt C, Forabosco P, Wiethoff S, Heidari M, Johnstone DM, Botia JA, Collingwood JF, Hardy J, Milward EA, Ryten M, Houlden H (2015) Gene co- expression networks shed light into diseases of brain iron accumulation. *Neurobiol Dis* 87**:** 59-68

Broccoli V, Rubio A, Taverna S, Yekhlef L (2015) Overcoming the hurdles for a reproducible generation of human functionally mature reprogrammed neurons. *Exp Biol Med (Maywood)* 240**:** 787-794

Brunetti D, Dusi S, Giordano C, Lamperti C, Morbin M, Fugnanesi V, Marchet S, Fagiolari G, Sibon O, Moggio M, d'Amati G, Tiranti V (2014) Pantethine treatment is effective in recovering the disease phenotype induced by ketogenic diet in a pantothenate kinase-associated neurodegeneration mouse model. *Brain : a journal of neurology* 137**:** 57-68

Brunetti D, Dusi S, Morbin M, Uggetti A, Moda F, D'Amato I, Giordano C, d'Amati G, Cozzi A, Levi S, Hayflick S, Tiranti V (2012) Pantothenate kinase- associated neurodegeneration: altered mitochondria membrane potential and defective respiration in Pank2 knock-out mouse model. *Hum Mol Genet* 21: 5294-5305

Campanella A, Privitera D, Guaraldo M, Rovelli E, Barzaghi C, Garavaglia B, Santambrogio P, Cozzi A, Levi S (2012) Skin fibroblasts from pantothenate kinase-associated neurodegeneration patients show altered cellular oxidative status and have defective iron-handling properties. *Hum Mol Genet* 21: 4049- 4059

Colombelli C, Aoun M, Tiranti V (2015) Defective lipid metabolism in neurodegeneration with brain iron accumulation (NBIA) syndromes: not only a matter of iron. *J Inherit Metab Dis* 38: 123-136

Cozzi A, Santambrogio P, Privitera D, Broccoli V, Rotundo LI, Garavaglia B, Benz R, Altamura S, Goede JS, Muckenthaler MU, Levi S (2013) Human L- ferritin deficiency is characterized by idiopathic generalized seizures and atypical restless leg syndrome. *J Exp Med* 210: 1779-1791

Dusi S, Valletta L, Haack TB, Tsuchiya Y, Venco P, Pasqualato S, Goffrini P, Tigano M, Demchenko N, Wieland T, Schwarzmayr T, Strom TM, Invernizzi F, Garavaglia B, Gregory A, Sanford L, Hamada J, Bettencourt C, Houlden H, Chiapparini L, Zorzi G, Kurian MA, Nardocci N, Prokisch H, Hayflick S, Gout I, Tiranti V (2014) Exome sequence reveals mutations in CoA synthase as a cause of neurodegeneration with brain iron accumulation. *Am J Hum Genet* 94: 11-22

Garcia M, Leonardi R, Zhang YM, Rehg JE, Jackowski S (2012) Germline deletion of pantothenate kinases 1 and 2 reveals the key roles for CoA in postnatal metabolism. *PLoS One* 7: e40871

Hartig MB, Hortnagel K, Garavaglia B, Zorzi G, Kmiec T, Klopstock T, Rostasy K, Svetel M, Kostic VS, Schuelke M, Botz E, Weindl A, Novakovic I, Nardocci N, Prokisch H, Meitinger T (2006) Genotypic and phenotypic spectrum of PANK2 mutations in patients with neurodegeneration with brain iron accumulation. *Ann Neurol* **59:** 248-256

Hartig MB, Prokisch H, Meitinger T, Klopstock T (2012) Pantothenate kinase- associated neurodegeneration. *Curr Drug Targets* 13: 1182-1189

Hayflick SJ, Hartman M, Coryell J, Gitschier J, Rowley H (2006) Brain MRI in neurodegeneration with brain iron accumulation with and without PANK2 mutations. *Ajnr* 27: 1230-1233

Heidari M, Johnstone DM, Bassett B, Graham RM, Chua AC, House MJ, Collingwood JF, Bettencourt C, Houlden H, Ryten M, Olynyk JK, Trinder D, Milward EA (2016) Brain iron accumulation affects myelin-related molecular systems implicated in a rare neurogenetic disease family with neuropsychiatric features. *Mol Psychiatry*

Hick A, Wattenhofer-Donze M, Chintawar S, Tropel P, Simard JP, Vaucamps N, Gall D, Lambot L, Andre C, Reutenauer L, Rai M, Teletin M, Messaddeq N, Schiffmann SN, Viville S, Pearson CE, Pandolfo M, Puccio H (2013) Neurons and cardiomyocytes derived from induced pluripotent stem cells as a model for mitochondrial defects in Friedreich's ataxia. *Dis Model Mech* 6: 608-621

Indrigo M, Papale A, Orellana D, Brambilla R (2010) Lentiviral vectors to study the differential function of ERK1 and ERK2 MAP kinases. *Methods Mol Biol* 661: 205-220

Invernizzi F, D'Amato I, Jensen PB, Ravaglia S, Zeviani M, Tiranti V (2012) Microscale oxygraphy reveals OXPHOS impairment in MRC mutant cells. *Mitochondrion* 12: 328-335

Kuo YM, Duncan JL, Westaway SK, Yang H, Nune G, Xu EY, Hayflick SJ, Gitschier J (2005) Deficiency of pantothenate kinase 2 (Pank2) in mice leads to retinal degeneration and azoospermia. *Hum Mol Genet* 14: 49-57

Leonardi R, Zhang YM, Rock CO, Jackowski S (2005) Coenzyme A: back in action. *Prog Lipid Res* 44: 125-153

Levi S, Finazzi D (2014) Neurodegeneration with brain iron accumulation: update on pathogenic mechanisms. *Frontiers in pharmacology* 5: 99

Lill R, Srinivasan V, Muhlenhoff U (2014) The role of mitochondria in cytosolic- nuclear iron-sulfur protein biogenesis and in cellular iron regulation. *Curr Opin Microbiol* 22: 111-119

Lodi R, Cooper JM, Bradley JL, Manners D, Styles P, Taylor DJ, Schapira AH (1999) Deficit of in vivo mitochondrial ATP production in patients with Friedreich ataxia. *PNAS* 96: 11492-11495

Lu C, Cortopassi G (2007) Frataxin knockdown causes loss of cytoplasmic iron-sulfur cluster functions, redox alterations and induction of heme transcripts. *Arch Biochem Biophys* 457: 111-122

Marchetto MC, Brennand KJ, Boyer LF, Gage FH (2011) Induced pluripotent stem cells (iPSCs) and neurological disease modeling: progress and promises. *Hum Mol Genet* 20: R109-115

Marchetto MC, Carromeu C, Acab A, Yu D, Yeo GW, Mu Y, Chen G, Gage FH, Muotri AR (2010) A model for neural development and treatment of Rett syndrome using human induced pluripotent stem cells. *Cell* 143: 527-539

Muckenthaler MU, Galy B, Hentze MW (2008) Systemic iron homeostasis and the iron-responsive element/iron-regulatory protein (IRE/IRP) regulatory network. *Annu Rev Nutr* **28:** 197-213

Pandolfo M (2003) Friedreich ataxia. *Semin Pediatr Neurol* 10: 163-172

Peitz M, Jungverdorben J, Brustle O (2013) Disease-specific iPS cell models in neuroscience. *Curr Mol Med* 13: 832-841

Rana A, Seinen E, Siudeja K, Muntendam R, Srinivasan B, van der Want JJ, Hayflick S, Reijngoud DJ, Kayser O, Sibon OC (2010) Pantethine rescues a Drosophila model for pantothenate kinase-associated neurodegeneration.
PNAS 107: 6988-6993

Santambrogio P, Dusi S, Guaraldo M, Rotundo LI, Broccoli V, Garavaglia B, Tiranti V, Levi S (2015) Mitochondrial iron and energetic dysfunction distinguish fibroblasts and induced neurons from pantothenate kinase- associated neurodegeneration patients. *Neurobiol Dis* 81: 144-153

Santambrogio P, Erba BG, Campanella A, Cozzi A, Causarano V, Cremonesi L, Galli A, Della Porta MG, Invernizzi R, Levi S (2011) Over-expression of mitochondrial ferritin affects the JAK2/STAT5 pathway in K562 cells and causes mitochondrial iron accumulation. *Haematologica* 96: 1424-1432

Siudeja K, Srinivasan B, Xu L, Rana A, de Jong J, Nollen EA, Jackowski S, Sanford L, Hayflick S, Sibon OC (2011) Impaired Coenzyme A metabolism affects histone and tubulin acetylation in Drosophila and human cell models of pantothenate kinase associated neurodegeneration. *EMBO Mol Med* 3: 755- 766

Srinivasan B, Baratashvili M, van der Zwaag M, Kanon B, Colombelli C, Lambrechts RA, Schaap O, Nollen EA, Podgorsek A, Kosec G, Petkovic H, Hayflick S, Tiranti V, Reijngoud DJ, Grzeschik NA, Sibon OC (2015) Extracellular 4'-phosphopantetheine is a source for intracellular coenzyme A synthesis. *Nat Chem Biol* **11:** 784-792

Tiscornia G, Vivas EL, Izpisua Belmonte JC (2011) Diseases in a dish: modeling human genetic disorders using induced pluripotent cells. *Nat Med* 17: 1570-1576

Tong WH, Rouault TA (2006) Functions of mitochondrial ISCU and cytosolic ISCU in mammalian iron-sulfur cluster biogenesis and iron homeostasis. *Cell Metab* 3: 199-210

Zhang Y, Pak C, Han Y, Ahlenius H, Zhang Z, Chanda S, Marro S, Patzke C, Acuna C, Covy J, Xu W, Yang N, Danko T, Chen L, Wernig M, Sudhof TC (2013) Rapid single-step induction of

functional neurons from human pluripotent stem cells. *Neuron* 78: 785-798

Zhou B, Westaway SK, Levinson B, Johnson MA, Gitschier J, Hayflick SJ (2001) A novel pantothenate kinase gene (PANK2) is defective in Hallervorden-Spatz syndrome. *Nat Genet* 28: 345-349

Zizioli D, Tiso N, Guglielmi A, Saraceno C, Busolin G, Giuliani R, Khatri D, Monti E, Borsani G, Argenton F, Finazzi D (2015) Knock-down of pantothenate kinase 2 severely affects the development of the nervous and vascular system in zebrafish, providing new insights into PKAN disease. *Neurobiol Dis* 85: 35-48

Zorzi G, Zibordi F, Chiapparini L, Bertini E, Russo L, Piga A, Longo F, Garavaglia B, Aquino D, Savoiardo M, Solari A, Nardocci N Iron-related MRI images in patients with pantothenate kinase-associated neurodegeneration (PKAN) treated with deferiprone: results of a phase II pilot trial. *Mov Disord* 26: 1756-1759

CHAPTER 5

Alteration of coenzyme A biosynthetic pathway in neurodegeneration with brain iron accumulation syndromes

Paola Venco*, Sabrina Dusi*, Lorella Valletta* and Valeria Tiranti*1

*Unit of Molecular Neurogenetics, Pierfranco and Luisa Mariani Centre for the Study of Mitochondrial Disorders in Children, Foundation IRCCS Neurological Institute 'Carlo Besta', 20126 Milan, Italy

Biochem. Soc. Trans: 2014 Aug;42(4):1069-74. doi: 10.1042/BST20140106

Abstract

NBIA (neurodegeneration with brain iron accumulation) comprehends a heterogeneous group of neurodegenerative diseases having as a common denominator, iron overload in specific brain areas, mainly basal ganglia and globus pallidus. In the past decade a bunch of disease genes have been identified, but NBIA pathomechanisms are still not completely clear. PKAN (pantothenate kinase-associated neurodegeneration), an autosomal recessive disorder with progressive impairment of movement, vision and cognition, is the most common form of NBIA. It is caused by mutations in the *PANK2* (pantothenate kinase 2) gene, coding for a mitochondrial enzyme that phosphorylates vitamin B5 in the first reaction of the CoA (coenzyme A biosynthetic pathway. A distinct form of NBIA, denominated CoPAN (CoA synthase protein-associated neurodegeneration), is caused by mutations in the *CoASY* (CoA synthase) gene coding for a bifunctional mitochondrial enzyme, which catalyses the final steps of the CoA biosynthesis. These two inborn errors of CoA metabolism further support the concept that dysfunctions in CoA synthesis may play a crucial role in the pathogenesis of NBIA.

Introduction

To date, ten genes have been associated with specific forms of NBIA (neurodegeneration with brain iron accumulation) [1]. As reported in Table 1, only two forms are caused by mutations in genes coding for proteins directly involved in iron metabolism: neuroferritinopathy due to *FTL* (ferritin light) chain gene (MIM #606159) mutation [2] and acaeruloplasminaemia linked to mutations in the *CP* (caeruloplasmin) gene (MIM #117700) [3]. The other NBIA disease genes encode proteins with a variety of functions: some are involved in fatty acid metabolism and autophagy while others have still unknown roles (Table 1).

PKAN (pantothenate kinase-associated neurodegenera- tion) accounts for approximately 50 % of NBIA cases and is caused by mutations in the *PANK2* (pantothenate kinase type 2) gene, whereas, recently, a novel subtype of NBIA, denominated CoPAN (CoA synthase protein- associated neurodegeneration) (MIM #609855), has been associated with mutations in *CoASY* (CoA synthase) gene [4]. As a high-energy carrier of acetyl and acyl groups, CoA (coenzyme A) is central to diverse cellular metabolic processes including citric acid cycle, fatty acid biosynthesis, β-oxidation, cholesterol and sphingolipid synthesis. In addition, CoA is a crucial factor in regulating a variety of enzymatic reactions and cellular metabolic processes. A reduction of CoA levels in PANK-deficient *Drosopftila* fumble mutants [5] and in mice lacking both *Pank1* and *Pank2* genes [6] have been demonstrated. Moreover, the demonstration of CoASY interaction with components of the PI3K/mTOR/S6K

(phosphoinositide 3-kinase/mammalian target of rapamycin/S6 kinase) signalling cascade poses an interesting link between CoA biosynthesis and the regulation of cellular metabolism [7,8].

Here we will discuss the main features of PANK2 and CoASY, and their relationship with CoA metabolism and neurodegeneration.

NBIA DISORDERS AND ASSOCIATED GENES			
DISEASE	DISEASE GENE	INHERITANCE	SYMPTOMS
Neuroferritinopathy	FTL (19q13.3)	Autosomal Dominant	Extrapyramidal signs, dystonia, orofacial dystonia, cognitive decline.
Aceruloplasminemia	CP (3q23.25)	Autosomal Recessive	Iron not only in the basal ganglia but also in liver, pancreas and myocardium, cognitive impairment, diabetes mellitus, retinal degeneration, blepharospasm, facial and neck

			dystonia, chorea, dysarthria, ataxia.
Pantothenate Kinase-Associated Neurodegeneration (PKAN)	*PANK2* (20p12.3)	Autosomal Recessive	Dystonia, spasticity, cognitive decline, pigmentary retinopathy.
PLA2G6-Associated Neurodegeneration (PLAN)	*PLA2G6* (22q12.13)	Autosomal Recessive	Infantile neuroaxonal dystrophy, progressive motor and mental retardation, cerebellar ataxia, pyramidal signs.
Mitochondrial Membrane Protein Associated Neurodegeneration (MPAN)	C19orf12 (19q12)	Autosomal Recessive	Iron-containing deposits, dystonia, parkinsonism, psychiatric symptoms, spastic paraparesis.
FA2H-Associated Neurodegeneration (FAHN)	FA2H (16q23)	Autosomal Recessive	Spastic quadriparesis, severe ataxia, dystonia.

Kufor-Rakeb disease	ATP13A2 (1p36)	Autosomal Recessive	Early onset levodopa-responsive parkinsonism with pyramidal tract involvement, dementia.
Woodhouse-Sakati Syndrome	*DCAF17* (2q31.1)	Autosomal Recessive	Hypogonadism, alopecia, diabetes mellitus, mental retardation, deafness, electrocardiographic abnormalities.
β-propeller Protein-Associated Neurodegeneration (BPAN)	*WDR45* (Xp11.23)	X-Linked	Cognitive impairment, progressive dystonia-parkinsonism, corticospinal signs.
COASY protein-associated neurodegeneration (CoPAN)	COASY (17q12.21)	Autosomal Recessive	Oro-mandibular dystonia, dysarthria, spastic dystonic

			paraparesis, obsessive-compulsive behaviour

CoA

CoA is an indispensable cofactor in all living organisms, where it functions as an acyl group carrier and carbonyl- activating group in a multitude of biochemical transform- ations, including the TCA (tricarboxylic acid) cycle and fatty acid metabolism. *De novo* synthesis of CoA is a highly conserved pathway that includes five enzymatic steps: pantothenic acid (vitamin B5) phosphorylation, cysteine conjugation, decarboxylation, conjugation to an adenosyl group and phosphorylation. In mammals, the first step is catalysed by PANK, whereas the last two steps are catalysed by CoASY, a mitochondrial bifunctional enzyme endowed with both PPAT (4r-phosphopantetheine adenylyltransferase) and DPCK (dephospho-CoA kinase) activities.

The reaction catalysed by PANK is the primary rate- limiting step in CoA biosynthesis and it is controlled by CoA and CoA thioesters the end-products of the pathway. Feedback regulation of PANK by different CoA molecular species controls overall CoA availability in response to cell metabolic status. In bacteria, a second level of regulation is evident at PPAT (or CoAD). CoA consists of 3r-phosphoadenosine linked through the 5r position of the ribose, to pantothenic acid via pyrophosphate linkage. The carboxyl end of

pantothenic acid is linked through a peptidic link to 2-mercaptoethanol amine. The thiol group at the end is essential to the chemical reactions where CoA is involved in, so the enzymes involved in CoA biosynthesis are very specific in incorporating cysteine, but not other amino acids [9]. CoA is utilized in about 100 biosynthetic and degrading reactions. Over 4 % of cellular reactions utilize CoA. Tissue levels can vary widely depending on the organ in question, diet and fed/fasting state. The ratio of free CoA to acyl-CoA is important for regulating many key metabolic enzymes, such as acyl-CoA synthetase, PDH (pyruvate dehydrogenase) and 2-OG (2-oxoglutarate) dehydrogenase. The level of CoA is regulated by numerous extracellular stimuli, including hormones, glucocorticoids, nutrients and cellular metabolites [10]. In plants, the steps that convert pantothenate to CoA are almost certainly cytosolic [11,12]. CoA is required in mitochondria for the citric acid cycle, in chloroplasts for fatty acid synthesis, and in peroxisomes for β-oxidation. CoA must be imported into these organelles from the cytosol. Yeast and mammalian mitochondria and peroxisomes likewise import CoA because they cannot make it [13]. Mitochondrial CoA transporters belonging to the MCF (mitochondrial carrier family) have been identified in yeast [14] and human [15]. The compartmentalization of CoA in all eukaryotes appears to be closely regulated, with cytosol and organelles maintaining separate CoA pools whose levels can modulate fluxes through CoA-dependent reactions. Mammalian cytosolic concentrations are estimated to be in the range 0.02–0.14 mM in animal tissues, whereas mitochondrial concentrations are much higher: from 2 to over 5 mM [16].

PANK2

Approximately half of the NBIA cases can be explained by *PANK2* gene mutations causing PKAN. By linkage analysis, the defective gene was mapped to chromosome 20p12.3 [17]. Early onset is associated with the classic presentation, whereas patients with later onset often show atypical features. There are differences in expression pattern among the *PANK* genes. *PANK1* is expressed in heart, liver and kidney, whereas *PANK3* is expressed most abundantly in the liver. In contrast with these two genes, *PANK2* is ubiquitously expressed, including in retina and infant basal ganglia [17]. *PANK2* dysfunction is compatible with life, and two functional homologues, *PANK1* and *PANK3*, encode for proteins located in the cytosol and may compensate for the loss of PANK2. There is also a PANK4 protein, which is fairly dissimilar from PANK1, PANK2 and PANK3 and apparently lacks enzymatic activity. Human full-length PANK2 is cleaved at two sites by the mitochondrial processing peptidase, generating a transient

59.2 kDa intermediate and a long-lived 47.4 kDa mature protein. Mitochondrial targeting sequences are located in both the largest precursor peptide and the intermediate peptide, and the biochemical activity of the 48 kDa protein is confirmed [18]. Investigations of human *PANK2* expression indicated two different transcripts, predicted to encode two protein isoforms; the longest PANK2 isoform localize to mitochondria [19].

PANK is known to catalyse the first out of five steps in CoA biosynthesis, which utilizes pantothenate, cysteine and ATP. CoA is

synthesized from vitamin B5 or pantothenate, which is taken up by endothelial cells via a sodium-dependent multivitamin transporter and then passes to the blood for delivery to the rest of the body. Mutations in *PANK2* are expected to result in defective CoA biosynthesis, which could lead to a variety of metabolic defects. Recently it has been hypothesized that diminished CoA pools have injurious effect on histone and tubulin acetylation, contributing to the neurological phenotype of PKAN [20]. However, it is not known how mutations in *PANK2* cause the spectrum of clinical symptoms exhibited by PKAN patients. Iron was increased in the cytoplasm of degenerating neurons, implying that neurons manifest iron overload before their degeneration and that iron overload may contribute to neuronal loss in PKAN. In a recent study, the 'eye of the tiger' was identified ***Q1*** as an ovoid region in the globus pallidus that was markedly depleted of viable neurons, but rich in large spheroids that consisted of degenerating neurons, and smaller spheroids composed of dystrophic axons [21]. MRI studies on pre- symptomatic patients with PKAN [21] may support the possibility that neuronal loss precedes iron accumulation and that iron accumulation may be a sec-ondary effect.

A metabolic study on plasma derived from PKAN patients, has reported reduced lipid and cholesterol biosynthesis, impaired bile acid metabolism and reduced levels of certain sphingomyelin species. Sphingomyelins are the principal component of the myelin sheath wrapping the axons of neuronal cells [22]. A recent study have investigated the metabolic phenotype in PKAN patients in order to address questions of energy balance, nutrition status and lipid metabolism [23]. The study of PANK2 function is complex. The

generation of animal models of disease by knocking out the gene in fruitflies and mice have generated incomplete phenotypes, lacking signs of NBIA. A PKAN model of *Drosopftila* has a brain phenotype characterized by

the formation of vacuoles and absence of iron accumulation. ***Q2*** This model has shown mitochondrial dysfunction, decreased levels of CoA, increased protein oxidation and reduced lifespan [24]. Interestingly, it was demonstrated that these alterations could be rescued by providing pantethine in the diet [5]. In 2005, *Pank2*-null mice were generated [25], which showed growth reduction, retinal degeneration and male infertility due to azoospermia, but no movement disorder or brain iron accumulation, even after 18 months of age. In contrast, a pantothenic acid-deficient diet was able to elicit a movement disorder and azoospermia in mice without evidence of iron accumulation in brain [26]. Human and mouse PANK2 proteins show an identity of 90 %, although the mouse polypeptide does not have an N-terminal extension, which is present in human PANK2. A recent study has demonstrated that murine PANK2 is mainly located in the mitochondrial inter-membrane space [27] as is the human protein [28]. *Pank2*-null mice show alteration of mitochondrial membrane potential in neurons derived from sciatic nerve and hair bulge stem cells of adult mice. The same alteration is also present in neonatal hippocampal neurons. Electron microscopy analysis on cultured neurons derived from *Pank2*-null mice, have shown aberrant swollen mitochondria with remodelled cristae [27]. On the basis of the role of CoA in several crucial metabolic pathways and considering the data obtained by the metabolomics study in patients with PKAN [22]

indicating the presence of impairment in lipid metabolism, a recent work tested the hypothesis to challenge *Pank2*-null mouse model with a diet containing high fat levels. A ketogenic diet consists of a low-glucose and high-lipid content, stimulating lipid use by mitochondrial *β*-oxidation and ketone body production in the liver. *Pank2*-null mice on a ketogenic diet demonstrated the clinical signs present in patients with PKAN, namely more severe movement disorder and neurodegeneration. Pantethine administration to these mice determined a rescue of the clinical phenotype [29] including the movement disorder and the extension of lifespan as previously demonstrated in *Drosopftila* [5]. It is known that pantethine is rapidly converted into cysteamine and pantothenate by pantetheinase [30]. Although pantethine is not able to cross the blood–brain barrier, cysteamine can cross the blood–brain barrier and can exert positive effects on the striatum and substantia nigra [31]. These data, together with data obtained in PKAN *Drosopftila* model, strongly suggest that pantethine administration to patients with PKAN should be considered as a possible and non-toxic therapeutic approach.

CoASY

A recent finding of human *CoASY* mutations in NBIA renews interest in CoA biosynthesis. In fact, in human, CoASY is a mitochondrial bifunctional enzyme of 62 kDa, with both PPAT and DPCK activities involved in the last two reactions of *de novo* CoA synthesis [32]. Although CoASY does not share a significant amino acidic sequence similarity with prokaryotes, a missense CoASY mutation

Q3 identified in PKAN patients [4] involves a residue highly conserved from bacteria to humans. In prokaryotes, plants and fungi, the PPAT and DPCK proteins are encoded by two different genes. PPAT, also named CoaD, catalyses the transfer of adenylyl group from ATP to 4-phospho- pantethine and appears as a homohexamer arranged in a dimer of trimers. It seems to be the second point of biosynthesis regulation [33]. To investigate the mechanism of this regulation, crystal structures of bacterial PPAT have been determined in presence of substrates and products. These studies show the preferentially binding of the molecules with only one of the two dimers, creating asymmetric units, and demonstrate an allosteric mechanism of catalysis [34,35]. Moreover crystal structure of PPAT-CoA mimics the PPAT-dPCoA (3r-dephospho-CoA) and PPAT-Ppant (4r-phosphopantetheinyl), showing similar conformational changes that prevent any other substrates interaction and suggesting that the asymmetry of binding of CoA plays a negative feedback regulation [36,37].

The DPCK, also named CoAE catalyses the phos- phorylation of the 3r hydroxy group of ribose using ATP as a phosphate donor and

appears in solution and in crystal structure respectively as monomer in *Haemopftilus influenzae* [38], or as homotrimers in bacteria [39]. Despite their difference in the quaternary structure, the sequence of DPCK in these microorganisms share a 48 % homology and have a very similar tertiary structure with several differences localized in residues involved in trimerization. The crystal reveals three conserved domains, typical of nucleosides kinase: the nucleotide-binding domain or P-loop; the substrate-binding domain; the lid domain. Interestingly, one of the human CoASY mutations is localized in conserved domain of P-loop [4], so further crystallization studies are necessary to understand the structure and regulation of the protein.

Conclusions and future perspectives

The aim of this review was to remark the importance of the new discovery about the second inborn error of CoA pathway associated with NBIA and to underline the potential link between CoA synthesis and neurodegeneration.

It is evident that two different and crucial pathways, namely CoA biosynthesis and iron metabolism, which are apparently not connected, play a crucial role in the pathogenesis of NBIA. CoA is an essential metabolic cofactor, which is involved in a wide variety of metabolic processes. On the other side, regulation of iron metabolism is also crucial since both iron deficiency and iron overload can cause diseases. Some researchers have hypothesized that iron accumulation may be just an epiphenomenon, and not a primary cause of NBIA diseases [40]. During normal aging process, brain iron accumulation is

present also in healthy people, but is also associated with various neurodegenerative diseases, such as Parkinson's disease, AD (Alzheimer's disease) and multiple sclerosis [41]. Iron has been evidenced as a potential damaging element for tissues either directly or because it changes the cellular environment, making it more prone to toxins. On the other hand, iron deposition may be just a consequence of microglial response to neuronal death and may not have a causative role in disease [42]. In addition, it remains unexplained why mutations in the enzymes involved in CoA biosynthetic pathway cause neurodegeneration. The hypothesis of cysteine accumulation, due to PANK2 malfunctioning, which produces free radical formation, appears plausible, but the pathophysiology of PKAN is not understood [43].

Moreover, it is necessary to find a different mechanism to explain the role of CoASY mutations.

This new finding support the idea that a dysfunction in CoA synthesis plays a crucial role in the pathogenesis of NBIA and thus in the development and functioning of the nervous system. This was previously suggested by other studies: PKAN *Drosopftila* model, manifest neurological symptoms and a significant decrease of CoA levels [5], and CoA level is reduced in mice lacking both *Pank1* and *Pank2* genes [6]. In addition, it has been demonstrated that CoASY associates specifically with S6K, a kinase regulator of cell size and growth, which is activated in response to mitogenic stimuli and nutrients via PI3K and mTOR signalling pathways [7,8].

Moreover, a recent study shows that the inhibition of acetyl-CoA synthesis induces autophagy, whereas stimula- tion of acetyl-CoA synthesis inhibits autophagy induced by different stimuli [44].

Nevertheless, further investigations are necessary to find a connection between CoA metabolism, lipid metabolism and mitochondrial dysfunctions, due to the mitochondrial localization of both PANK2 and CoASY [4,45–48]. Additional research will be requested to better define the sub-mitochondrial compartments in which PANK2 and CoASY are located and to understand whether the other enzymes of the CoA biosynthesis, PPCDC (phosphopantothenoylcysteine decarboxylase) and PPCS (phosphopantothenoylcysteine synthetase), are exclusively present in the cytoplasm. It would be relevant to clarify whether an exclusively mitochondrial CoA biosynthetic pathway is present and how the exchange of CoA between the different cellular compartments is regulated.

These studies will pave the way to understanding the molecular mechanisms involved in CoA metabolism, its connection with iron management in the brain, mitochondria function and neurodegeneration

Funding

The support of Telethon [grant number GGP11088 (to V.T.)] and of Mariani Foundation of Milan is gratefully acknowledged. This work was supported by TIRCON project of the European Commission's Seventh Framework Programme (FP7/2007–2013, HEALTH-F2-2011) [grant number 277984].

References

1 Kalman, B., Lautenschlaeger, R., Kohlmayer, F., Büchner, B., Kmiec, T., Klopstock, T., and Kuhn, K.A. (2012) An international registry for neurodegeneration with brain iron accumulation. Orphanet. J. Rare. Dis. 7, 66.

2 Chinnery, P.F., Crompton, D.E., Birchall, D., Jackson, M.J., Coulthard, A., Lombès, A., Quinn, N., Wills, A., Fletcher, N., Mottershead, J.P., Cooper, P., Kellett, M., Bates, D., and Burn, J. (2007) Clinical features and natural history of neuroferritinopathy caused by the FTL1 460InsA mutation. Brain. 130, 110-119.

3 McNeill, A., Pandolfo, M., Kuhn, J., Shang, H., and Miyajima, H. (2008) The neurological presentation of ceruloplasmin gene mutations. Eur. Neurol. 60, 200-5.

4 Dusi, S., Valletta, L., Haack, T.B., Tsuchiya, Y., Venco, P., Pasqualato, S., Goffrini, P., Tigano, M., Demchenko, N., Wieland, T., Schwarzmayr, T., Strom, T.M., Invernizzi, F., Garavaglia, B., Gregory, A., Sanford, L., Hamada, J., Bettencourt, C., Houlden, H., Chiapparini, L., Zorzi, G., Kurian, M.A., Nardocci, N.,

Prokisch, H., Hayflick, S., Gout, I., and Tiranti, V. (2014) Exome sequence reveals mutations in CoA synthase as a cause of neurodegeneration with brain iron accumulation. Am. J. Hum. Genet. 94, 11-22.

5 Rana, A., Seinen, E., Siudeja, K., Muntendam, R., Srinivasan, B., van der Want, J.J., Hayflick, S., Reijngoud, D.J., Kayser, O., and Sibon, O.C. (2010). Pantethine rescues a Drosophila model for pantothenate kinase-associated neurodegeneration. Proc. Natl. Acad. Sci. U.S.A. 107, 6988-93.

6 Garcia, M., Leonardi, R., Zhang, Y.M., Rehg, J.E., and Jackowski, S. (2012) Germline deletion of pantothenate kinases 1 and 2 reveals the key roles for CoA in postnatal metabolism. PLoS. One. 7, e40871.

7 Nemazanyy, I., Panasyuk, G., Zhyvoloup, A., Panayotou, G., Gout, I.T., and Filonenko, V. (2004) Specific interaction between S6K1 and CoA synthase: a potential link between the mTOR/S6K pathway, CoA biosynthesis and energy metabolism. FEBS. Lett. 578, 357-62.

8 Breus, O., Panasyuk, G., Gout, I.T., Filonenko, V., and Nemazanyy, I. (2009) CoA synthase is in complex with p85alphaPI3K and affects PI3K signaling pathway. Biochem. Biophys. Res. Commun. 385, 581-5.

9 Strauss, E. and Begley, T.P. (2005) The selectivity for cysteine over serine in coenzyme A biosynthesis. Chembiochem. 6, 284-286.

10 Tahiliani, A. G. and Beinlich, C.J. (1991) Pantothenic acid in health and disease. Vitam. Horm. 46, 165-228.

11 Webb, M.E., and Smith, A.G. (2011) Pantothenate Biosynthesis in Higher Plants. Adv. Bot. Res. 58, 203-255.

12 Gerdes, S., Lerma-Ortiz, C., Frelin, O., Seaver, S.M., Henry, C.S., de Crécy-Lagard, V., and Hanson, A.D. (2012) Plant B vitamin pathways and their compartmentation: a guide for the perplexed. J. Exp. Bot. 63, 5379-95.

13 Agrimi, G., Russo, A., Scarcia, P., and Palmieri, F. (2012) The human gene SLC25A17 encodes a peroxisomal transporter of coenzyme A, FAD and NAD+. Biochem. J. 443, 241-7.

14 Prohl, C., Pelzer, W., Diekert, K., Kmita, H., Bedekovics, T., Kispal, G., and Lill, R. (2001) The yeast mitochondrial carrier Leu5p and its human homologue Graves' disease protein are required for accumulation of coenzyme A in the matrix. Mol. Cell. Biol. 21, 1089-97.

15 Fiermonte, G., Paradies, E., Todisco, S., Marobbio, C.M., and Palmieri, F. (2009) A novel member of solute carrier family 25 (SLC25A42) is a transporter of coenzyme A and adenosine 3',5'-diphosphate in human mitochondria. J. Biol. Chem. 284, 18152-9.

16 Leonardi, R., Zhang, Y.M., Rock, C.O., and Jackowski, S. (2005) Coenzyme A: back in action. Prog. Lipid. Res. 44, 125-153.

17 Zhou, B., Westaway, S.K., Levinson, B., Johnson, M.A., Gitschier, J., and Hayflick, S.J. (2001) A novel pantothenate kinase gene (PANK2) is defective in Hallervorden-Spatz syndrome. Nat. Genet. 28, 345-349.

18 Kotzbauer, P.T., Truax, A.C., Trojanowski, J.Q. and Lee, V.M.Y. (2005) Altered neuronal mitochondrial coenzyme A synthesis in neurodegeneration with brain iron accumulation

caused by abnormal processing, stability, and catalytic activity of mutant pantothenate kinase 2. J. Neurosci. 25, 689–98.

19 Hortnagel, K., Prokisch, H., and Meitinger, T. (2003) An isoform of hPANK2, deficient in pantothenate kinase-associated neurodegeneration, localizes to mitochondria. Hum. Mol. Genet. 12, 321-7.

20 Siudeja, K., Srinivasan, B., Xu, L., Rana, A., De Jong, J., Nollen, E.A.A, Jackowski, S., Sanford, L., Hayflick, S., and Sibon, O.C.M. (2011) Impaired Coenzyme A metabolism affects histone and tubulin acetylation in Drosophila and human cell models of pantothenate kinase associated neurodegeneration, EMBO Mol. Med. 3, 1-12.

21 Kruer, M.C., Hiken, M., Gregory, A., Malandrini, A., Clark, D., Hogarth, P., Grafe, M., Hayflick, S.J., and Woltjer, R.L. (2011) Novel histopathologic findings in molecularly-confirmed pantothenate kinase-associated neurodegeneration. Brain. 134, 947-58.

22 Leoni, V., Strittmatter, L., Zorzi, G., Zibordi, F., Dusi, S., Garavaglia, B., Venco, P., Caccia, C., Souza, A.L., Deik, A., Clish, C.B., Rimoldi, M., Ciusani, E., Bertini, E., Nardocci, N., Mootha, V.K., and Tiranti, V. (2012). Metabolic consequences of mitochondrial coenzyme A deficiency in patients with PANK2 mutations. Mol. Genet. Metab. 105, 463-71.

23 Williams, S., Gregory, A., Hogarth, P., Hayflick, S.J., and Gillingham, M.B. (2013) Metabolism and energy requirements in pantothenate kinase-associated neurodegeneration. Mol. Genet. Metab. 110, 336-41.

24 Bosveld, F., Rana, A., van der Wouden, P.E., Lemstra, W., Ritsema, M., Kampinga, H.H. and Sibon, O.C. (2008) De novo CoA biosynthesis is required to maintain DNA integrity during development of the Drosophila nervous system. Hum. Mol. Genet. 17, 2058–2069.

25 Kuo, Y.M., Duncan, J.L., Westaway, S.K., Yang, H., Nune, G., Xu, E.Y., Hayflick, S.J. and Gitschier, J. (2005) Deficiency of pantothenate kinase 2 (Pank2) in mice leads to retinal degeneration and azoospermia. Hum. Mol. Genet. 14, 49–57.

26 Kuo, Y.M., Hayflick, S.J. and Gitschier, J. (2007) Deprivation of pantothenic acid elicits a movement disorder and azoospermia in a mouse model of pantothenate kinase-associated neurodegeneration. J. Inherit. Metab. Dis. 30, 310–317.

27 Brunetti, D., Dusi, S., Morbin, M., Uggetti, A., Moda, F., d'Amato, I., Giordano, C., d'Amati, G., Cozzi, A., Levi, S., Hayflick, S., and Tiranti, V. (2012) Pantothenate kinase-associated neurodegeneration: altered mitochondria membrane potential and defective respiration in Pank2 knock-out mouse model. Hum. Mol. Genet. 21, 5294-305.

28 Leonardi, R., Rock, C.O., Jackowski, S., and Zhang, Y.M. (2007) Activation of human mitochondrial pantothenate kinase 2 by palmitoylcarnitine. Proc. Natl. Acad. Sci. USA. 104, 1494-9.

29 Brunetti, D., Dusi, S., Giordano, C., Lamperti, C., Morbin, M., Fugnanesi, V., Marchet, S., Fagiolari, G., Sibon, O., Moggio, M., d'Amati, G., and Tiranti V. (2013) Pantethine treatment is effective in recovering the disease phenotype induced by ketogenic

diet in a pantothenate kinase-associated neurodegeneration mouse model. Brain. 137, 57-68.

30 Kaskow, B.J., Proffitt, J.M., Blangero, J., Moses, E.K., and Abraham, L.J. (2012) Diverse biological activities of the vascular non-inflammatory molecules - the Vanin pantetheinases. Biochem. Biophys. Res. Commun. 417, 653–8.

31 Gibrat, C., and Cicchetti, F. Potential of cystamine and cysteamine in the treatment of neurodegenerative diseases. (2011) Prog. Neuropsychopharmacol. Biol. Psychiatry. 35, 380–9.

32 Aghajanian, S., and Worrall, D.M. (2002). Identification and characterization of the gene encoding the human phosphopantetheine adenylyltransferase and dephospho-CoA kinase bifunctional enzyme (CoA synthase). Biochem. J. 365, 13–18.

33 Daugherty M., Polanuyer, B., Farrell, M., Scholle, M., Lykidis, A., de Crécy-Lagard, V., and Osterman, A. (2002) Complete reconstitution of the human coenzyme A biosynthetic pathway via mparative genomics. J. Biol. Chem. 277, 21431–21439.

34 Izard, T., and Geerlof, A. (1999) The crystal structure of novel bacterial adenylyltransferase reveals half of sites reactivity. EMBO. J. 18, 2021-30.

35 Izard, T. (2002). The crystal structures of phosphopantetheine adenylyltransferase with bound substrates reveal the enzyme's catalytic mechanism. J. Mol. Biol. 315, 487-95.

36 Izard, T. (2003) A novel adenylate binding site confers phosphopantetheine adenylyltransferase interactions with coenzyme A. J. Bacteriol. 185, 4074-80.

37 Rock, C.O., Park, H.W., and Jackowski, S. (2003) Role of feedback regulation of pantothenate kinase (CoaA) in control of coenzyme A levels in Escherichia coli. J. Bacteriol. 185, 3410-5.

38 Obmolova, G., Teplyakov, A., Bonander, N., Eisenstein, E., Howard, A.J., and Gilliland, G.L. (2001) Crystal structure of dephospho-coenzyme A kinase from Haemophilus influenzae. J. Struct. Biol. 136, 119-25.

39 O'Toole, N., Barbosa, J.A., Li, Y., Hung, L.W., Matte, A., and Cygler, M. (2003) Crystal structure of a trimeric form of dephosphocoenzyme A kinase from Escherichia coli. Protein. Sci. 12, 327-36.

40 Schneider, S.A., Dusek, P., Hardy, J., Westenberger, A., Jankovic, J. and Bhatia, K.P. (2013) Genetics and Pathophysiology of Neurodegeneration with Brain Iron Accumulation (NBIA). Curr. Neuropharmacol. 11, 59-79.

41 Stankiewicz, J., Panter, S.S., Neema, M., Arora, A., Batt, C.E., and Bakshi, R. (2007) Iron in chronic brain disorders: imaging and neurotherapeutic implications. Neurotherapeutics. 4, 371-86.

42 Schneider, S.A., Hardy, J., and Bhatia, K.P. (2009) Iron accumulation in syndromes of neurodegeneration with brain accumulation 1 and 2: causative or consequential? J. Neurol. Neurosurg. Psychiatry. 80, 589-590.

43 Fleming, R.E., and Ponka, P. (2012) Iron overload in human disease. N. Engl. J. Med. 366, 348-59.

44 Mariño, G., Pietrocola, F., Eisenberg, T., Kong, Y., Malik, S.A., Andryushkova, A., Schroeder, S., Pendl, T., Harger, A., Niso-Santano, M., Zamzami, N., Scoazec, M., Durand, S., Enot, D.P., Fernández, A.F., Martins, I., Kepp, O., Senovilla, L., Bauvy, C., Morselli, E., Vacchelli, E., Bennetzen, M., Magnes, C., Sinner, F., Pieber, T., López-Otín, C., Maiuri, M.C., Codogno, P., Andersen, J.S., Hill, J.A., Madeo, F., and Kroemer, G. (2014) Regulation of autophagy by cytosolic acetyl-coenzyme a. Mol Cell. 53, 710-25.

45 Hörtnagel, K., Prokisch, H., and Meitinger, T. (2003) An isoform of hPANK2, deficient in pantothenate kinase-associated neurodegeneration, localizes to mitochondria. Hum. Mol. Genet. 12, 321-327.

46 Alfonso-Pecchio, A., Garcia, M., Leonardi, R., and Jackowski, S. (2012). Compartmentalization of mammalian pantothenate kinases. PLoS. One. 7, e49509.

47 Zhyvoloup, A., Nemazanyy, I., Panasyuk, G., Valovka, T., Fenton, T., Rebholz, H., Wang, M.L., Foxon, R., Lyzogubov, V., Usenko, V., et al. (2003). Subcellular Localization and Regulation of Coenzyme A Synthase. J. Biol. Chem. 278, 50316-21.

48 Rhee, H.W., Zou, P., Udeshi, N.D., Martell, J.D., Mootha, V.K., Carr, S.A., and Ting, A.Y. (2013). Proteomic mapping of mitochondria in living cells via spatially-restricted enzymatic tagging. Science. 339, 1328-31.

SUMMARY

During my PhD program I have been involved in a project organized principally in three sections: in the first part, I characterized C19orf12 gene, coding for a mitochondrial membrane protein, which mutations are responsible for a subtype of NBIA called MPAN (Mitochondrial membrane Protein Associated Neurodegeneration). In the second part I applied exome sequencing on selected patients without molecular diagnosis, and we found that mutations in CoA Synthase (COASY) were responsibible for a form of NBIA, that we called CoPAN (COASY protein-associated neurodegeneration). In the third part I obtained new cellular models for NBIA disorders (specifically for PKAN subtype) and MPAN (in progress) in order to understand their pathogenetic mechanisms.

To achieve these aims, I initially focused on C19orf12 coding protein, a 17kDa mitochondrial membrane-associated protein whose function is still unknown. So, the first thing was to study wild-type and mutants C19orf12 sub-cellular localization in native conditions and under oxidative stress. I showed that wild-type C19orf12 protein was not exclusively present in mitochondria, but also in the Endoplasmic Reticulum (ER) and MAM (Mitochondria Associated Membrane), while mutant C19orf12 variants presented a different localization. Moreover, after induction of oxidative stress, a GFP-tagged C19orf12 wild-type protein was able to relocate to the cytosol. On the contrary, mutant isoforms were not able to respond to oxidative stress. During these experiments we noticed bright aggregates by the wild-type

protein, surrounding mitochondria, so we performed colocalization study using the specific autophagy marker LC3, suggesting that these were not autophagosomes. In support of the hypothesis of an involvement in autophagy, we observed that overexpression of wild-type C19orf12 resulted in conversion of autophagic marker LC3 and reduction of levels of p62. On the contrary, induction of delocalization by oxidative stress results in reduction of autophagy LC3 conversion. Interestingly, the overexpression of mutants, unable to properly gain its intracellular localization, fails to promote autophagy induction and levels of basal autophagy remain unchanged during exposure to oxidative stress. Finally high mitochondrial calcium concentration and increased H_2O_2 induced apoptosis were found in fibroblasts derived from one patient as compared to controls. Then we carried out secondary structure prediction of the full *C19orf12* sequence and modeling of the predicted soluble region (*C19orf12*$_{1\text{-}40/81\text{-}151}$) to understand functional and structural properties of the wild-type protein and the effects of the mutations.

Our *in silico* investigation suggested that, the glycine zipper motifs of C19orf12 form helical regions spanning the membrane. The N- and C-terminal regions with respect to the transmembrana portion, on the contrary, are predicted to rearrange in a structural domain, which is homolog to the N-terminal regulatory domain of the magnesium transporter MgtE, suggesting that C19orf12 may act as a regulatory protein for human MgtE transporters.

The second part of my PhD program was focused on the characterization of a new disease gene, coenzyme A synthase

(COASY), found mutated using whole Exome Sequencing strategy. COASY codes for a bifunctional enzyme (PPAT and DPCK activities) involved in the last two steps of coenzyme A biosynthesis. In order to verify if we have identified the second inborn error of CoA biosynthesis leading to NBIA, we performed traditional Sanger sequencing in a cohort of NBIA subject and we found another mutant patient. Then we performed western-blot analysis showed that the protein was absent in patient-derived skin fibroblasts.

To better analyze the effects of the mutation on catalytic activity of COASY, we expressed wild type and mutant human DPCK domain in bacteria as His-tag fusion protein. We also expressed PPAT domain and wild type and mutant human COASY. After protein purification we measured Coenzyme A *in vitro* synthesis through HPLC analysis.

Wild-type COASY was able to synthesizes CoA, whereas mutant enzymes had an about 40-50% reduced activity compared to wild-type enzyme. Consequently, we analyzed CoA levels in fibroblasts derived from affected subjects and the level of CoA was approximately 20% of that produced by control fibroblasts. Additional experiment were performed on yeast cells, about growth and HPLC analysis on mitochondria isolated from the strains, and we observed a significant reduction of CoA concentration in the mutant strains.

Due to the fact that existing cellular models and *in vivo* models for NBIA don't recapitulate the neuropathological signs typical of the human disorder, we tried to obtain new cellular models. We started from PKAN patients and MPAN patients (work in progress). We generated human induced pluripotent stem cells (hiPSCs)

reprogramming PKAN fibroblasts that were fully characterized. We then differentiated control and PKAN hiPSCs into a pure and stable population of self-renewable neuronal precursor cells (NPCs). Stable NPC cultures were established with equal efficiency from all controls and PKAN hiPSCs and were competent to differentiate into neurons and astrocytes. To generate functional neurons, we used over-expression of Neurogenin2, a neurogenic factor, which pushes the reprogramming towards glutamatergic neurons. The mitochondrial functionality of neurons was evaluated studying the integrity of mitochondrial membrane potential using the mitochondria-specific fluorescent probe tetramethylrhodamine-methyl-ester (TMRM). PKAN neurons exhibited a statistically significant reduction (about 20% lower) in TMRM incorporation respect to control neurons and, at ultrastructural analysis, aberrant mitochondria with damaged cristae. Next we investigated respiratory activity as a critical parameter of mitochondrial function by microscale oxygraphy. PKAN neurons showed values significant lower than control, which indicate mitochondrial dysfunctions. Thus, we monitored ROS levels in basal conditions using the fluorescent ROS-sensitive dichlorofluorescein (DCF) and they were strongly enhanced in the PKAN compared to control neurons. Trying to have a model not only for mitochondrial dysfunction but also for iron accumulation, we analyzed iron mitochondrial pathways, investigating the activity of two ISC-containing enzymes and heme content in neurons. We reported a significant reduction of aconitase activity and heme content. These results provide evidence that iron metabolism is impaired in PKAN neurons, which exhibit a manifested cellular iron deficient phenotype.

Taken together these observations, even though they regarded different NBIA subtype, suggest that Whole Exome sequencing is useful to find new disease genes, that CoA have an important function in the pathological mechanism of this syndrome, that further studies are necessary to understand the function of C19orf12 gene, but that reprogramming is a successful method for modeling NBIA.

CONCLUSIONS

It is difficult to write the conclusion of a thesis concerning a syndrome having as common denominator only iron overload in the brain, and with a big variability of clinical presentation, inheritance and molecular diagnosis. Despite in the last years, thank to genetic, remarkable advances in the identification of new disease genes, their function and their pathogenetic role remain sometimes elusive. So, in attempt to find another common denominator for this syndrome here I propose as the main focus on my PhD program, the characterization of these disease gene with development of cellular models, highlighting the cellular processes that lead to neurodegeneration.

In the first part of my PhD I characterized C19orf12 gene, using fibroblasts' derived patients, over-expression of the protein and in silico analyses. We have demonstrated that C19orf12 is not present only in mitochondria but also in ER and MAM, and that mutations cause a mis-localization of the protein. MAM are zones of contact

between ER and mitochondria, and have a role in lipid transfer and Ca^{2+} ions exchange (Berridge MJ. 2003) (Hamasaki M. 2013). Their first role may be correlated with the putative role of C19orf12 in lipid metabolism, the second with our data that show high levels of mitochondrial Ca^{2+} in fibroblasts patients compared to control. As a consequence, patient-derived fibroblasts were more sensitive to Ca^{2+} dependent apoptotic stimuli like H_2O_2 as compared to control. Moreover we proposed a putative role as stimulatory effect on autophagy. Altogether these data point the attention on different emerging aspects for NBIA: mitochondria-ER function, lipid metabolism, calcium metabolism, autophagosome formation, oxidative stress. Moreover in silico analysis suggested a putative role for C19orf12 as a magnesium transport. Magnesium has been recently associated with learning and memory. (Barbagallo M. 2009) (Slutsky I. 2004). So my work paves the way to different hypothesis for C19orf12 gene, but other experiments are required to clearly understand its function.

In the second paper we have performed whole exome sequencing analysis in one subject with clinical presentation suggestive of NBIA but without any mutations in previously associated genes.
The overall study was carried out using patient derived fibroblasts, His-tag fusion proteins, and also saccharomyces cerevisiae as models, and at the end we have identified the second inborn error of CoA biosynthesis leading to NBIA due to mutations in COASY gene. The first one was associated with PANK2 mutations. (Zhou B. 2001). This finding highlights the role of CoA pathway for the function of nervous

system, but it is unclear why CoA synthesis defect is compatible with life (patients can survive up to the third decade of life). Maybe there are alternative strategies to synthesize CoA, and maybe they have to be researched in mitochondria considering that both PANK2 and COASY are mitochondrial enzymes. (Alfonso-Pecchio 2012) (Zhyvoloup A. 2003) (Rhee HW. 2013) .The potential link between CoA synthesis and neurodegeneration it is also suggested by other studies: PKAN drosophila models manifest neurological symptoms and a significant decrease of CoA levels (Rana A. 2010) and CoA level is reduced in *Pank2* $^{-/-}$ mouse model, even if mice don't recapitulate the neurodegenerative phenotype (Garcia M. 2012). Due to the fact that CoA works like a high energy carrier of acetyl and acyl groups and it is involved in many metabolic reactions, for example in synthesis of phospholipids and sphingolipids, and that the role of iron accumulation is not clear in this subtype of NBIA, we propose defects in membrane remodeling as the primary cause of neurodegeneration. According to this hypothesis, mitochondrial CoA deficiency may damage cell and organelles membranes and lead to oxidative stress, which would alter iron homeostasis (Levi and Finazzi 2014).

This hypothesis is supported by the reduced amounts of newly synthetized acetyl-CoA compared to controls, that may be influence membranes' integrity, and at the end alteration of mitochondrial structure and functionality and strong impact on neurological function. In addition, it has been demonstrated a link between CoA biosynthase and mTOR pathway, which is implicated in numerous metabolic and signaling processes (Nemazanyy 2004). Nevertheless, further studies are necessary to definitely prove this hypotheses, and to find the

strong connection between CoA metabolism, lipid metabolism, mitochondria dysfunctions and cellular processes that lead to neurodegeneration. And maybe new modeling approaches for NBIA pathologies come to the aid of this goal and eventually to the developing of a therapy.

Then the third part of my PhD program was focus on the opportunity to generate iPSCs from human skin fibroblasts, and later, due to their capacity to be differentiated into the cell-type of interest, to investigate the pathological properties of human neuronal cells from them (Amamoto and Arlotta 2014). We started to modeling PKAN syndrome, because PANK2 mutations account for 50% of NBIA cases, but the final goal is to prepare a iPSCs bank of NBIA where different neural cell types and different NBIA subtype can be collected and studied. This goal represents a future challenge also because NBIA animal models have been crucial in the investigation of disease aspects but till now they aren't able to recapitulate whole neurological phenotype and the hallmark of the iron deposition in the brain. Furthermore, as I try to prove in my PhD thesis, the overwhelming majority of neurological disease is of sporadic nature (Christian K. 2012), rendering animal modeling ineffective, while they share many interest characteristics with monogenic forms of disease. (Sterneckert JL. 2014). According to this observation patient-specific iPSCs represent a an opportunity not only to study NBIA, but alto other disease that affect the nervous system. (Yu D. 2013)
The first result of our work is the successful generation of a new PKAN model by generating iPSC- derived neurons, suggesting that

PANK2 deficiency does not affect the neuronal fate commitment and differentiation of these cells, as would be expected considering that the patients have a normal brain development. This PKAN model shows abnormal phenotypes in human neuronal and highlight CoA treatment as a potential therapeutic option. Nonetheless, we have not detected any iron deposition in PKAN neurons yet. Two different reasons might account for this result. On one hand, the period of time where human neurons in culture were observed might not be long enough considering that iron deposition is detectable in patients only few or more years after birth (Marchetto MC. 2010). On the other hand, iron accumulation in patients is restricted to pallidal GABAergic and, less frequently, dopaminergic neurons of substantia nigra. We favored to conduct our study on forebrain-specific glutamatergic excitatory neurons since this system is among the fewest that can be derived from hiPSCs providing a homogeneous neuronal network with robust functional activities. Overall, these data indicate that this new human neuronal model represents a powerful platform for investigating pathogenic mechanism of disease and testing the efficacy of therapeutic compounds.

In conclusion, these three studies will pave the way to understand the molecular mechanisms involved in NBIA, in particular the connection between ad altered lipid metabolis, as a result of CoA biosynthesis defect, iron management in the brain, mitochondria function and neurodegeneration.

FUTURE PERSPECTIVES

Neurological diseases include heterogeneous group of disorders ranging from pediatric neurodevelopment diseases, heterogeneous monogenic disorders (like NBIA) to late-onset neurodegenerative diseases, most of which are poorly understood and the treatment options remain limited to supportive therapies rather than correction of the underlying deficiencies. (Prohaska R. 2012).

NBIA disorders are a group of rare syndromes characterized by high genetic and clinical heterogeneity and relatively loose genotype/phenotype correlation. Using rare genetically defined disorders, make them very interesting and useful to understand disease mechanisms that lead to neurodegeneration. On the contrary most of late-onset neurodegenerative diseases (such as PD, AD and ALS) are complex neurological diseases where several genes with rare and/or common variants can influence disease risk as well as environmental factors can contribute to disease development. So even if NBIA pathogenesis is still not clear, my PhD work demonstrates that new integrated approaches including, generation of appropriate cellular models, whole exome sequencing and reprogramming, are needed to unravel the highly complex biological processes presented in different neurological disorders.

Thanks to new sequencing technologies many new genes associated to inherited conditions, including several neurological diseases, have been identified in the last few years and will be identified in a more rapid turnaround time, bypassing many problems typical of the traditional approaches, for example the requirement of large pedigrees

(Johnson JO. 2010) (Zimprich A. 2011). Despite this improvement in diagnosis, some protein functions are still unknown (like C19orf12), or the hallmark of this syndrome, the iron accumulation, is far to be clear. But in our studies we propose some hypothesis: lipid metabolism as one of the main causes of NBIA, or also mitochondria dysfunction as a concurrent cause for it (Colombelli C. 2014) (Brunetti D 2014). Undoubtedly much more work is needed to comprehend all the mechanisms and the connections that cause NBIA, and neurodegeneration in general. To this aim, somatic cellular reprogramming seems to represent an opportunity to study the behavior of live neurons from patients with monogenic neurodegenerative diseases even if many improvements are necessary to refine the technology. From the literature a general pattern has emerging regarding the inability of neurons to establish proper connections and neuronal maturation suitable for modeling defects. Furthermore the overwhelming and attractive advantage to study the nervous system in the context of each patient's own unique genetic constellation, represents also the risk of a high variability that elicits the big effort to establish a meaningful parallel between the dish and the pathology. (Yu D. 2013). In this sense is necessary to create an appropriate cell banking, in order to analyze multiple clones of the same disease or syndrome. We in collaboration with San Raffaele Scientific Institute are concerting efforts to create a NBIA iPSCs bank, and till now we have obtained stem cells for PKAN, CoPAN, MPAN, BPAN subtype, but many investigations are to be done to study them and eventually propose some effective therapeutic compounds.

REFERENCES

Alfonso-Pecchio, A., Garcia, M., Leonardi, R., and Jackowski, S. « Compartmentalization of mammalian pantothenate kinases.» *PLoS. One.* , 2012: 7, e49509.

Amamoto, R., and P. Arlotta. "Development-inspired reprogramming of the mammalian central nervous system." *Science*, 2014: 343: 1239882.

Barbagallo M., Belvedere M, Dominguez LJ. «Magnesium homeostasis and aging.» *Magnes Res.*, 2009: 22(4):235-46.

Berridge MJ., Bootman MD, Roderick HL. « Calcium signalling: dynamics, homeostasis and remodelling.» *Nat Rev Mol Cell Biol* , 2003: 4:517-529.

Brunetti D, Dusi S, Giordano C., Lamperti C., Morbin M., Fugnanesi V., Marchet S., Fagiolari G., Sibon O., Moggio M., d'Amati G., Tiranti V.,. «Panthetine treatment is effective in recovering the disease phenotype induced by ketogenic diet in a pantothenate kinase-associated neurodegeneration mouse mode.» *Brain*, 2014: 137: 57-68.

Christian K., Song H., Ming G.,. «Application of reprogrammed patient cell to investigate the etiology of neurological and psychiatric disorders.» *Front Biol*, 2012: 7:179-188.

Colombelli C., Aoun M., Tiranti V.,. «Defective lipid metabolism in neurodegeneration with brain iron accumulation (NBIA) syndrome: not only a matter of iron.» *J inherit Metab Dis*, 2014.

Garcia M., Leonardi R., Zhang YM., Rehg JE, Jackowski S. «Germline deletion of pantothenate kinases 1 and 2 reveals the key roles for CoA in postnatal metabolism.» *Plos One*, 2012.

Hamasaki M., Furuta N, Matsuda A, Nezu A, Yamamoto A, Fujita N, Oomori H, Noda T, Haraguchi T, Hiraoka Y, Amano A, Yoshimori T. « Autophagosomes form at ER-mitochondria contact sites. .» *Nature*, 2013: 21;495(7441):389-93.

Johnson JO., Mandrioli J, Benatar M, Abramzon Y, Van Deerlin VM. « Exome sequencing reveals VCP mutations as a cause of familial ALS.» *Neuron* , 2010: 68, 857–864.

Levi, S., and D., Finazzi. "Neurodegeneration with brain iron accumulation: update on pathogenic mechanism." *frontiers in pharmacology*, 2014.

Marchetto MC., Carromeu, C., Acab, A., Yu, D., Yeo, G.W., Mu, Y., Chen, G.,Gage, F.H., and Muotri, A.R. « A model for neural development and treatment of Rett syndrome using human induced pluripotent stem cells. .» *Cell* , 2010: 143,527–539.

Nemazanyy, I., Panasyuk, G., Zhyvoloup A., Panayotou, G., Gout, I.T., and Filonenko, V. « Specific interaction between S6K1 and CoA synthase: a potential link between the mTOR/S6K pathway, CoA biosynthesis and energy metabolism.» *FEBS. Lett. 578, 357*, 2004: 578, 357.

Prohaska R., Ody Sibo CM., Rudnicki D., Danek A., Walker R. «Brain, blood and iron: perspective on the roles of erythrocyte and iron in neurodegeneration.» *Neuro of Disease*, 2012.

Rana A., Seinen E., Siudeja K., Muntendam R., Srinivasan, B., Van der Want, J.J., Hayflick, S., Reijngoud, D.J., Kayser, O., Sibon, O.C. «Pantethine rescues a Drosophila model for pantothenate kinase-associated neurodegeneration.» *Proc. Nat. Acad. Sci. USA. 107*, 2010: 6988-93.

Rhee HW., Zou, P., Udeshi, N.D., Martell, J.D., Mootha, V.K., Carr, S.A., and Ting, A.Y. « Proteomic mapping of mitochondria in living

cells via spatially-restricted enzymatic tagging.» *Science*, 2013: 339, 1328-31.

Slutsky I., Sadeghpour S, Li B, Liu G. « Enhancement of synaptic plasticity through chronically reduced Ca2+ flux during uncorrelated activity.» *Neuron.* , 2004: 2;44(5):835-49.

Sterneckert JL., Peter Reinhardt,Hans R. Schöler. «Investigating human disease using stem cell models.» *Nature review*, 2014: 15: 625-630.

Yu D., Marchetto MC, Gage F. «Therapeutic translation of iPSCs for Treating Neurological Disease.» *Cell Stem Cell*, 2013: 12: 678-688.

Zhou B., Westaway S.K., Levinson B., Johnson M.A., Gitschier, J., Hayflick, S.J. «A novel pantothenate kinase gene (PANK2) is defective in Hallervorden-Spatz syndrome.» *Nat. Genet. 28*, 2001: 345-349.

Zhyvoloup A., Nemazanyy, I., Panasyuk, G., Valovka, T., Fenton, T., Rebholz, H., Wang, M.L., Foxon, R., Lyzogubov, V., Usenko, V. «Subcellular Localization and Regulation of Coenzyme A Synthase.» *J. Biol. Chem. 2*, 2003: 278, 50316-21.

Zimprich A., Benet-Pagès A, Struhal W, Graf E, Eck SH, Offman MN, Haubenberger D, Spielberger S. « A mutation in VPS35, encoding a subunit of the retromer complex, causes late-onset Parkinson disease. .» *Am. J. Hum. Genet*, 2011: 89, 168–175. .